THE STRUCTURAL RESPONSE OF UNSYMMETRICALLY LAMINATED COMPOSITE CYLINDERS[1]

T. A. Butler[2]
M. W. Hyer[3]
Department of Mechanical Engineering
University of Maryland
College Park, MD 20742
Technical Report 89-2
August 1989

(1) Work supported by Grant NAG-1-665 from the Structural Mechanics Branch of Langley Research Center.
Grant Monitor: Dr. Michael P. Nemeth

(2) Currently, Martin-Marietta Naval and Aero Systems
6711 Baymeadow Drive
Glen Burnie, MD 21061

(3) Currently, Professor, Department of Engineering Science and Mechanics, Virginia Polytechnic Institute and State University, Blacksburg, VA 24061-0219

ABSTRACT

The responses of an unsymmetrically laminated fiber-reinforced composite cylinder to an axial compressive load, a torsional load, and the temperature change associated with cooling from the processing temperature to the service temperature are investigated. These problems are consider axisymmetric and the response is studied in the context of linear elastic material behavior and geometrically linear kinematics. Four different laminates are studied: a general unsymmetric laminate; two unsymmetric but more conventional laminates; and a conventional quasi-isotropic symmetric laminate. The responses based on closed-form solutions for different boundary conditions are computed and studied in detail. Particular emphasis is directed at understanding the influence of elastic couplings in the laminates. The influence of coupling decreased from a large effect in the general unsymmetric laminate, to practically no effect in the quasi-isotropic laminate. For example, the torsional loading of the general unsymmetric laminate resulted in a radial displacement. The temperature change also caused a significant radial displacement to occur near the ends of the cylinder. On the otherhand, the more conventional unsymmetric laminate and the quasi-isotropic cylinder did not deform radially when subjected to a torsional load. From the results obtained, it is clear the degree of elastic coupling can be controlled and indeed designed into a cylinder, the degree and character of the coupling being dictated by the application.

Preface

This report constitutes the thesis of Theresa A. Butler submitted for the partial fulfillment of a Master of Science in Mechanical Engineering at the University of Maryland, College Park.

Acknowledgements

The work reported on herein was conducted under the partial support of Grant NAG-1-665 from the Structural Mechanics Branch of the Langley Research Center to the University of Maryland. The symbolic computation used in the study was carried out by the second author while he was on leave from the University of Maryland and in residence at the Langley Research Center. The use of the facilities of the Langley Research Center are appreciated, as is the financial support of the Grant. The advice from and interaction with the Grant Monitor, Dr. Michael P. Nemeth, are also appreciated.

TABLE OF CONTENTS

LIST OF ABBREVIATIONS

Γ	Total potential energy
u_i	Displacement field
B_i	Body force distribution
$T_i^{(v)}$	Surface Tractions
U	Strain energy
σ_x	Normal stress in the x direction
σ_θ	Normal stress in the θ direction
σ_r	Normal stress in the r direction
$\tau_{\theta r}$	Shear stress on θ surface acting in r direction
τ_{xr}	Shear stress on x surface acting in r direction
$\tau_{x\theta}$	Shear stress on x surface acting in θ direction
ϵ_x	Strain acting in the x direction
ϵ_θ	Strain acting in the θ direction
ϵ_r	Strain acting in the r direction
$\epsilon_{\theta r}$	Shear strain on θ surface acting in r direction
ϵ_{xr}	Shear strain on x surface acting in r direction
$\epsilon_{x\theta}$	Shear strain on x surface acting in θ direction
R	Mean radius of cylinder (in)
L	Length of cylinder (in)
u	Axial displacement
w	Radial displacement

v	Circumferential displacement
u°	Axial midplane displacement
w°	Radial midplane displacement
v°	Circumferential midplane displacement
r	Radius somewhere on cylinder in r-θ coordinates
t	Wall thickness of cylinder (in)
N_x	Force resultant in x direction (lb/in)
N_θ	Force resultant in θ direction (lb/in)
$N_{x\theta}$	Shear resultant (lb/in)
M_x	Moment resultant in x direction (in-lb/in)
M_θ	Moment resultant in θ direction (in-lb/in)
$M_{x\theta}$	Twist moment resultant (in-lb/in)
N_x^T	Force resultant in x direction due to temperature
N_θ^T	Force resultant in θ direction due to temperature
$N_{x\theta}^T$	Shear force resultant due to temperature
M_x^T	Moment resultant in x direction due to temperature
M_θ^T	Moment resultant in θ direction due to temperature
$M_{x\theta}^T$	Twist moment resultant due to temperature
α_x	Coefficient of thermal expansion in x direction
α_θ	Coefficient of thermal expansion in θ direction

$\alpha_{x\theta}$	Shear coefficient of thermal expansion
ΔT	Change in temperature
C_{ij}	Stiffness matrix i,j = 1,2,3,4,5,6
Q	Reduced stiffness matrix
E_x	Young's modulus in x direction
E_y	Young's modulus in y direction
E_s	Shear modulus
μ_x	Poisson's ratio when material is loaded in the x direction
μ_y	Poisson's ratio when material is loaded in the y direction
Q_{ij}	Transformed reduced stiffness matrix i,j = 1,2,6
A_{ij}	Laminate stretching stiffness matrix i,j = 1,2,6
B_{ij}	Laminate bending/stretching stiffness matrix i,j = 1,2,6
D_{ij}	Laminate bending stiffness matrix i,j = 1,2,6
n	sin θ
m	cos θ
θ	Fiber angle
k_x	Curvature in x direction
k_θ	Curvature in θ direction
$k_{x\theta}$	Twist curvature

Chapter 1 - Introduction

Since their introduction as a structural material, fiber-reinforced composites have been used primarily as a replacement for more traditional materials such as metal. Despite the wide range of tailoring, elastic couplings, and directional dependence available with fiber-reinforced composite materials, they have not been used with these characteristics in mind. Rather, the inherent lighter weight, integrated design, and near-net-shape manufacturing capability of these materials have been the prime reasons for their increased use. As a result, composite structures today are overweight, conservatively designed, and in many applications, not that much better than, say, a lithium aluminum structure designed for the same purpose. There are exceptions to this, the forward sweep experimental aircraft technology being a prime example. While in some applications a design that does not utilize fiber-reinforced materials may be the best design, it is fair to say at this point in the development of composite structures that their potential in many applications, traditional and not so traditional, has not been fully explored. It has not been fully explored for two major reasons. First, the majority of thinking is still metals, or isotropic, in nature. A culture based on the availability of directional dependency and elastic

couplings does not yet exist. Second, analysis of structures and materials with nonisotropic behavior and the wide variety of elastic couplings available with composite materials has not matured. For sure it is possible to use numerical methods such as finite-elements and obtain numbers for a particular problem, or a series of problems. However, such an approach provides no insight as to what characteristics of composites materials are important and may provide benefits to a particular class of problems. Solving simple problems in the context of the more complex behavior of composite materials can lead to insight into how certain characteristics of the responses of composite materials influence the behavior of structures. This latter approach to understanding the behavior, and hence understanding the full potential of fiber-reinforced composite materials, is one of the purposes of this thesis. Specifically, this thesis examines the response of cylinders fabricated with fiber-reinforced materials, the cylinders being presumably filament wound from a graphite/polymer, and the winding sequence being completely general, in particular, unsymmetric. Herein the term 'unsymmetric' will be used as the commonly accepted description of a composite laminate that does not exhibit elastic symmetry with respect to its geometric midplane. It is well known that due to the elevated temperatures associated with the processing of polymer matrix

composites, an unsymmetric laminating sequence in a flat laminate can cause severe warpage of the laminate as it cools to a lower service temperature [1, 2]. An unsymmetrically laminated cylinder, on the other hand, will remain cylindrical when cooled from the elevated processing temperature. Thus, unsymmetrically laminated cylinders offer a real possibility of exploiting the advantages of unsymmetric laminates, if there are indeed any advantages. Clearly what may be considered an advantage depends on the application. Hence, understanding and cataloging the response of unsymmetrically laminated cylinders is an important first step, before specific applications are investigated. Some work has been done in this regard but only for one very special case. [3]

Here the response of an unsymmetrically laminated cylinder to an axial compressive load, a torsional load, and due to the temperature change associated with cooling from the processing temperature to the service temperature are investigated. These problems are all considered axisymmetric, and the response will be studied in the context of linear elastic material behavior and geometrically linear kinematics. Clearly these studies are the precursor to studies aimed at investigating the potential for utilizing unsymmetrically laminated construction for delaying the collapse of cylinders due to either an axial load, a torsional load, or both. Such

problems are geometrically nonlinear problems and can only be studied after completely understanding the linear counterparts. The thermal problem is important because there may be thermally induced warpage of the cylinder near its ends. Such warpage would influence the pre-collapse response in the nonlinear analysis. The second purpose of the work described here, then, is to develop and solve the equations which govern the behavior of unsymmetrically laminated cylinders subjected to axial compression, torsion, and a temperature change, and translate the solutions into software so numerical results for specific examples can be easily obtained and studied.

The next chapter introduces the basic nomenclature relevant to fiber-reinforced composites as it pertains to the present class of problems. Emphasis is on the constitutive behavior of the material. The third chapter develops the equations assumed to govern the behavior of the cylinders, namely, Sanders' kinematic approximations [4] in conjunction with the constitutive behavior and the first variation in the total potential energy. [5] The variation formulation is preferred over the Newtonian approach because boundary conditions associated with the kinematics of the problem are developed as part of the variational process. The proper boundary conditions are not as easily formulated when using the Newtonian approach.

The fourth chapter briefly outlines the computer

programs written to implement the closed-form solution of the governing equations for the various cases studied. The fifth chapter presents numerical results for the three loading cases, namely compression, torsion, and a temperature change. The responses of several laminates are studied, one laminate being more unorthodox than the others. The unorthodox laminate is studied to explore the full range of responses that can be exhibited with composite materials. Two laminates felt to be viable alternatives to current conventional designs are also studied. These laminates are compared to what could be considered a conventional counterpart. Concluding remarks and recommendations for future research are discussed in Chapter 6.

Chapter 2 - Some Basic Definitions Associated with Fiber-Reinforced Composite Materials

A single layer of a fiber reinforced composite material is referred to as a lamina. The lamina coordinate system, illustrated in fig. 1, defines the x axis in the fiber direction, the y axis perpendicular to the fibers and in the plane of the lamina, and the z axis perpendicular to the plane of the lamina. For an anisotropic material Hooke's Law can be defined as

$$\begin{bmatrix} \sigma_x \\ \sigma_y \\ \sigma_z \\ \tau_{yz} \\ \tau_{xz} \\ \tau_{xy} \end{bmatrix} = \begin{bmatrix} C_{11} & C_{12} & C_{13} & C_{14} & C_{15} & C_{16} \\ C_{12} & C_{22} & C_{23} & C_{24} & C_{25} & C_{26} \\ C_{13} & C_{23} & C_{33} & C_{34} & C_{35} & C_{36} \\ C_{14} & C_{24} & C_{34} & C_{44} & C_{45} & C_{46} \\ C_{15} & C_{25} & C_{35} & C_{45} & C_{55} & C_{56} \\ C_{16} & C_{26} & C_{36} & C_{46} & C_{56} & C_{66} \end{bmatrix} \begin{bmatrix} \epsilon_x \\ \epsilon_y \\ \epsilon_z \\ \epsilon_{yz} \\ \epsilon_{xz} \\ \epsilon_{xy} \end{bmatrix} \quad (1)$$

This results in 21 independent elastic constants, C_{ij}, being required to describe the material. The C matrix is called the stiffness matrix. By considering materials which exhibit some degree of symmetry, the number of independent elastic constants is reduced. For example, particular to the study here, an orthotropic material has only 9 independent constants. Hooke's law then takes the

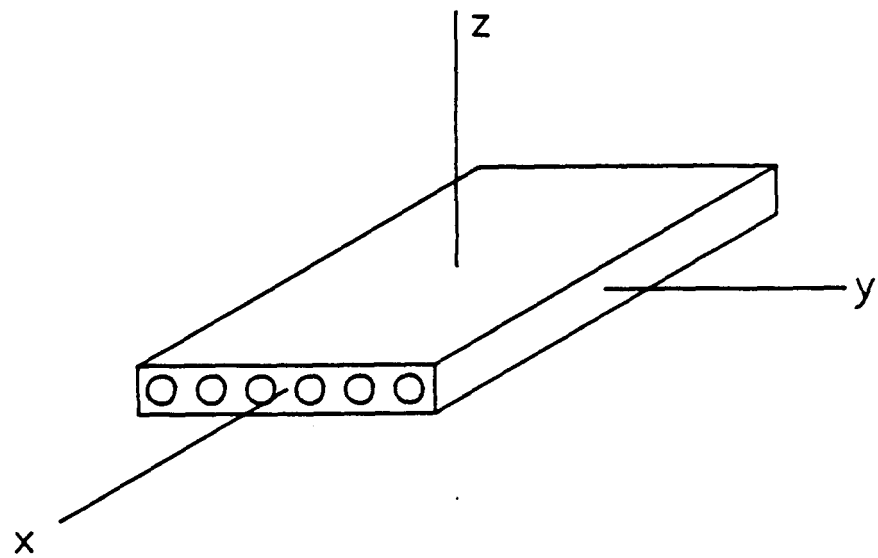

FIGURE 1 LAMINA COORDINATE SYSTEM

form

$$\begin{bmatrix} \sigma_x \\ \sigma_y \\ \sigma_z \\ \tau_{yz} \\ \tau_{xz} \\ \tau_{xy} \end{bmatrix} = \begin{bmatrix} C_{11} & C_{12} & C_{13} & 0 & 0 & 0 \\ C_{12} & C_{22} & C_{23} & 0 & 0 & 0 \\ C_{13} & C_{23} & C_{33} & 0 & 0 & 0 \\ 0 & 0 & 0 & C_{44} & 0 & 0 \\ 0 & 0 & 0 & 0 & C_{55} & 0 \\ 0 & 0 & 0 & 0 & 0 & C_{66} \end{bmatrix} \begin{bmatrix} \epsilon_x \\ \epsilon_y \\ \epsilon_z \\ \epsilon_{yz} \\ \epsilon_{xz} \\ \epsilon_{xy} \end{bmatrix} \quad (2)$$

The stiffness matrix can be written in terms of the engineering material properties, namely Young's moduli, Poisson's ratios, and shear moduli.

For the plane stress state, $\sigma_z = \tau_{xz} = \tau_{yz} = 0$, and the 6 x 6 matrix can be reduced to a 3 x 3 matrix. For this situation Hooke's Law for an orthotropic material becomes [6]

$$\begin{bmatrix} \sigma_x \\ \sigma_y \\ \tau_{xy} \end{bmatrix} = \begin{bmatrix} Q_{xx} & Q_{xy} & 0 \\ Q_{yx} & Q_{yy} & 0 \\ 0 & 0 & Q_{ss} \end{bmatrix} \begin{bmatrix} \epsilon_x \\ \epsilon_y \\ \epsilon_{xy} \end{bmatrix}. \quad (3)$$

The Q matrix is called the reduced stiffness matrix and is defined as

$$Q_{xx} = \frac{E_x}{1 - \mu_x \mu_y} \tag{4}$$

$$Q_{xy} = \frac{\mu_x E_y}{1 - \mu_x \mu_y} \tag{5}$$

$$Q_{yx} = Q_{xy} \tag{6}$$

$$Q_{yy} = \frac{E_y}{1 - \mu_x \mu_y} \tag{7}$$

$$Q_{ss} = E_s \tag{8}$$

$$\mu_y = \mu_x \left(\frac{E_y}{E_x} \right) \quad , \tag{9}$$

where E_x and E_y are Young's moduli in the x and y directions, respectively; μ_x and μ_y are Poisson's ratios when the material is loaded in the x and y directions, respectively; and E_s is the shear modulus of the material. The reduced stiffness matrix can obviously be related to the C_{ij}. Here it is more convenient to use the engineering properties directly.

When several laminae are bonded together they form a laminate. Each lamina of the laminate can have a unique

fiber angle relative to a global, structural, or laminate coordinate system. For example, a cylinder may have one layer wound helically at 45° to the cylinder axis, another layer wound at -45° to the cylinder axis, and yet a third layer with fibers parallel with the axis. Since any analysis is usually conducted in the global system, the reduced stiffness matrix for each lamina must be transformed from the lamina coordinate system to the global or laminate coordinate system. The global coordinate system is denoted as the 1-2 system and the transformation is shown in fig. 2. This transformation results in what is called the transformed reduced stiffness matrix. Thus, for the plane stress case, referred to the laminate coordinate system, Hooke's Law becomes

$$\begin{bmatrix} \sigma_1 \\ \sigma_2 \\ \tau_{12} \end{bmatrix} = \begin{bmatrix} Q_{11} & Q_{12} & Q_{16} \\ Q_{21} & Q_{22} & Q_{26} \\ Q_{61} & Q_{62} & Q_{66} \end{bmatrix} \begin{bmatrix} \epsilon_1 \\ \epsilon_2 \\ \epsilon_{12} \end{bmatrix} , \qquad (10)$$

with the Q matrix defined as

$$Q_{11} = Q_{xx}m^4 + 2(Q_{xy} + Q_{ss})\, m^2n^2 + Q_{yy}n^4 , \qquad (11)$$

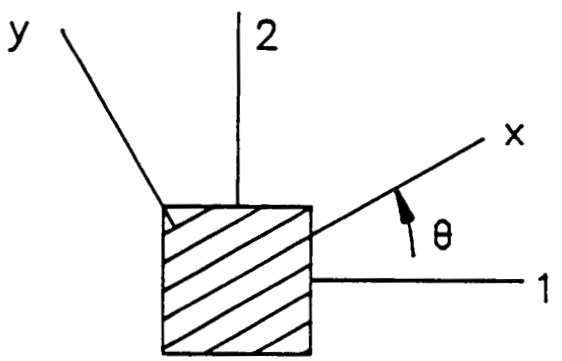

FIGURE 2 LAMINA (x–y) AND LAMINATE (1–2) COORDINATE SYSTEMS

$$Q_{12} = Q_{21} = (Q_{xx} + Q_{yy} - 4Q_{ss})\, m^2 n^2 + Q_{xy}(n^4 + m^4) \quad , \tag{12}$$

$$Q_{16} = Q_{61} = (Q_{xx} - Q_{xy} - 2Q_{ss})\, n\, m^3 + (Q_{xy} - Q_{yy} + 2Q_{ss})\, n^3\, m \quad , \tag{13}$$

$$Q_{22} = Q_{xx} n^4 + 2(Q_{xy} + 2Q_{ss})\, n^2\, m^2 + Q_{yy} m^4 \quad , \tag{14}$$

$$Q_{26} = Q_{62} = (Q_{xx} - Q_{xy} - 2Q_{ss})\, n\, m^3 + (Q_{xy} - Q_{yy} - 2Q_{ss})\, n\, m^3 \quad , \tag{15}$$

$$Q_{66} = (Q_{xx} + Q_{yy} - 2Q_{xy} - 2Q_{ss})\, n^2\, m^2 + Q_{ss}(m^4 + n^4) \quad , \tag{16}$$

where $m = \cos\theta$ and $n = \sin\theta$, θ being defined in fig. 2. The subscripts 1 and 2 on the stresses and strains in eq. 10 indicate these quantities are referred to the 1-2 coordinate system.

Assuming the Kirchhoff hypothesis is valid for a laminate, [5,6] the strains, ϵ_1, ϵ_2, ϵ_{12}, of eq. 10 can be written in terms of the laminates's midplane extensional strains, ϵ°_1, ϵ°_2, ϵ°_{12}, and the midplane curvatures, k°_1, k°_2, k°_{12}, as

$$\epsilon_1 = \epsilon^\circ_1 + z\, k^\circ_1 \tag{17}$$

$$\epsilon_2 = \epsilon^\circ_2 + z\, k^\circ_2 \tag{18}$$

$$\epsilon_{12} = \epsilon^\circ_{12} + z\, k^\circ_{12} \,. \tag{19}$$

The stress resultants for a laminate can be defined as

$$N_1 \equiv \int_{z=-t/2}^{t/2} \sigma_1 \, dz \tag{20}$$

$$M_1 \equiv \int_{z=-t/2}^{t/2} z\, \sigma_1 \, dz \tag{21}$$

$$N_2 \equiv \int_{z=-t/2}^{t/2} \sigma_2 \, dz \tag{22}$$

$$M_2 \equiv \int_{z=-t/2}^{t/2} z\, \sigma_2 \, dz \tag{23}$$

$$N_{12} \equiv \int_{z=-t/2}^{t/2} \tau_{12}\, dz \tag{24}$$

$$M_{12} \equiv \int_{z=-t/2}^{t/2} z\, \tau_{12}\, dz, \tag{25}$$

where t is the thickness of the laminate and it is implied that the z = 0 location is at the laminate geometric midplane. The N's are the force resultants and the M's are the moment resultants.

Since the midplane strains and curvatures are not functions of z, substitution of eq. 10 into eq. 20 results in

$$\begin{aligned} N_1 = {} & \epsilon_1^\circ \int_{-t/2}^{t/2} Q_{11}\, dz + \epsilon_2^\circ \int_{-t/2}^{t/2} Q_{12}\, dz \\ & + \epsilon_{12}^\circ \int_{-t/2}^{t/2} Q_{16}\, dz + k_1^\circ \int_{-t/2}^{t/2} z\, Q_{11} dz \\ & + k_2^\circ \int_{-t/2}^{t/2} z\, Q_{12}\, dz + k_{12}^\circ \int_{-t/2}^{t/2} z\, Q_{12} dz. \end{aligned} \tag{26}$$

Because fiber angles can vary from layer to layer, the Q's do vary with z but are piecewise constant with z. The integrals become sums, the sums being defined as

$$A_{11} = \int_{-t/2}^{t/2} Q_{11}\, dz$$

$$= \sum_{k=1}^{N_{layer}} Q_{11_k}(z_k - z_{k-1}) \qquad (27)$$

$$A_{12} = \int_{-t/2}^{t/2} Q_{12}\, dz$$

$$= \sum_{k=1}^{N_{layer}} Q_{12_k}(z_k - z_{k-1}) \qquad (28)$$

$$A_{16} = \int_{-t/2}^{t/2} Q_{16}\, dz$$

$$= \sum_{k=1}^{N_{layer}} Q_{16_k}(z_k - z_{k-1}) \quad , \qquad (29)$$

where z_k is the z location of the interface between the k^{th} and the $(k-1)^{th}$ layers, and $z_0 = -t/2$ and $z_n = +t/2$.

Similar relations can be derived from eqs. 22 and 24 to produce a 3 x 3 A matrix. The A matrix is called the laminate inplane stiffness matrix and an abbreviated form can be written as

$$A_{ij} = \sum_{k=1}^{N_{layer}} Q_{ij_k} (z_k - z_{k-1}) \qquad i,j = 1,2,6 \ . \tag{30}$$

The integrals multiplying the curvatures are defined in abbreviated form as

$$B_{ij} = \int_{-t/2}^{t/2} z \ Q_{ij} \, dz$$

$$= \sum_{k=1}^{N_{layer}} Q_{ij_k} \left(\frac{z_k^2 - z_{k-1}^2}{2}\right) \qquad i,j = 1,2,6 \ . \tag{31}$$

Considering eqs. 20, 22, and 24, the B_{ij} defines another 3 x 3 matrix. The B matrix is called the laminate bending/stretching stiffness matrix.

The results so far lead to a relation of the form

$$\begin{bmatrix} N_1 \\ N_2 \\ N_{12} \end{bmatrix} = \begin{bmatrix} A_{11} & A_{12} & A_{16} \\ A_{12} & A_{22} & A_{26} \\ A_{16} & A_{26} & A_{66} \end{bmatrix} \begin{bmatrix} \epsilon_1^\circ \\ \epsilon_2^\circ \\ \epsilon_{12}^\circ \end{bmatrix}$$

$$+ \quad \begin{bmatrix} B_{11} & B_{12} & B_{16} \\ B_{12} & B_{22} & B_{26} \\ B_{16} & B_{26} & B_{66} \end{bmatrix} \quad \begin{bmatrix} k_1^\circ \\ k_2^\circ \\ k_{12}^\circ \end{bmatrix} \tag{32}$$

More will be said regarding the B matrix shortly.

The moment equations, eqs. 21, 23, 25, can be defined similarly. For example, substituting eq. 10 into eq. 21 results in

$$M_1 = \epsilon_1^\circ \int_{-t/2}^{t/2} z\, Q_{11}\, dz + \epsilon_2^\circ \int_{-t/2}^{t/2} z\, Q_{12}\, dz$$

$$+ \epsilon_{12}^\circ \int_{-t/2}^{t/2} z\, Q_{16}\, dz + k_1^\circ \int_{-t/2}^{t/2} z^2\, Q_{11} dz$$

$$+ k_2^\circ \int_{-t/2}^{t/2} z^2\, Q_{12}\, dz + k_{12}^\circ \int_{-t/2}^{t/2} z^2\, Q_{12} dz \,. \tag{33}$$

Defining

$$D_{ij} = \int_{-t/2}^{t/2} z^2\, Q_{ij}\, dz \qquad i,j = 1,2,6 \,, \tag{34}$$

since the Q's are piecewise constant with z, the integral

becomes a sum, namely

$$D_{ij} = \sum_{k=1}^{N_{layer}} Q_{ij_k} \left(\frac{z_k^3 - z_{k-1}^3}{3} \right) \quad i,j = 1,2,6 \; . \tag{35}$$

Considering also eqs. 23 and 25, the D_{ij} forms a third 3 x 3 matrix. This matrix is referred to as the laminate bending stiffness matrix.

Arrangement of the six stress resultants into matrix form leads to the load-midplane deformation relationship

$$\begin{bmatrix} N_1 \\ N_2 \\ N_{12} \\ M_1 \\ M_2 \\ M_{12} \end{bmatrix} = \left[\begin{array}{ccc|ccc} A_{11} & A_{12} & A_{16} & B_{11} & B_{12} & B_{16} \\ A_{12} & A_{22} & A_{26} & B_{12} & B_{22} & B_{26} \\ A_{16} & A_{26} & A_{66} & B_{16} & B_{26} & B_{66} \\ \hline B_{11} & B_{12} & B_{16} & D_{11} & D_{12} & D_{16} \\ B_{12} & B_{22} & B_{26} & D_{12} & D_{22} & D_{26} \\ B_{16} & B_{26} & B_{66} & D_{16} & D_{26} & D_{66} \end{array}\right] \begin{bmatrix} \epsilon_1^\circ \\ \epsilon_2^\circ \\ \epsilon_{12}^\circ \\ k_1^\circ \\ k_2^\circ \\ k_{12}^\circ \end{bmatrix} . \tag{36}$$

The 6 x 6 matrix of eq. 36 is called the laminate stiffness matrix, or the ABD matrix. When viewed in the context of eq. 36, it is clear that composites exhibit elastic couplings simply not present with isotropic

materials. The existence of the elements of the B matrix implies that force resultants (N_1, N_2, N_{12}) and curvatures are coupled, and moment resultants (M_1, M_2, M_{12}) and extensioned strains are coupled. Because of the D_{16} and D_{26} terms, bending moment resultants (M_1, M_2) cause twist curvatures (k_{12}°) and twisting moment resultants (M_{12}) cause bending curvatures (k_1°, k_2°). This is a very powerful characteristic of fiber-reinforced materials. For specific fiber orientations, some of the elements of the ABD matrix are zero. For a symmetric laminate B is identically zero. Furthermore, if for every layer with fiber angle θ there is an identical layer with fiber angle $-\theta$, the laminate is said to be balanced and A_{16} and A_{26} are zero. (See fig. 2.) Finally, if each layer has a fiber angle of 0° or 90°, $D_{16} = D_{26} = 0$. While the analysis of composite structures is simpler if these elements of the ABD matrix are zero, it is not clear there is any structural advantage to having these zero. It is the specific intent of this thesis to investigate the ramifications of them not being zero.

Writing out eq. 36,

$$N_1 = A_{11}\,\epsilon_1^\circ + A_{12}\,\epsilon_2^\circ + A_{16}\,\epsilon_{12}^\circ + B_{11}\,k_1^\circ + B_{12}\,k_2^\circ + B_{16}\,k_{12}^\circ \qquad (37)$$

$$N_2 = A_{12}\,\epsilon_1^\circ + A_{22}\,\epsilon_2^\circ + A_{26}\,\epsilon_{12}^\circ + B_{12}\,k_1^\circ + B_{22}\,k_2^\circ + B_{26}\,k_{12}^\circ \quad (38)$$

$$N_{12} = A_{16}\,\epsilon_1^\circ + A_{26}\,\epsilon_2^\circ + A_{66}\,\epsilon_{12}^\circ + B_{16}\,k_1^\circ + B_{26}\,k_2^\circ + B_{66}\,k_{12}^\circ \quad (39)$$

$$M_1 = B_{11}\,\epsilon_1^\circ + B_{12}\,\epsilon_2^\circ + B_{16}\,\epsilon_{12}^\circ + D_{11}\,k_1^\circ + D_{12}\,k_2^\circ + D_{16}\,k_{12}^\circ \quad (40)$$

$$M_2 = B_{12}\,\epsilon_1^\circ + B_{22}\,\epsilon_2^\circ + B_{26}\,\epsilon_{12}^\circ + D_{12}\,k_1^\circ + D_{22}\,k_2^\circ + D_{26}\,k_{12}^\circ \quad (41)$$

$$M_{12} = B_{16}\,\epsilon_1^\circ + B_{26}\,\epsilon_2^\circ + B_{66}\,\epsilon_{12}^\circ + D_{16}\,k_1^\circ + D_{26}\,k_2^\circ + D_{66}\,k_{12}^\circ . \quad (42)$$

Thermal Expansion Effects

Thermal expansion effects of the fiber-reinforced

material can be included by returning to Hooke's Law. With thermal expansion effects Hooke's Law becomes

$$\begin{bmatrix} \sigma_1 \\ \sigma_2 \\ \tau_{12} \end{bmatrix} = \begin{bmatrix} Q_{11} & Q_{12} & Q_{16} \\ Q_{12} & Q_{22} & Q_{26} \\ Q_{16} & Q_{26} & Q_{66} \end{bmatrix} \begin{bmatrix} \epsilon_1 - \alpha_1 \Delta T \\ \epsilon_2 - \alpha_2 \Delta T \\ \epsilon_{12} - \alpha_{12} \Delta T \end{bmatrix} , \qquad (43)$$

where α_1, α_2, and α_{12} are the lamina coefficients of thermal expansion as measured in the global 1-2 coordinate system. The quantities α_1, α_2, and α_3 are defined as

$$\alpha_1 = \alpha_x m^2 + \alpha_y n^2 \qquad (44)$$

$$\alpha_2 = \alpha_x n^2 + \alpha_y m^2 \qquad (45)$$

$$\alpha_{12} = 2 m n (\alpha_x - \alpha_y) , \qquad (46)$$

where α_x is the lamina coefficient of thermal expansion in the fiber direction, and α_y is the lamina coefficient of thermal expansion perpendicular to the fibers in the plane of the lamina.

Using the definitions of force and moment resultants, eqs. 20-25, and substituting for σ_1, σ_2, and τ_{12} from eq. 43, each force and moment resultant can be calculated to

include thermal expansion effects. The integrals which led to the ABD matrix are not affected by the inclusion of the thermal effects. However, the thermal effects do lead to additional integrals. With thermal effects, for example,

$$N_1 = A_{11}\ \epsilon_1^\circ + A_{12}\ \epsilon_2^\circ + A_{16}^\circ\ \epsilon_{12}$$

$$+ B_{11}\ k_1^\circ + B_{12}\ k_2^\circ + B_{16}\ k_{12}^\circ$$

$$- \Delta T \int_{-t/2}^{t/2} (Q_{11}\ \alpha_1 + Q_{12}\ \alpha_2 + Q_{16}\ \alpha_{12})\ dz\ . \tag{47}$$

Since it has the proper units, the integral is interpreted as an equivalent thermal inplane load, N_1^T, i.e.,

$$N_1^T = \Delta T \int_{-t/2}^{t/2} (Q_{11}\ \alpha_1 + Q_{12}\ \alpha_2 + Q_{16}\ \alpha_{12})\ dz\ . \tag{48}$$

Since the Q's and α's are piecewise constant with z, the integrals can be replaced by summations, namely,

$$N_1^T = \sum_{k=1}^{N_{layer}} (Q_{11_k}\ \alpha_{1_k} + Q_{12_k}\ \alpha_{2_k} + Q_{16_k}\ \alpha_{12_k})$$

$$(z_k - z_{k-1}) \Delta T \quad . \qquad (49)$$

Considering N_2, N_{12}, M_1, M_2, M_{12} results in similar definitions of thermally-induced loads, namely,

$$N_2^T = \sum_{k=1}^{N_{layer}} (Q_{12_k} \alpha_{1_k} + Q_{22_k} \alpha_{2_k} + Q_{26_k} \alpha_{12_k})$$

$$(z_k - z_{k-1}) \Delta T \quad , \qquad (50)$$

$$N_{12}^T = \sum_{k=1}^{N_{layer}} (Q_{16_k} \alpha_{1_k} + Q_{26_k} \alpha_{2_k} + Q_{66_k} \alpha_{12_k})$$

$$(z_k - z_{k-1}) \Delta T \quad , \qquad (51)$$

$$M_1^T = \sum_{k=1}^{N_{layer}} (Q_{11_k} \alpha_{1_k} + Q_{12_k} \alpha_{2_k} + Q_{16_k} \alpha_{12_k})$$

$$(\frac{z_k^2 - z_{k-1}^2}{2}) \Delta T \quad , \qquad (52)$$

$$M_2^T = \sum_{k=1}^{N_{layer}} (Q_{12_k} \alpha_{1_k} + Q_{22_k} \alpha_{2_k} + Q_{26_k} \alpha_{12_k})$$

$$\left(\frac{z_k^* - z_{k-1}^*}{2}\right) \Delta T \quad , \tag{53}$$

$$M_{12}^T = \sum_{k=1}^{N_{layer}} \left(Q_{16_k} \alpha_{1_k} + Q_{26_k} \alpha_{2_k} + Q_{66_k} \alpha_{12_k}\right)$$

$$\left(\frac{z_k^* - z_{k-1}^*}{2}\right) \Delta T \ . \tag{54}$$

The latter three are thermally-induced moments.

With the above developments, the final form from the stress resultants, including the thermal effects, is

$$N_1 = A_{11} \epsilon_1^\circ + A_{12} \epsilon_2^\circ + A_{16} \epsilon_{12}^\circ + B_{11} k_1^\circ + B_{12} k_2^\circ + B_{16} k_{12}^\circ - N_1^T \tag{55}$$

$$N_2 = A_{12} \epsilon_1^\circ + A_{22} \epsilon_2^\circ + A_{26} \epsilon_{12}^\circ + B_{12} k_1^\circ + B_{22} k_2^\circ + B_{26} k_{12}^\circ - N_2^T \tag{56}$$

$$N_{12} = A_{16} \epsilon_1^\circ + A_{26} \epsilon_2^\circ + A_{66} \epsilon_{12}^\circ$$

$$+ B_{16} k_1^\bullet + B_{26} k_2^\bullet + B_{66} k_{12}^\bullet - N_{12}^T \tag{57}$$

$$M_1 = B_{11} \epsilon_1^\bullet + B_{12} \epsilon_2^\bullet + B_{16} \epsilon_{12}^\bullet$$

$$+ D_{11} k_1^\bullet + D_{12} k_2^\bullet + D_{16} k_{12}^\bullet - M_1^T \tag{58}$$

$$M_2 = B_{12} \epsilon_1^\bullet + B_{22} \epsilon_2^\bullet + B_{26} \epsilon_{12}^\bullet$$

$$+ D_{12} k_1^\bullet + D_{22} k_2^\bullet + D_{26} k_{12}^\bullet - M_2^T \tag{59}$$

$$M_{12} = B_{16} \epsilon_1^\bullet + B_{26} \epsilon_2^\bullet + B_{66} \epsilon_{12}^\bullet$$

$$+ D_{16} k_1^\bullet + D_{26} k_2^\bullet + D_{66} k_{12}^\bullet - M_{12}^T. \tag{60}$$

The definition of the ABD matrix and the inclusion of thermal effects are important ingredients for the next step, namely, the development of a structural level theory for cylinder behavior. A quick review of this chapter indicates that all that has been done is to define thickness-integrated properties. These relations developed shift emphasis to the laminate midplane, yet nothing has

been said as to how the N's, M's, ϵ's, or k's vary from point to point on the midplane, say, with distance along the cylinder. This is done in the next chapter.

Chapter 3 - Sanders' Shell Theory: Axisymmetric Problem

3.1 The Variational Statement

To derive the equations governing the deformation of a cylindrical shell, the variational method in combination with the total potential energy is used. The total potential energy of a three dimensional solid is [5]

$$\Gamma = U - \int\int\int_V B_i u_i \, dV - \int\int_{S_1} T_i^{(v)} u_i dS, \tag{61}$$

where U is the strain energy of the solid and the other terms are due to the applied loads. Since this study will not involve applied loads, but rather displacement boundary conditions,

$$\int\int\int_V B_i u_i \, dV - \int\int_{S_1} T_i^{(v)} u_i \, dS = 0 \tag{62}$$

and so

$$\Gamma = U \tag{63}$$

With this, the first variation of the total potential

energy reduces to

$$\delta\Gamma = \delta U = \int\int\int_V (\sigma_x \delta\epsilon_x + \sigma_\theta \delta\epsilon_\theta + \sigma_r \delta\epsilon_r + \tau_{\theta r} \delta\epsilon_{\theta r} + \tau_{xr} \delta\epsilon_{xr} + \tau_{x\theta} \delta\epsilon_{x\theta}) \, dV. \tag{64}$$

This expression will be applied to cylinders. Figure 3 illustrates the coordinate system used to describe a cylinder with a mean radius R and a length L. The cylinder thickness will be denoted as t, and, as in the last chapter, t represents the thickness of the laminate which constitutes the cylinder wall. The subscripts x, θ, and r on the stresses and strains in eq. 64 indicate that these quantities are referred to the global cylindrical coordinate system.

3.2 Kinematic Assumptions

To use the variational statement of eq. 64, the strain field must be defined. Since the strains are related to the displacements, it is the displacement fields that must be defined. For the axisymmetric case, the axial displacement, u(x,z), and the radial displacement, w(x,z), of an arbitrary point A are illustrated in fig. 4 and are

FIGURE 3 THE CYLINDER COORDINATE SYSTEM

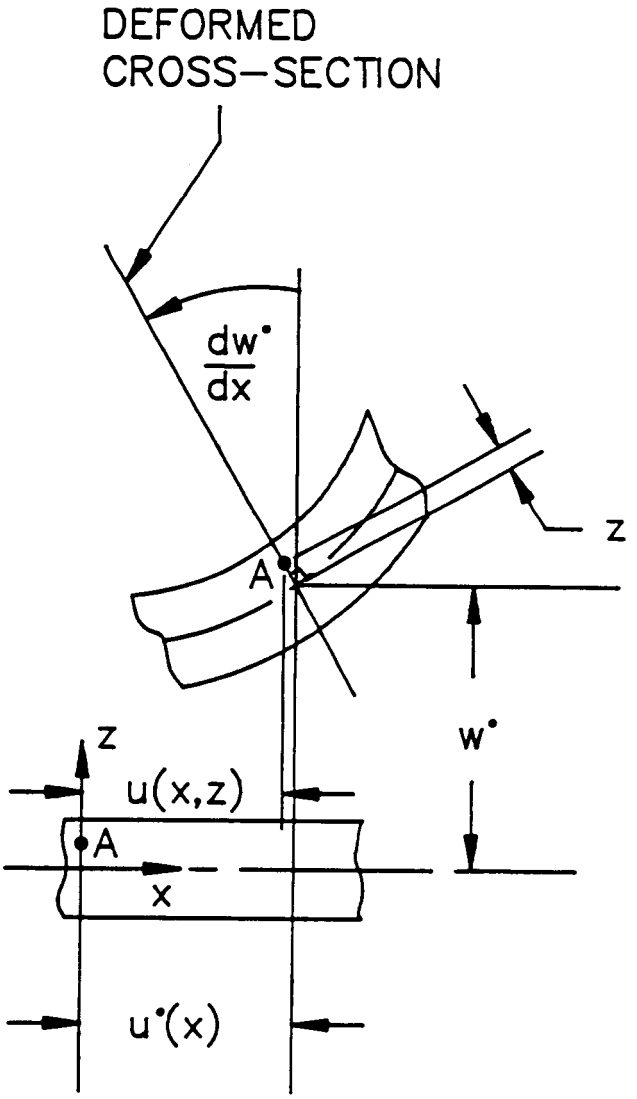

FIGURE 4 THE AXIAL AND RADIAL DISPLACEMENTS OF CYLINDER

equal to

$$u(x,z) = u^{\circ}(x) - z \frac{dw^{\circ}(x)}{dx} \tag{65}$$

$$w(x,z) = w^{\circ}(x), \tag{66}$$

where the superscript $^{\circ}$ refers to the displacements of the cylinder reference surface which is located at the mean radius. The distance z is measured from the reference surface, i.e., $z = 0$ is the geometric midsurface of the cylinder wall. The circumferential displacement, $v(x,z)$, of an arbitrary point A is illustrated in fig. 5 and it is found to be

$$v(x,z) = \left(1 + \frac{z}{R}\right) v^{\circ}(x). \tag{67}$$

This form of v, as opposed to

$$v(x,z) = v^{\circ}(x) \quad , \tag{68}$$

is referred to as the Sander's kinematic assumption [4], while the latter is attributed to Donnell [7]. With Sander's kinematic assumption, the validity of the Kirchhoff hypothesis is implied. Note: The three problems of compression, torsion, and temperature change are assumed to be axisymmetric and so the displacements are not

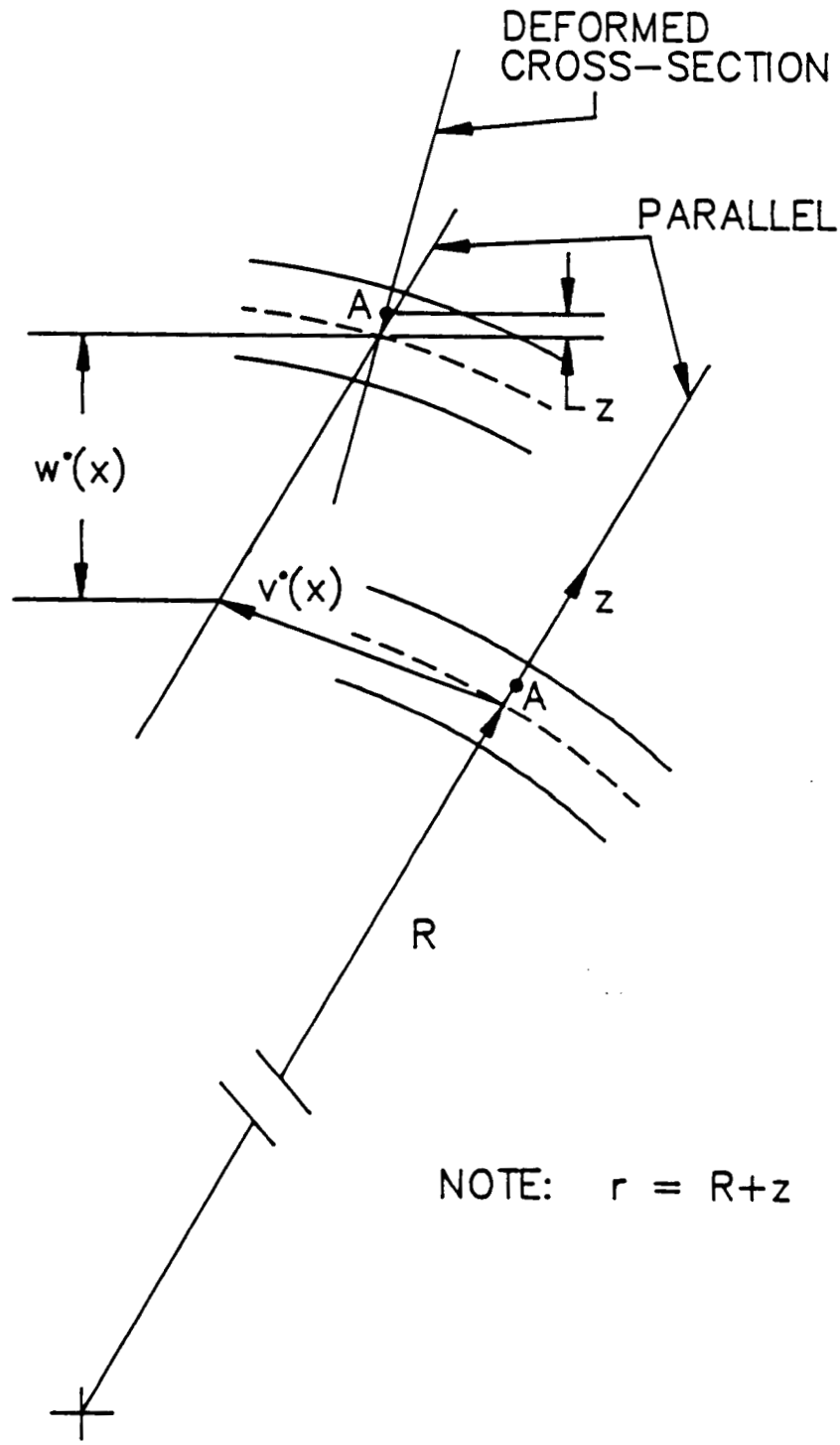

FIGURE 5 KINEMATICS OF CIRCUMFERENTIAL DISPLACEMENTS OF CYLINDER

functions of θ. Furthermore, the stresses, strains, and the stress resultants are assumed to be independent of θ and so derivatives with respect to θ will be set equal to zero.

Knowing the displacements, the strain field can now be defined using the strain-displacement relations.

3.3 The Strain Field

The strain-displacement relations in polar coordinates for the axisymmetric case are as follows [8]:

$$\epsilon_x(x,r) = \frac{\partial u(x,r)}{\partial x} \tag{69}$$

$$\epsilon_\theta(x,r) = \frac{w(x,r)}{r} \tag{70}$$

$$\epsilon_r(x,r) = \frac{\partial w(x,r)}{\partial r} \tag{71}$$

$$\epsilon_{\theta r}(x,r) = \frac{-v(x,r)}{r} + \frac{\partial v(x,r)}{\partial r} \tag{72}$$

$$\epsilon_{xr}(x,r) = \frac{\partial u(x,r)}{\partial r} + \frac{\partial w(x,r)}{\partial x} \tag{73}$$

$$\epsilon_{x\theta}(x,r) = \frac{\partial v(x,r)}{\partial x} \quad . \tag{74}$$

Substituting the displacements of eqs. 65-67 into the strain-displacement equations, eqs. 69-74, leads to

$$\epsilon_x(x,z) = \frac{du^\circ(x)}{dx} - z\,\frac{d^2w^\circ(x)}{dx^2} \tag{75}$$

$$\epsilon_\theta(x,z) = \frac{w^\circ(x)}{R} \tag{76}$$

$$\epsilon_r(x,z) = \frac{dw^\circ(x)}{dz} = 0 \tag{77}$$

$$\epsilon_{\theta r}(x,z) = 0 \tag{78}$$

$$\epsilon_{xr}(x,z) = 0 \tag{79}$$

$$\epsilon_{x\theta}(x,z) = \frac{dv^\circ(x)}{dx} + \frac{z}{R}\,\frac{dv^\circ(x)}{dx} \tag{80}$$

where in the above equations it has been assumed that the shell is thin so

$$r = R + z = R\,(1 + \frac{z}{R}) \approx R \tag{81}$$

and use has been made of the fact that

$$dr = dz. \tag{82}$$

In addition, the functional dependence on r has been switched to the functional dependence on z. As can be seen, three of the six strains are zero, the nonzero ones being $\epsilon_x(x,z)$, $\epsilon_\theta(x,z)$, and $\epsilon_{x\theta}(x,z)$. Therefore, the variational statement, eq. 64, simplifies to

$$\delta\Gamma = \int_V (\sigma_x \delta\epsilon_x + \sigma_\theta \delta\epsilon_\theta + \tau_{x\theta} \delta\epsilon_{x\theta}) dV. \tag{83}$$

3.4 The Euler Equations and Boundary Conditions

Substitution of eqs. 75, 76, and 80 into the simplified variational statement, eq. 83, leads to the governing equations and boundary conditions. The quantity dV in polar coordinates is approximated for thin shells as follows:

$$dV = r\, d\theta\, dr\, dx \tag{84}$$

$$dV = (R + z)\, d\theta\, dz\, dx \tag{85}$$

$$dV = R(1 + z/R)\, d\theta\, dz\, dx \approx R\, d\theta\, dz\, dx. \tag{86}$$

Using eqs. 84-86 and eqs. 75-80, the variational statement

of eq. 83 becomes

$$\delta\Gamma = \int_{x=-L/2}^{L/2} \int_{\theta=0}^{2\pi} \int_{z=-t/2}^{t/2} \left[\sigma_x \, \delta\left(\frac{du^*(x)}{dx} - z \, \frac{d^2w^*}{dx^2} \right) + \sigma_\theta \, \delta\left(\frac{w^*}{R} \right) + \tau_{x\theta} \, \delta\left(\frac{dv^*}{dx} + \frac{z \, dv^*}{R \, dx} \right) \right] dz \, Rd\theta \, dx, \tag{87}$$

where the limits on the integral define the volume of the cylinder, and the points x = 0 and z = 0 are located at the mean radius midway along the cylinder length. Integration with respect to z can be done independently and in doing so the following stress resultants are defined:

$$N_x \equiv \int_{z=-t/2}^{t/2} \sigma_x \, dz \tag{88}$$

$$M_x \equiv \int_{z=-t/2}^{t/2} z \, \sigma_x \, dz \tag{89}$$

$$N_\theta \equiv \int_{z=-t/2}^{t/2} \sigma_\theta \, dz \tag{90}$$

$$N_{x\theta} \equiv \int_{z=-t/2}^{t/2} \tau_{x\theta}\, dz \tag{91}$$

$$M_{x\theta} \equiv \int_{z=-t/2}^{t/2} z\, \tau_{x\theta}\, dz. \tag{92}$$

With the integration on θ and substitution of eqs. 88-92, the variational statement of eq. 87 becomes

$$\delta\Gamma = 2\pi R \int_{x=-L/2}^{L/2} [\, N_x\, \delta\left(\frac{du^\circ}{dx}\right) - M_x\, \delta\left(\frac{d^2w^\circ}{dx^2}\right)$$

$$+ \frac{N_\theta}{R}\, \delta w^\circ + N_{x\theta}\, \delta\left(\frac{dv^\circ}{dx}\right)$$

$$+ \frac{M_{x\theta}}{R}\, \delta\left(\frac{dv^\circ}{dx}\right)]\, dx. \tag{93}$$

Integration by parts leads to

$$\delta\Gamma = 2\pi R \left[\left(N_x\, \delta u^\circ \right) \Big|_{-L/2}^{L/2} - \right.$$

$$\left. \left(M_x\, \delta \left(\frac{dw^\circ}{dx} \right) \right) \Big|_{-L/2}^{L/2} \right.$$

$$+ \left(\frac{dM_x}{dx} \delta w^\circ \right)\Big|_{-L/2}^{L/2} + \left(N_{x\theta} \delta v^\circ \right)\Big|_{-L/2}^{L/2}$$

$$+ \left(\frac{M_{x\theta}}{R} \delta v^\circ \right)\Big|_{-L/2}^{L/2}$$

$$+ \int_{x=-L/2}^{L/2} \left[\left(\frac{-dN_x}{dx} \right) \delta u^\circ + \left(\frac{-dN_{x\theta}}{dx} - \frac{d}{dx} \left(\frac{M_{x\theta}}{R} \right) \right) \delta v^\circ \right.$$

$$\left. + \left(\frac{-d^2M_x}{dx^2} + \frac{N_\theta}{R} \right) \delta w^\circ \right] dx \quad . \qquad (94)$$

Of course the first variation must be zero and so eq. 94 reveals the Euler equations and the associated boundary conditions for the problem. The Euler equations are:

$$\frac{dN_x}{dx} = 0, \qquad (95)$$

$$\frac{d}{dx} \left(N_{x\theta} + \frac{M_{x\theta}}{R} \right) = 0, \qquad (96)$$

$$\frac{d^2M_x}{dx^2} - \frac{N_\theta}{R} = 0, \qquad (97)$$

while the boundary conditions are:

$$\text{either } N_x = 0 \quad \text{or} \quad u^\circ \text{ specified} \tag{98}$$

$$\text{either } M_x = 0 \quad \text{or} \quad \frac{dw^\circ}{dx} \text{ specified} \tag{99}$$

$$\text{either } \frac{dM_x}{dx} = 0 \quad \text{or} \quad w^\circ \text{ specified} \tag{100}$$

$$\text{either } \left(N_{x\theta} + \frac{M_{x\theta}}{R} \right) = 0 \quad \text{or} \quad v^\circ \text{ specified.} \tag{101}$$

It should be noted that the quantities $N_{x\theta}$ and $M_{x\theta}/R$ always appear summed. This quantity will be referred to as $\overline{N_{x\theta}}$, i.e.,

$$\overline{N_{x\theta}} = N_{x\theta} + \frac{M_{x\theta}}{R} , \tag{102}$$

and is interpreted to mean that the Sanders' theory does not use either $N_{x\theta}$ or $M_{x\theta}$ separately. Donnell's theory, on the other hand, makes no mention of $M_{x\theta}$. Obviously $M_{x\theta}/R$ is a result of the z/R term in eq. 67.

3.5 Solving the Euler Equations

Referring to eqs. 17-19 and 75-80, and using the

notation of Ch. 2 by letting the subscripts 1 = x and 2 = θ, for the cylinder problem

$$\epsilon_x^\circ = \frac{du^\circ}{dx} \tag{103}$$

$$\epsilon_\theta^\circ = \frac{w^\circ}{R} \tag{104}$$

$$\epsilon_{x\theta}^\circ = \frac{dv^\circ}{dx} \tag{105}$$

$$k_x^\circ = -\frac{d^2w^\circ}{dx^2} \tag{106}$$

$$k_\theta^\circ = 0 \tag{107}$$

$$k_{x\theta}^\circ = \frac{1}{R}\frac{dv^\circ}{dx} \tag{108}$$

Rewriting eq. 36 for the x-θ coordinate frame, substituting eqs. 103-108 into eq. 36, and writing out each stress resultant with the equivalent thermal loads included leads to the expressions for the stress resultants pertinent to axisymmetric cylinder problems. These stress resultants are:

$$N_x = A_{11}\frac{du^\circ}{dx} + A_{12}\frac{w^\circ}{R} + \left(A_{16} + \frac{1}{R}B_{16}\right)\frac{dv^\circ}{dx}$$

$$- B_{11} \frac{d^2 w^\circ}{dx^2} - N_x^T \quad , \tag{109}$$

$$N_\theta = A_{12} \frac{du^\circ}{dx} + A_{22} \frac{w^\circ}{R} + (A_{26} + \frac{1}{R} B_{26}) \frac{dv^\circ}{dx}$$

$$- B_{12} \frac{d^2 w^\circ}{dx^2} - N_\theta^T \quad , \tag{110}$$

$$\overline{N_{x\theta}} = (A_{16} + \frac{B_{16}}{R}) \frac{du^\circ}{dx}$$

$$+ (A_{26} + \frac{B_{26}}{R}) \frac{w^\circ}{R} + (A_{66} + \frac{2 B_{66}}{R} + \frac{D_{66}}{R^2}) \frac{dv^\circ}{dx}$$

$$- (B_{16} + \frac{D_{16}}{R}) \frac{d^2 w^\circ}{dx^2} - \overline{N}_{x\theta}^T \quad , \tag{111}$$

$$M_x = B_{11} \frac{du^\circ}{dx} + B_{12} \frac{w^\circ}{R} + (B_{16} + \frac{1}{R} D_{16}) \frac{dv^\circ}{dx}$$

$$- D_{11} \frac{d^2 w^\circ}{dx^2} - M_x^T \quad , \tag{112}$$

$$M_\theta = B_{12} \frac{du^\circ}{dx} + B_{22} \frac{w^\circ}{R} + (B_{26} + \frac{1}{R} D_{26}) \frac{dv^\circ}{dx}$$

$$- D_{12} \frac{d^2 w^\circ}{dx^2} - M_\theta^T \quad , \tag{113}$$

where

$$\bar{N}^{T}_{x\theta} = N^{T}_{x\theta} + \frac{M^{T}_{x\theta}}{R} \quad . \tag{114}$$

Using eqs. 109-114, the Euler equations, eqs. 95-97 become

$$A_{11} \frac{d^2u^\circ}{dx^2} + (A_{16} + B_{16}) \frac{d^2v^\circ}{dx^2} + \frac{1}{R} A_{12} \frac{dw^\circ}{dx} - B_{11} \frac{d^3w^\circ}{dx^3} = 0 , \tag{115}$$

$$(A_{16} + \frac{1}{R} B_{16}) \frac{d^2u^\circ}{dx^2} + (A_{66} + \frac{2}{R} B_{66} + \frac{1}{R^2} D_{66}) \frac{d^2v^\circ}{dx^2} + (A_{26} + \frac{1}{R} B_{26}) \frac{1}{R} \frac{dw^\circ}{dx} - (B_{16} + \frac{1}{R} D_{16}) \frac{d^3w^\circ}{dx^3} = 0 , \tag{116}$$

$$B_{11} \frac{d^3u^\circ}{dx^3} - \frac{1}{R} A_{12} \frac{du^\circ}{dx} + (B_{16} + \frac{1}{R} D_{16}) \frac{d^3v^\circ}{dx^3}$$

$$- \frac{1}{R}\left(A_{26} + \frac{1}{R} B_{26}\right) \frac{dv^\circ}{dx} - D_{11} \frac{d^4 w^\circ}{dx^4}$$

$$+ \frac{2}{R} B_{12} \frac{d^2 w^\circ}{dx^2} - \frac{1}{R^2} A_{22} w^\circ + \frac{1}{R} N_\theta^T$$

$$= 0 \quad , \qquad (117)$$

Before proceeding, some of the influences of elastic couplings should be discussed in the context of the stress resultants, eqs. 109-113, and the governing equations, eqs. 115-117. For a symmetric laminate the B_{ij} are equal to zero and the stress resultants equations become

$$N_x = A_{11} \frac{du^\circ}{dx} + A_{12} \frac{w^\circ}{R} + A_{16} \frac{dv^\circ}{dx}$$

$$- N_x^T \quad , \qquad (109a)$$

$$N_\theta = A_{12} \frac{du^\circ}{dx} + A_{22} \frac{w^\circ}{R} + A_{26} \frac{dv^\circ}{dx}$$

$$- N_\theta^T \quad , \qquad (110a)$$

$$\overline{N_{x\theta}} = A_{16} \frac{du^\circ}{dx} + A_{26} \frac{w^\circ}{R}$$

$$+ \left(A_{66} + \frac{D_{66}}{R^2} \right) \frac{dv^\circ}{dx}$$

$$- \frac{D_{16}}{R} \frac{d^2w^\circ}{dx^2} - N_{x\theta}^T , \qquad (111a)$$

$$M_x = \frac{1}{R} D_{16} \frac{dv^\circ}{dx} - D_{11} \frac{d^2w^\circ}{dx^2} \qquad (112a)$$

$$M_\theta = \frac{1}{R} D_{26} \frac{dv^\circ}{dx} - D_{12} \frac{d^2w^\circ}{dx^2} \qquad (113a)$$

The differential equations become

$$A_{11} \frac{d^2u^\circ}{dx^2} + A_{16} \frac{d^2v^\circ}{dx^2} + \frac{1}{R} A_{12} \frac{dw^\circ}{dx}$$

$$= 0 , \qquad (115a)$$

$$A_{16} \frac{d^2u^\circ}{dx^2} + \left(A_{66} + \frac{1}{R^2} D_{66}\right) \frac{d^2v^\circ}{dx^2} +$$

$$A_{26} \frac{1}{R} \frac{dw^\circ}{dx} - \frac{1}{R} D_{16} \frac{d^3w^\circ}{dx^3}$$

$$= 0 , \qquad (116a)$$

$$- \frac{1}{R} A_{12} \frac{du^\circ}{dx} + \frac{1}{R} D_{16} \frac{d^3 v^\circ}{dx^3}$$

$$- \frac{1}{R} A_{26} \frac{dv^\circ}{dx} - D_{11} \frac{d^4 w^\circ}{dx^4}$$

$$- \frac{1}{R^2} A_{22} w^\circ + \frac{1}{R} N_\theta^T$$

$$= 0 , \qquad (117a)$$

Comparing eqs. 109-113 with eqs. 109a-113a, it is seen that with an unsymmetric laminate the curvature of the radial displacement in the axial direction, i.e., d^2w°/dx^2, contributes to the axial and circumferential force resultants through B_{11} and B_{12}, respectively. For symmetric laminates the radial displacement influences the axial and the circumferential force resultants only through the A_{12} and A_{22}, respectively. These A terms are related to Poisson effects. Similarly, B_{11} and B_{12} cause the axial displacement gradient, du°/dx, to influence the axial moment resultant, M_x, and the circumferential moment resultant, M_θ, respectively. For symmetric laminates the axial displacement gradient has absolutely no influence on the moment resultants. It is interesting to note that even for a symmetric laminate, the circumferential displacement

gradient, dv°/dx, influences the axial and the circumferential force resultants through A_{16} and A_{26} respectively, the shear force resultants through A_{66} and D_{66} respectively, and the moment resultants through D_{16} and D_{26}.

For a balanced symmetric laminate, $A_{16} = A_{26} = 0$ and the stress resultants become

$$N_x = A_{11} \frac{du^{\circ}}{dx} + A_{12} \frac{w^{\circ}}{R} - N_x^T , \qquad (109b)$$

$$N_\theta = A_{12} \frac{du^{\circ}}{dx} + A_{22} \frac{w^{\circ}}{R} - N_\theta^T , \qquad (110b)$$

$$\overline{N_{x\theta}} = \left(A_{66} + \frac{D_{66}}{R^2} \right) \frac{dv^{\circ}}{dx} - \frac{D_{16}}{R} \frac{d^2w^{\circ}}{dx^2} \qquad (111b)$$

$$M_x = \frac{1}{R} D_{16} \frac{dv^{\circ}}{dx} - D_{11} \frac{d^2w^{\circ}}{dx^2} \qquad (112b)$$

$$M_\theta = \frac{1}{R} D_{26} \frac{dv^{\circ}}{dx} - D_{12} \frac{d^2w^{\circ}}{dx^2} \qquad (113b)$$

While the governing equations become

$$A_{11} \frac{d^2u^\circ}{dx^2} + \frac{1}{R} A_{12} \frac{dw^\circ}{dx}$$

$$= 0 , \qquad (115b)$$

$$(A_{66} + \frac{1}{R^2} D_{66}) \frac{d^2v^\circ}{dx^2}$$

$$- \frac{1}{R} D_{16} \frac{d^3w^\circ}{dx^3} = 0 , \qquad (116b)$$

$$- \frac{1}{R} A_{12} \frac{du^\circ}{dx} + \frac{1}{R} D_{16} \frac{d^3v^\circ}{dx^3}$$

$$- \frac{1}{R^2} A_{22} w^\circ - D_{11} \frac{d^4w^\circ}{dx^4}$$

$$+ \frac{1}{R} N_\theta^T = 0 , \qquad (117b)$$

The axial and circumferential force resultants do not depend on the circumferential displacement gradient, dv°/dx, and the shear force resultant does not depend on the axial displacement gradient, du°/dx. For an orthotropic laminate and metal, $D_{16} = D_{26} = 0$, and there is further decoupling of displacements and stress resultants.

In general, the meaning of these couplings is quite profound. However, for the cylinder the presence of the

couplings just discussed mean that in an unbalanced and/or an unsymmetric laminate, twisting causes axial forces (see eq. 109) and radial growth or bulging (see eq. 111), and axial compression causes twisting (see eq. 109) and radial growth beyond the normal Poisson effect (see eq. 109).

3.6 Solution of the Governing Equations

Equations 115-117 constitute a system of ordinary linear differential equations with constant coefficients. There is a homogeneous and a particular solution. The solution to the homogeneous portion of these equations is assumed to be of the form:

$$u^{\circ}(x) = U\, e^{s\,x} \quad ; \quad v^{\circ}(x) = V\, e^{s\,x} \quad ;$$

$$w^{\circ}(x) = W\, e^{s\,x} \quad . \qquad (118)$$

Substituting these assumed forms into eqs. 115-117 results in

$$\left[A_{11}\, s^2 \right] U + \left[\left(A_{16} + \frac{1}{R} B_{16}\right) s^2 \right] V$$

$$+ \left[\frac{1}{R} A_{12} s - B_{11} s^3 \right] W = 0 , \qquad (119)$$

$$\left[\left(A_{16} + \frac{1}{R} B_{16} \right) s^2 \right] U$$

$$+ \left[\left(A_{66} + \frac{2}{R} B_{66} + \frac{1}{R^2} D_{66} \right) s^2 \right] V$$

$$+ \left[\left(A_{26} + \frac{1}{R} B_{26} \right) \frac{1}{R} s - \left(B_{16} + \frac{1}{R} D_{16} \right) s^3 \right] W$$

$$= 0 , \qquad (120)$$

$$\left[\frac{1}{R} A_{12} s - B_{11} s^3 \right] U$$

$$+ \left[\left(A_{26} + \frac{1}{R} B_{26} \right) \frac{1}{R} s - \left(B_{16} + \frac{1}{R} D_{16} \right) s^3 \right] V$$

$$+ \left[D_{11} s^4 + \frac{1}{R^2} A_{22} - \frac{2}{R} B_{12} s^2 \right] W$$

$$= 0 . \qquad (121)$$

Writing eqs. 119-121 in matrix form and introducing the matrix T_{ij}, leads to

$$\begin{bmatrix} T_{11} & T_{12} & T_{13} \\ T_{12} & T_{22} & T_{23} \\ T_{13} & T_{23} & T_{33} \end{bmatrix} \begin{bmatrix} U \\ V \\ W \end{bmatrix} = \begin{bmatrix} 0 \\ 0 \\ 0 \end{bmatrix} , \qquad (122)$$

where

$$T_{11} = A_{11} s^2 \qquad (123)$$

$$T_{12} = (A_{16} + \frac{1}{R} B_{16}) s^2 \qquad (124)$$

$$T_{13} = \frac{1}{R} A_{12} s - B_{11} s^3 \qquad (125)$$

$$T_{22} = (A_{66} + \frac{2}{R} B_{66} + \frac{1}{R^2} D_{66}) s^2 \qquad (126)$$

$$T_{23} = (A_{26} + \frac{1}{R} B_{26}) \frac{1}{R} s - (B_{16} + \frac{1}{R} D_{16}) s^3 \qquad (127)$$

$$T_{33} = D_{11} s^4 + \frac{1}{R^2} A_{22} - \frac{2}{R} B_{12} s^2 \qquad (128)$$

Equation 122 is a standard eigenvalue problem and the eigenvalues, s_i, are found by setting the determinant of

the T matrix equal to zero and solving for the s's. The determinant is of the form

$$| T | = C_8 s^8 + C_6 s^6 + C_4 s^4 = 0 . \qquad (129)$$

The quantities, C_8, C_6, and C_4, of eq. 129 are constants and are equal to

$$C_8 = 2 A_{11} B_{66} \frac{D_{11}}{R} - 2 A_{16} B_{16} \frac{D_{11}}{R}$$

$$- 2 A_{11} B_{16} \frac{D_{16}}{R} + 2 A_{16} B_{11} \frac{D_{16}}{R}$$

$$- 2 B_{11}^2 \frac{B_{66}}{R} + 2 B_{11} \frac{B_{16}^2}{R}$$

$$+ A_{11} D_{66} \frac{D_{11}}{R^2} - B_{16}^2 \frac{D_{11}}{R^2}$$

$$- B_{11}^2 \frac{D_{66}}{R^2} - A_{11} \frac{D_{16}^2}{R^2}$$

$$+ 2 B_{11} B_{16} \frac{D_{16}}{R^2} + A_{11} A_{66} D_{11}$$

$$- A_{16}^2 D_{11} - A_{11} B_{16}^2 + 2 A_{16} B_{11} B_{16}$$

$$- A_{66} B_{11}^2 \qquad (130)$$

$$C_6 = 2 A_{16}^2 \frac{B_{12}}{R} - 2 A_{12} B_{16} \frac{D_{16}}{R^3}$$

$$+ 2 A_{12} A_{66} \frac{B_{11}}{R} - 2 A_{16} A_{26} \frac{B_{11}}{R}$$

$$+ 2 A_{11} A_{26} \frac{D_{16}}{R^2} - 2 A_{12} A_{16} \frac{D_{16}}{R^2}$$

$$- 2 B_{11} B_{16} \frac{B_{26}}{R^3} + 4 A_{16} B_{12} \frac{B_{16}}{R^2}$$

$$+ 2 B_{12} \frac{B_{16}^2}{R^3} - 2 A_{12} \frac{B_{16}^2}{R^2}$$

$$- 2 A_{26} B_{11} \frac{B_{16}}{R^2} - 2 A_{11} B_{12} \frac{D_{66}}{R^3}$$

$$+ 2 A_{12} B_{11} \frac{D_{66}}{R^3} + 2 A_{11} B_{26} \frac{D_{16}}{R^3}$$

$$- \quad 4 \; A_{11} \; B_{12} \; \frac{B_{66}}{R^2} \quad + \quad 4 \; A_{12} \; B_{11} \; \frac{B_{66}}{R^2}$$

$$+ \quad 2 \; A_{11} \; B_{16} \; \frac{B_{26}}{R^2} \quad - \quad 2 \; A_{16} \; B_{11} \; \frac{B_{26}}{R^2}$$

$$+ \quad 2 \; A_{11} \; A_{26} \; \frac{B_{16}}{R} \quad - \quad 2 \; A_{12} \; A_{16} \; \frac{B_{16}}{R}$$

$$- \quad 2 \; A_{11} \; A_{66} \; \frac{B_{12}}{R} \qquad (131)$$

$$C_4 = A_{11} \; A_{22} \; \frac{A_{66}}{R^2} \quad - \quad A_{12}^2 \; \frac{A_{66}}{R^2}$$

$$- \quad A_{11} \; \frac{A_{26}^2}{R^2} \quad + \quad 2 \; A_{12} \; A_{16} \; \frac{A_{26}}{R^2}$$

$$- \quad A_{16}^2 \; \frac{A_{22}}{R^2} \quad - \quad 2 \; A_{12}^2 \; \frac{B_{66}}{R^3}$$

$$+ \quad 2 \; A_{11} \; A_{22} \; \frac{B_{66}}{R^3} \quad - \quad A_{12}^2 \; \frac{D_{66}}{R^4}$$

$$+ \quad A_{11} \; A_{22} \; \frac{D_{66}}{R^4} \quad - \quad 2 \; A_{11} \; A_{26} \; \frac{B_{26}}{R^3}$$

$$+ \quad 2 \; A_{12} \; A_{16} \; \frac{B_{26}}{R^4} \quad + \quad 2 \; A_{12} \; A_{26} \; \frac{B_{16}}{R^3}$$

$$+ \quad 2 \; A_{12} \; B_{16} \; \frac{B_{26}}{R^3} \quad - \quad 2 \; A_{16} \; A_{22} \; \frac{B_{16}}{R^3}$$

$$- \quad A_{11} \; \frac{B_{26}^2}{R^4} \quad - \quad A_{22} \; \frac{B_{16}^2}{R^4} \qquad (132)$$

Solving eq. 129 for s results in eight eigenvalues. Four eigenvalues are repeated zeros and the other four are given by

$$s_1, s_2, s_3, s_4 = \pm \left(\frac{- C_6 \pm \sqrt{C_6^2 - 4 \; C_8 \; C_4}}{2 \; C_8} \right)^{\frac{1}{2}} . \qquad (133)$$

The associated eigenvectors are defined by Φ and ϕ. Here

$$U_i = \Phi_i \; W_i \qquad (134)$$

$$V_i = \phi_i \; W_i \qquad (135)$$

i = 1,2,3,4, corresponding to the four nonzero roots, s_i.

To find the proper form for the repeated zero root

solutions, assume the following displacements:

$$u^{\circ}(x) = U_5 + U_6 x + U_7 x^2 + U_8 x^3 \quad (136)$$

$$v^{\circ}(x) = V_5 + V_6 x + V_7 x^2 + V_8 x^3 \quad (137)$$

$$w^{\circ}(x) = W_5 + W_6 x + W_7 x^2 + W_8 x^3 . \quad (138)$$

Equations 136-138 and their derivatives are substituted into equations 115-117. After matching terms with like powers of x, it is found that some of the constants in eqs. 136-138 are zero and what remains is

$$u^{\circ}(x) = U_5 + U_6 x \quad (139)$$

$$v^{\circ}(x) = V_5 + V_6 x \quad (140)$$

$$w^{\circ}(x) = W_5 . \quad (141)$$

Substitution of eqs. 139-141 into eq. 117 reveals a relationship between W_5, U_6, and V_6 such that

$$W_5 = \left(-\frac{A_{12}\,R}{A_{22}}\right) U_6 + \frac{(-A_{26} - B_{26})R}{A_{22}} V_6 , \tag{142}$$

or

$$W_5 = \alpha\, U_6 + \beta\, V_6 , \tag{143}$$

where

$$\alpha = \left(-\frac{A_{12}\,R}{A_{22}}\right) \tag{144}$$

$$\beta = \frac{(-A_{26} - B_{26})R}{A_{22}} \tag{145}$$

By inspection, the particular solution to the system of differential equations is

$$u_p^{\bullet} = 0 = v_p^{\bullet} \tag{146}$$

$$w_p^{\bullet} = \frac{R}{A_{22}}\, N_{\theta}^{T} , \tag{147}$$

with the subscript p denoting the particular solution. Collecting the various portions of the solutions leads to the following expressions for the displacements:

$$u^{\circ}(x) = \phi_1 W_1 e^{s_1 x} + \phi_2 W_2 e^{s_2 x}$$

$$+ \phi_3 W_3 e^{s_3 x} + \phi_4 W_4 e^{s_4 x}$$

$$+ U_5 + U_6 x \; ; \qquad (148)$$

$$v^{\circ}(x) = \Phi_1 W_1 e^{s_1 x} + \Phi_2 W_2 e^{s_2 x}$$

$$+ \Phi_3 W_3 e^{s_3 x} + \Phi_4 W_4 e^{s_4 x}$$

$$+ V_5 + V_6 x \; ; \qquad (149)$$

$$w^{\circ}(x) = W_1 e^{s_1 x} + W_2 e^{s_2 x} + W_3 e^{s_3 x}$$

$$+ W_4 e^{s_4 x} + \alpha U_6 + \beta V_6$$

$$+ \frac{R}{A_{22}} N_{\theta}^{T} \; . \qquad (150)$$

As it turns out, the eigenvalues, s_i, and assorted eigenvectors, Φ_i and ϕ_i, in eqs. 148-150 are complex. This

complicates the algebra. Since the displacements are real, the complex nature can be eliminated by algebraic manipulation. In particular, the four nonzero eigenvalues are of the form

$$s_2 = a_2 + i\,b_2 \quad ; \quad s_1 = \bar{s}_2 = a_2 - i\,b_2$$

$$s_4 = -a_2 - i\,b_2 \quad ; \quad s_3 = \bar{s}_4 = -a_2 + i\,b_2 \tag{151}$$

The associated eigenvectors are of the form

$$\Phi_i = (\pm g_2 \pm i\,f_2) \quad \text{and} \quad \phi_i = (\pm j_2 \pm i\,k_2)\,. \tag{152}$$

The nonsubscript i being $\sqrt{-1}$, not an index. Expanding,

$$\Phi_2 = (g_2 + i\,f_2) \quad ; \quad \Phi_1 = \overline{\Phi_2} = (g_2 - i\,f_2)$$

$$\Phi_4 = (-g_2 - i\,f_2) \quad ; \quad \Phi_3 = \overline{\Phi_4} = (-g_2 + i\,f_2)$$

$$\phi_2 = (j_2 + i\,k_2) \quad ; \quad \phi_1 = \overline{\phi_2} = (j_2 - i\,k_2)$$

$$\phi_4 = (-j_2 - i\,k_2) \quad ; \quad \phi_3 = \overline{\phi_4} = (-j_2 + i\,k_2) \tag{153}$$

The W_i constants assume the form

$$W_2 = c_2 + i\, d_2 \quad ; \quad W_1 = c_1 + i\, d_1$$

$$W_4 = c_4 + i\, d_4 \quad ; \quad W_3 = c_3 + i\, d_3 \tag{154}$$

Starting with the equation for the displacement $w^*(x)$, eq. 150, the above eigenvalue and eigenvector definitions are substituted. The displacement $w^*(x)$ then assumes the form

$$\begin{aligned} w^*(x) = {} & (c_1 + i\, d_1)\, e^{(a_2 - i\, b_2)\, x} \\ & + (c_2 + i\, d_2)\, e^{(a_2 + i\, b_2)\, x} \\ & + (c_3 + i\, d_3)\, e^{(-a_2 + i\, b_2)\, x} \\ & + (c_4 + i\, d_4)\, e^{(-a_2 - i\, b_2)\, x} \\ & + \alpha\, U_6 + \beta\, V_6 + \frac{R}{A_{22}}\, N_\theta^T \,. \end{aligned} \tag{155}$$

Note that α and β are real. The real and imaginary parts

of the exponential terms are separated as follows:

$$e^{(x + i\,y)} = e^{x} (\cos y + i \sin y) , \qquad (156)$$

$$e^{\pm a_2 x} = \cosh a_2 x \pm \sinh a_2 x , \qquad (157)$$

and these are substituted into eq. 155. Since w° is real, the imaginary part of the right hand side of eq. 155 must equal zero, therefore,

$$c_2 = c_1 ; \quad c_3 = c_4 ; \quad d_1 = -d_2 ; \quad d_3 = -d_4 . \qquad (158)$$

Substitution and regrouping of this information into odd and even functions of x reveals

$$\left.\begin{aligned} w^{\circ}(x) = {} & 2 (c_2 + c_4) \cos b_2 x \cosh a_2 x \\ & - 2 (d_2 + d_4) \sin b_2 x \sinh a_2 x \\ & + \alpha U_6 + \beta V_6 + \frac{R}{A_{22}} N_{\Theta}^{T} \end{aligned}\right\} \text{even}$$

$$\text{odd} \left\{ \begin{array}{l} + \; 2 \; (\; c_2 \; - \; c_4 \;) \; \cos \; b_2 x \;\; \sinh \; a_2 x \\ \\ + \; 2 \; (\; d_4 \; - \; d_2 \;) \; \sin \; b_2 x \;\; \cosh \; a_2 x \end{array} \right. \quad . \qquad (159)$$

Separation into odd and even functions of x was done because the axial compression, torsion, and temperature change problems all lead to responses that are characterized by $w^{\circ}(x)$ being an even function of x. Therefore, the odd part of $w^{\circ}(x)$ must be zero. For this to be true

$$c_2 = c_4 \quad ; \quad d_2 = d_4 \; . \qquad (160)$$

Hence, the $w^{\circ}(x)$ displacement equation reduces to

$$w^{\circ}(x) = 2 \; C \cos \; b_2 x \;\; \cosh \; a_2 x$$

$$- \; 2 \; D \sin \; b_2 x \;\; \sinh \; a_2 x \; + \; \alpha \; U_6$$

$$+ \; \beta \; V_6 \; + \; \frac{R}{A_{22}} \;\; N_{\theta}^{T} \; . \qquad (161)$$

where

$$C = c_2 + c_4$$

$$D = d_2 + d_4 \ . \qquad (162)$$

Expressions for u*(x) and v*(x) can be derived similarly using the information found from the w*(x) equation, particularly eqs. 158, 160, and 162. These displacements are found to be

$$u^*(x) = 2C (g_2 \cos b_2 x \sinh a_2 x -$$

$$f_2 \sin b_2 x \cosh a_2 x)$$

$$- 2D (f_2 \cos b_2 x \sinh a_2 x +$$

$$g_2 \sin b_2 x \cosh a_2 x) + U_6 x \ ; \qquad (163)$$

and

$$v^*(x) = 2C (j_2 \cos b_2 x \sinh a_2 x -$$

$$k_2 \sin b_2 x \cosh a_2 x)$$

$$- 2D (k_2 \cos b_2 x \sinh a_2 x +$$

$$j_2 \sin b_2 x \cosh a_2 x) + V_6 x \quad . \qquad (164)$$

By choosing $w^\circ(x)$ to be even in x, $u^\circ(x)$ and $v^\circ(x)$ are odd in x. This was expected. The above solutions for $u^\circ(x)$, $v^\circ(x)$, and $w^\circ(x)$ are valid for any axisymmetric response that is characterized by $w^\circ(x)$ being an even function of x. The boundary conditions for each of the three problems lead to specific solutions based on the above general forms. In the next three sections the boundary conditions for the three cases considered here are presented.

3.7 The Boundary Conditions for Compression

Two sets of variationally consistent boundary conditions for axial compression of the cylinder will be considered. The first set of boundary conditions is

$$u^\circ (L/2) = -0.5 t \quad ; \qquad (165)$$

$$v^\circ (L/2) = 0 \quad ; \qquad (166)$$

$$w^\circ (L/2) = 0 \quad ; \qquad (167)$$

$$\frac{dw^\circ (L/2)}{dx} = 0 \quad . \qquad (168)$$

The second set of boundary conditions is

$$u^{\circ}\left(L/2 \right) = -0.5\, t \quad ; \tag{169}$$

$$\left(N_{x\theta}\left(L/2 \right) + \frac{M_{x\theta}\left(L/2 \right)}{R} \right) = 0 \quad ; \tag{170}$$

$$w^{\circ}\left(L/2 \right) = 0 \quad ; \tag{171}$$

$$\frac{dw^{\circ}\left(L/2 \right)}{dx} = 0 \quad . \tag{172}$$

It is important to note that only the conditions at one end of the cylinder are considered. By the symmetry conditions on $u^{\circ}(x)$, $v^{\circ}(x)$, and $w^{\circ}(x)$, conditions on the other end are automatically specified.

The first set of conditions corresponds to a cylinder that is restrained on each end against circumferential displacement, radial displacement, and rotation in the x direction. The ends of the cylinder are compressed toward each other with a displacement equal to a laminate thickness, t. The second set of conditions corresponds to a cylinder that is free to move circumferentially at each end but is restrained against radial displacements and rotation in the x direction. The ends of the cylinder are again compressed toward each other. This compression

condition is considered for the case where temperature effects are ignored and so $N_\theta^T = 0$ in eq. 117. Herein the above two sets of boundary conditions for compression will be referred to as boundary condition 1 and boundary condition 2, respectively. They will be abbreviated bc 1 and bc 2. These two sets of boundary conditions are used in conjunction with eqs. 161-164 to solve for the four unknowns, C, D, U_6, and V_6. After values for the unknowns are found, values of the displacements and force and moment resultants along the cylinder can be calculated.

3.8 The Boundary Conditions for Torsion

Two sets of variationally consistent boundary conditions for twisting the cylinder are considered. The first set is

$$u^\circ (L/2) = 0 \quad ; \tag{173}$$

$$v^\circ (L/2) = 0.5\ t \ ; \tag{174}$$

$$w^\circ (L/2) = 0 \quad ; \tag{175}$$

$$\frac{dw^\circ (L/2)}{dx} = 0 \quad . \tag{176}$$

The second set of boundary conditions is

$$N_x (L/2) = 0 \quad ; \tag{177}$$

$$v^{\circ} (L/2) = 0.5 \, t \quad ; \tag{178}$$

$$w^{\circ} (L/2) = 0 \quad ; \tag{179}$$

$$\frac{dw^{\circ} (L/2)}{dx} = 0 \quad . \tag{180}$$

The first set of boundary conditions correspond to the case of a cylinder with its ends restrained against axial displacement, radial displacement, and rotation in the axial direction, and with a circumferential displacement of one end of the cylinder relative to the other equal to one laminate thickness. The second set is similar to the first except that the cylinder is free to expand or contract in the axial direction. These conditions are denoted as bc 1 and bc 2. Here also the twisting is considered independent of temperature effects and so $N_{\theta}{}^{T} = 0$. Similar to compression, these two sets of boundary conditions are used to solve for the four unknowns C, D, U_6, V_6 and then to calculate the values of the displacements and force and moment resultants along the cylinder.

3.9 The Boundary Conditions for Thermal Expansion

There is only one set of boundary conditions that correspond to the case of free thermal expansion of the cylinder. They correspond to the ends of the cylinder being completely free of any applied loads. These are given by the variationally consistent boundary conditions

$$N_x(L/2) = 0 \quad ; \tag{181}$$

$$M_x(L/2) = 0 \quad ; \tag{182}$$

$$\frac{dM_x(L/2)}{dx} = 0 \quad ; \tag{183}$$

$$\overline{N_{x\theta}}(L/2) = 0 \quad . \tag{184}$$

Substituting the expressions for the displacements eqs. 161-164 into the force and moment resultant expressions, eqs. 109, 111, and 112; and substituting these results into the above equations leads to four equations from which to solve for the four unknowns, C, D, U_6, and V_6.

The next chapter outlines the three FORTRAN programs used to solve for the four unknowns, C, D, U_6, and V_6.

Chapter 4 - Creation of the Software

The preceding analyses were implemented into three FORTRAN computer programs, one for each of the three types of loading conditions. All three programs have the same logic, only the boundary conditions and some input information are different. Figure 6 illustrates a simplified flowchart of the programming logic. The programs were written for minimal user input but with as much generality as possible. Therefore, only the cylinder geometry, which includes the length and mean radius, and the material properties, which include Young's moduli in the x and y directions, shear modulus, Poisson's ratio, the thickness of each layer of the material, the number of layers, and the orientation of the fibers of each layer, are input. For thermal expansion, the two coefficients of thermal expansion, α_x and α_y, and the change in temperature are also input. After input, the reduced and transformed reduced stiffness matrices are calculated. The calculation of the transformed reduced stiffness matrix enables the ABD matrix to be calculated. The input and calculated values are then written to a data file. Numerical values for C_8, C_6, and C_4 of eqs. 130-132 are calculated using the above information. With numerical values for these variables, the roots or eigenvalues are found by solving eq. 133. From the eigenvalues, the eigenvectors are found directly

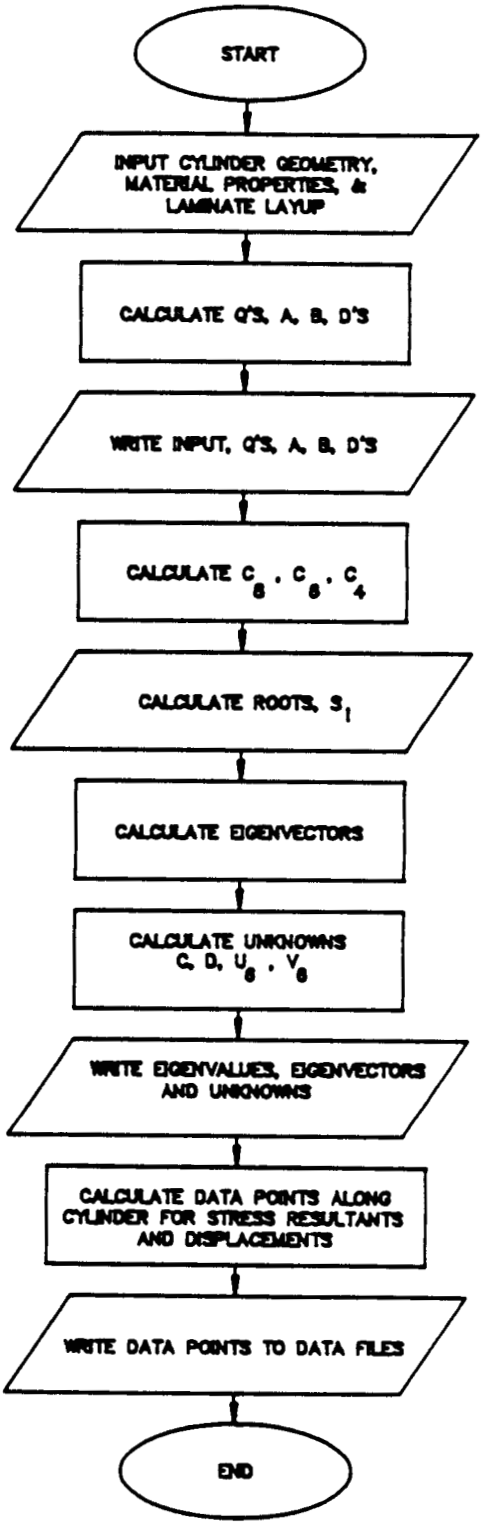

FIGURE 6 COMPUTER FLOWCHART

using Cramer's rule and a closed-form expression for the determinant of a 4 x 4 matrix. With the eigenvalues and eigenvectors known, the unknown constants can be found for the particular set of boundary conditions. The four unknowns are also found directly using Cramer's rule and a closed-form expression for the determinant of a matrix. Using the three equations for displacement, eqs. 161-164, and the six stress resultant equations, eqs. 109-113, 100 data points are calculated along the cylinder from the center at x = 0 to the end at x = + L/2. Each set of data points is written to its own data file for each of the displacements and stress resultants of each boundary condition. These files are used for plotting the results.

The listing and/or a copy on a floppy disk for each of the three programs is available upon request.

Chapter 5 - Results

To determine the character of the responses that are a result of the elastic couplings and directional dependence of fiber-reinforced materials, several specific examples of cylinders are studied for the three loading cases. The first example discussed could be considered somewhat unusual. However, it was chosen to determine the types of responses that can be exhibited by composite cylinders. The cylinder studied is a two layer cylinder with a stacking arrangement of $(23/-60)_T$. In the stacking sequence notation the number denotes the angle, in degrees, of the fibers relative to the axial direction of the cylinder. The first entry in the notation denotes the orientation of the inner layer, and subsequent entries correspond to layers further away from the inner radius. Clearly, such a cylinder is highly coupled in that it is both unbalanced and unsymmetric, i. e., $A_{16} \neq 0$, $A_{26} \neq 0$, and there are entries in the B_{ij} matrix. The other examples are more realistic and do not deviate too far from current design philosophies. However, these latter examples exhibit some characteristics not usually found in current designs.

The material properties of each layer are assumed to represent AS4/3501 graphite-epoxy. This material cures at 350 °F and has the following elastic properties:

E_x = 20. E6 psi ,

E_y = 1.3 E6 psi ,

E_s = 1.03 E6 psi ,

μ_x = .3 .

In each case, the cylinder geometry is:

mean radius R = 10.0 inches ,

length of cylinder L = 30.0 inches .

To illustrate the response of the various cylinders, the displacement and stress resultant responses of each cylinder as a function of axial distance along the cylinder is illustrated in a series of figures. The displacement response of the cylinders is normalized by the laminate thickness and axial distance is normalized by the length of the cylinders. Since the responses of the right and left halves of the cylinder are either even or odd functions of axial distance, the responses for just the right half of the cylinder are shown.

5.1 Response of the $(23/-60)_T$ Cylinder

5.1.1 Compression

The values of the various entries in the ABD matrix for the $(23/-60)_T$ laminate are:

the A matrix

$$A_{11} = .90107\ E5\ \ lb/in\ \ ,$$

$$A_{12} = .30097\ E5\ \ lb/in\ \ ,$$

$$A_{16} = .15812\ E5\ \ lb/in\ \ ,$$

$$A_{22} = .71799\ E5\ \ lb/in\ \ ,$$

$$A_{26} = -.22710\ E5\ \ lb/in\ \ ,$$

$$A_{66} = .36474\ E5\ \ lb/in\ \ , \qquad (185)$$

the B matrix

$$B_{11} = -152.45\ \ lb\ \ ,$$

$$B_{12} = 12.006\ \ lb\ \ ,$$

$$B_{16} = -96.633\ \ lb\ \ ,$$

$$B_{22} = 128.44\ \ lb\ \ ,$$

$$B_{26} = -89.747\ \ lb\ \ ,$$

$$B_{66} = 12.006 \text{ lb} , \quad (186)$$

and the D matrix

$$D_{11} = .75089 \text{ lb-in} ,$$

$$D_{12} = .25081 \text{ lb-in} ,$$

$$D_{16} = .13177 \text{ lb-in} ,$$

$$D_{22} = .59832 \text{ lb-in} ,$$

$$D_{26} = -.18925 \text{ lb-in} ,$$

$$D_{66} = .30395 \text{ lb-in} . \quad (187)$$

As can be seen, there are no zero entries in the matrix, this laminate construction exhibiting full coupling.

The axial displacement response of the $(23/-60)_T$ cylinder for the case of axial compression with the two boundary conditions is illustrated in fig. 7. The response is linear with x, a characteristic which is due to the dominance of the U_6 term of eq. 163, and starts at zero at mid-cylinder and goes to minus one-half at the right end. Recall, the compression condition is achieved by displacing one end of the cylinder relative to the other by one laminate thickness. Therefore, the right end moves one-half a laminate thickness in the negative x direction. As can be seen, the axial displacement response of the

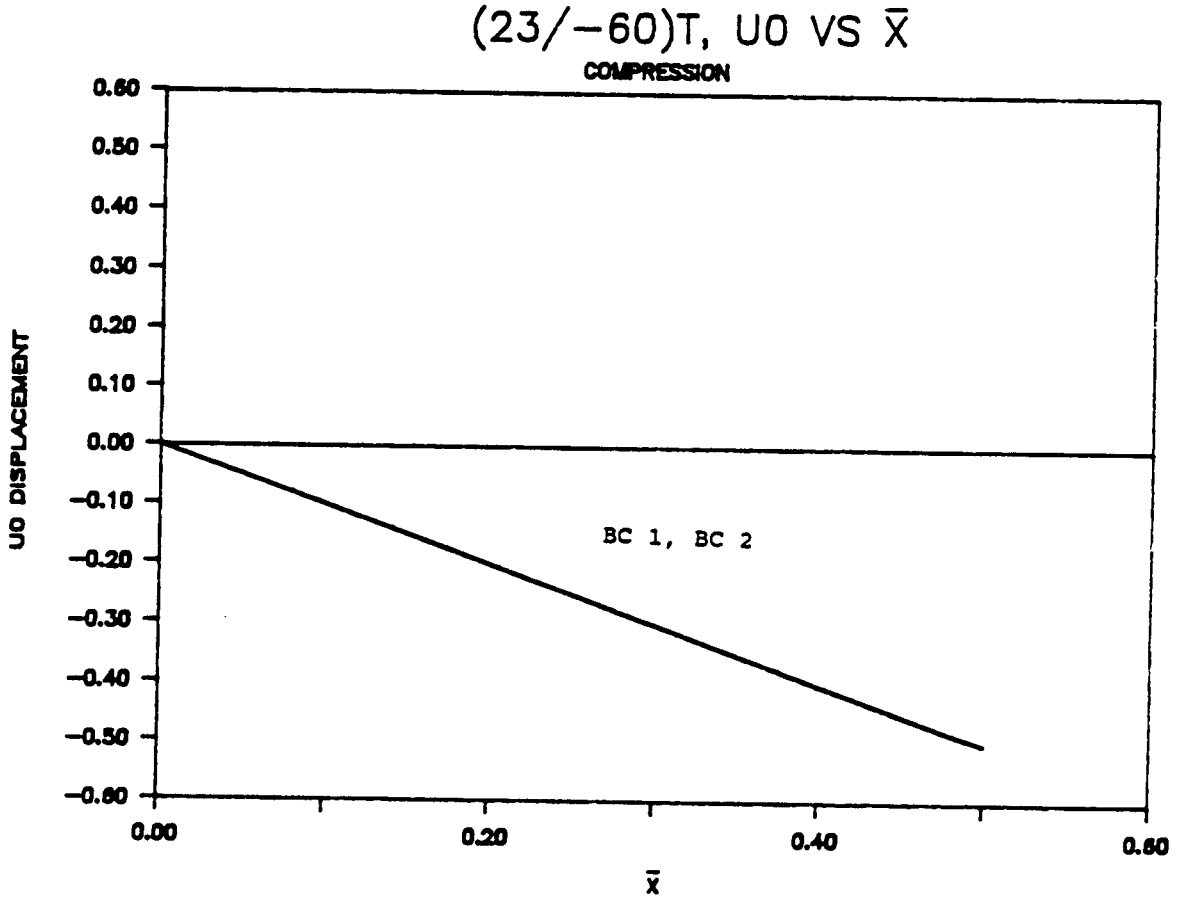

Figure 7 $(23/-60)_T$, $u^*(\bar{x})$ vs $\bar{x}$, Compression

cylinder is independent of boundary condition. On the other hand, the axial force resultant, illustrated in fig. 8, is strongly dependent on the boundary condition. The difference in the magnitudes of the axial force resultant in fig. 8 is due to differences in the circumferential boundary conditions. For metallic and balanced symmetric composite cylinders such a dependence simply does not exist. Circumferential displacements do not strongly influence, if they influence at all, the axial force characteristics. The highly coupled nature of the responses is a characteristic that is unique to fiber-reinforced material. This can be clearly seen by examining eq. 109, the expression for the axial force. The third term in the equation involves gradients of the circumferential displacement. In metallic and balanced symmetric composite cylinders, A_{16}, B_{16}, and B_{11} are all zero and so the axial force involves only the axial displacement gradient, through the first term in that equation, and the radial displacement, through the second term. The second term, as mentioned previously, represents the standard coupling of radial and axial responses due to Poisson effects. The results of fig. 8 indicate that the cylinder restrained against twist, bc 1, requires a larger axial compressive force to move the ends of the cylinder toward each other than the cylinder that is free to twist. The difference in the two force levels is a direct result

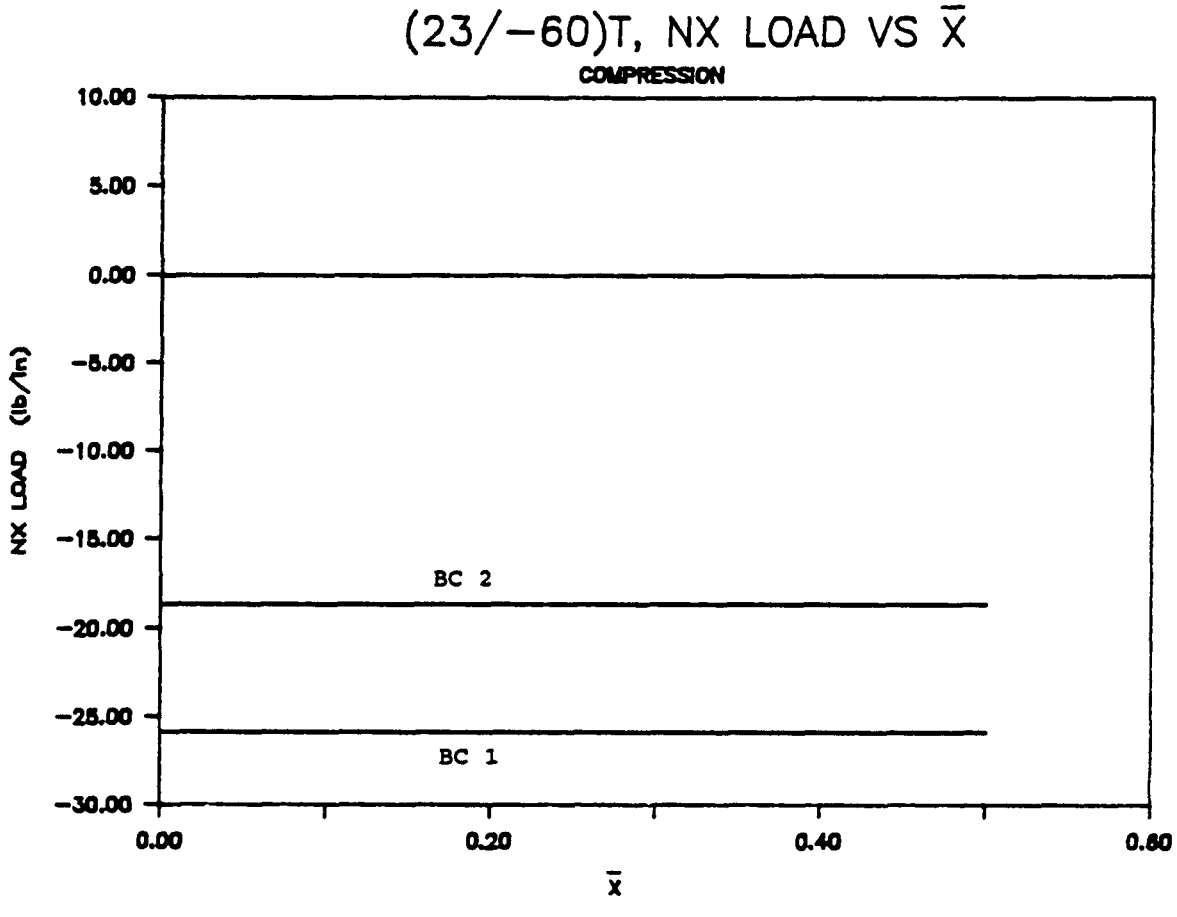

Figure 8 $(23/-60)_T$, N_X vs $\bar{x}$, Compression

of this twist term, specifically the A_{16} term.

To further illustrate the coupling of axial and circumferential responses, the circumferential displacement response of the cylinder for the two boundary conditions is shown in fig. 9. As expected, the circumferential displacement is strongly influenced by the type of boundary condition. Boundary condition 2 imposes no constraint on circumferential displacement at the ends of the cylinder and so the cylinder twists as it is compressed axially. As was seen in fig. 8, this freedom to twist reduces the axial force required to compress the cylinder. The twist response is a characteristic of V_6 in eq. 164. Boundary condition 1, on the other hand, restrains twist motion. The restraint is not complete because there is actually twisting of the cylinder between the ends and center of the cylinder. The twist displacements are not discernible on the scale of fig. 9. To complement fig. 9, the shear force resultant $\overline{N_{x\theta}}$ for the two boundary conditions is illustrated in fig. 10. This figure, like the previous three, typifies the coupling between axial and circumferential responses. To compress the circumferentially restrained cylinder, bc 1, requires a shear force resultant. The expression for $\overline{N_{x\theta}}$, eq. 111, clearly illustrates this. The constant A_{16} multiplies the axial strain, the axial strain being the dominant response for this case of compression. For the case

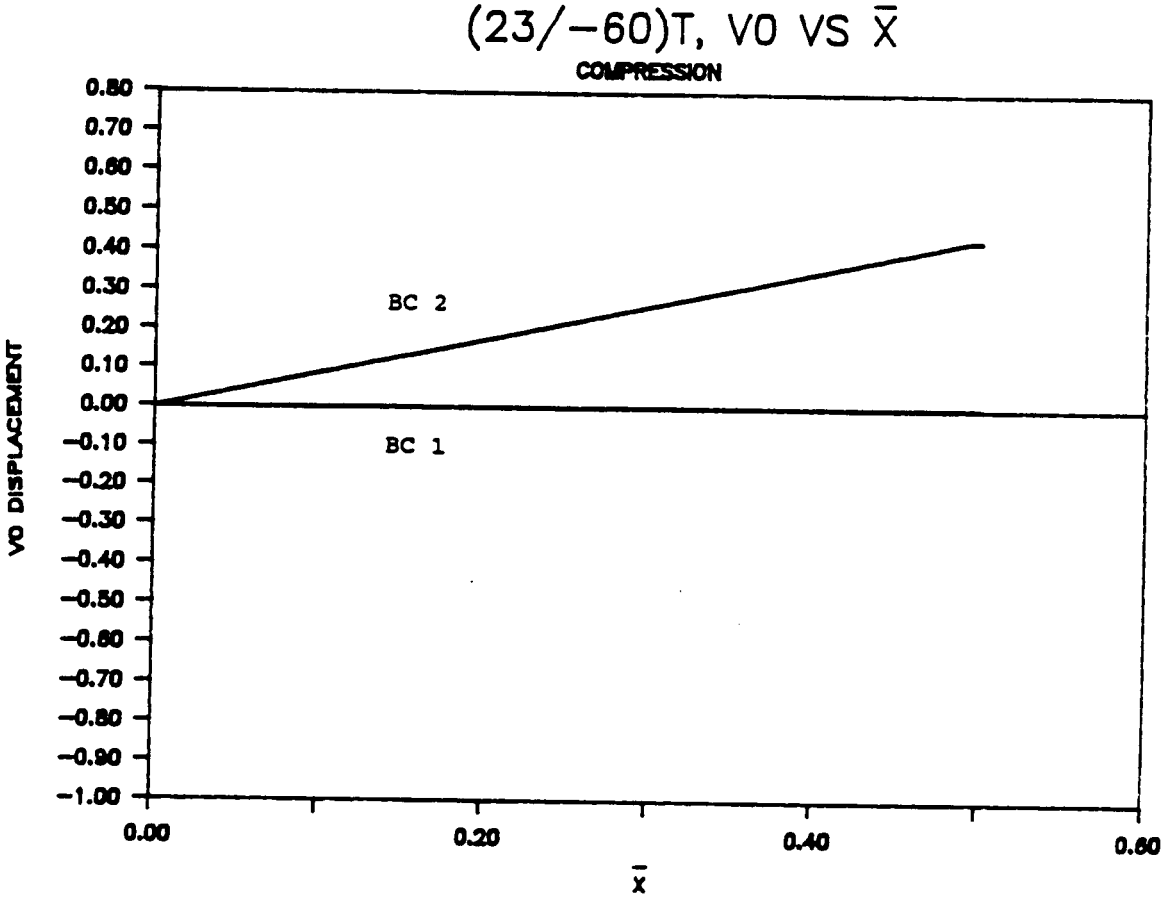

Figure 9 $(23/-60)_T$, $v^*(\bar{x})$ vs $\bar{x}$, Compression

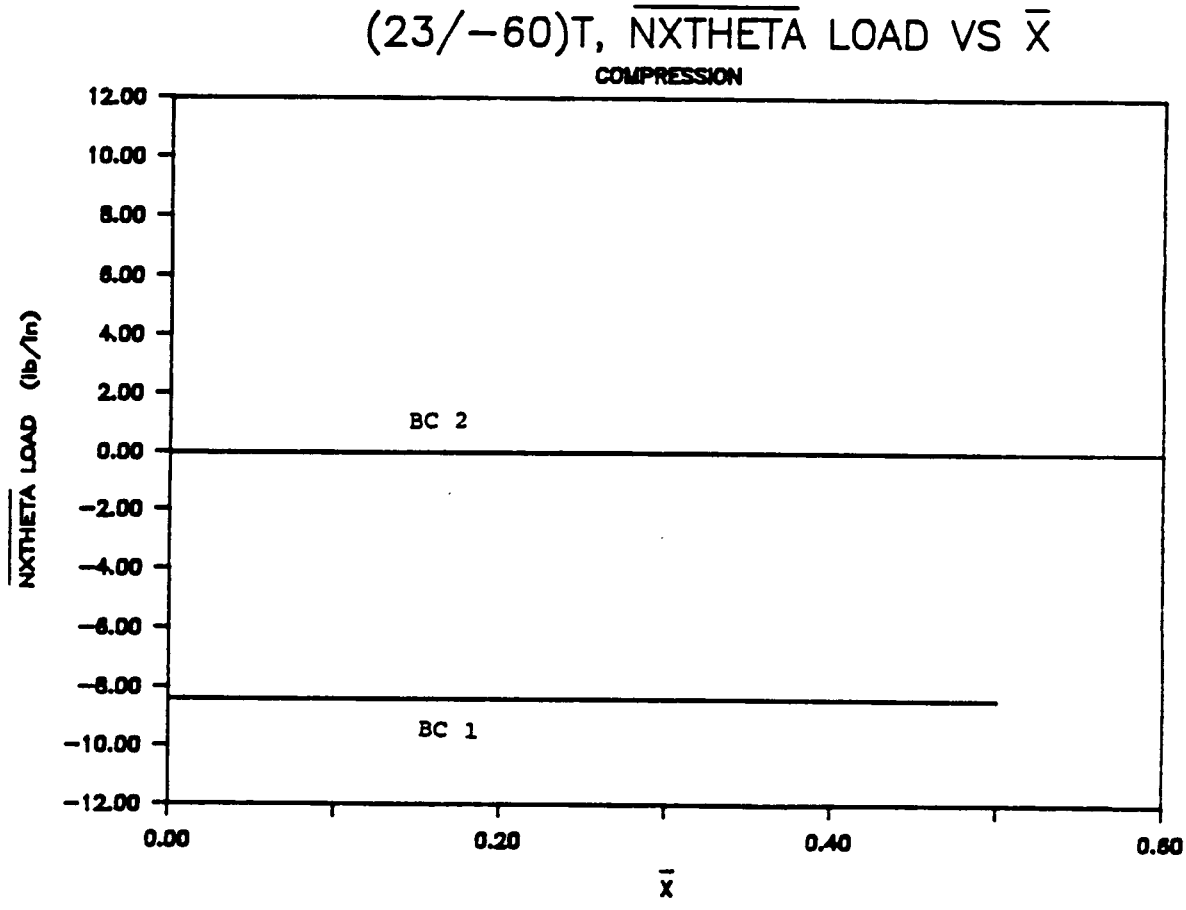

Figure 10 $(23/-60)_T$, $\overline{N_{x\theta}}$ vs $\bar{x}$, Compression

of a restrained cylinder the third term, the term normally associated with twist response, is zero, and so the majority of the contribution to $\overline{N_{x\theta}}$ is due to the axial strain term. For the unrestrained cylinder, the twist response is not zero and the third term cancels the first term in $\overline{N_{x\theta}}$. Note that A_{16} was responsible for the coupling in the expression for N_x, eq. 109.

The radial expansion of the cylinder, i.e., the w° displacement response, for the case of axial compression is shown in fig. 11. Due to Poisson effects, the axial compression of any type of cylinder, metallic or composite, results in radial expansion. Here, however, the various elastic couplings cause the cylinder with no twisting restraint to expand more. This results in a somewhat larger displacement gradient in the boundary layer at the supported end of the cylinder. The displacement gradient in the boundary layer influences the circumferential force resultant N_θ, as shown in fig. 12. Over the majority of the cylinder there is no change in the value of the radial displacement. The value of the circumferential force resultant is zero there. However, at the end of the cylinder, the radial displacement changes rapidly causing a circumferential force resultant there. For the cylinder with no twist restraint, this induced stress resultant is larger in magnitude than when the twist restraint is present. Examining eq. 110 it is seen that the

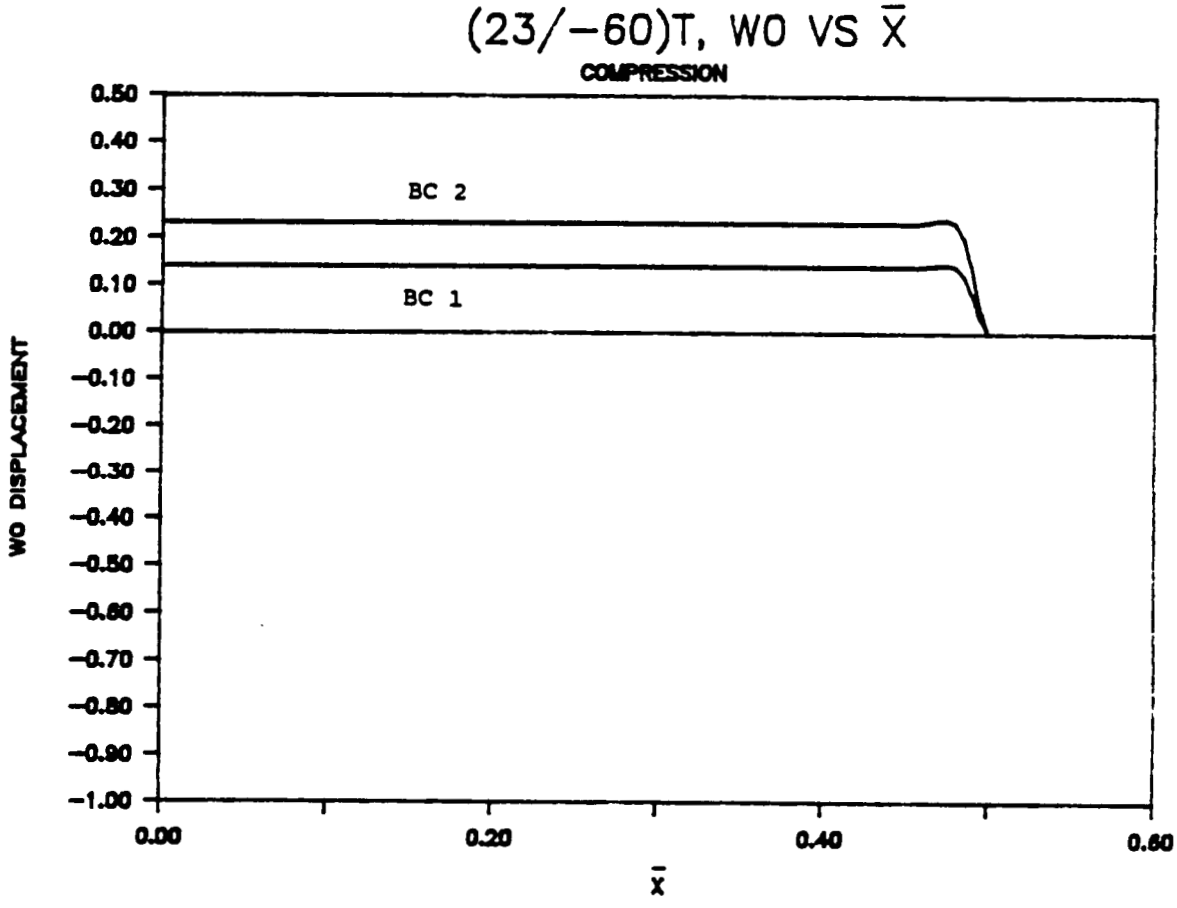

Figure 11 $(23/-60)_T$, $w^*(\bar{x})$ vs $\bar{x}$, Compression

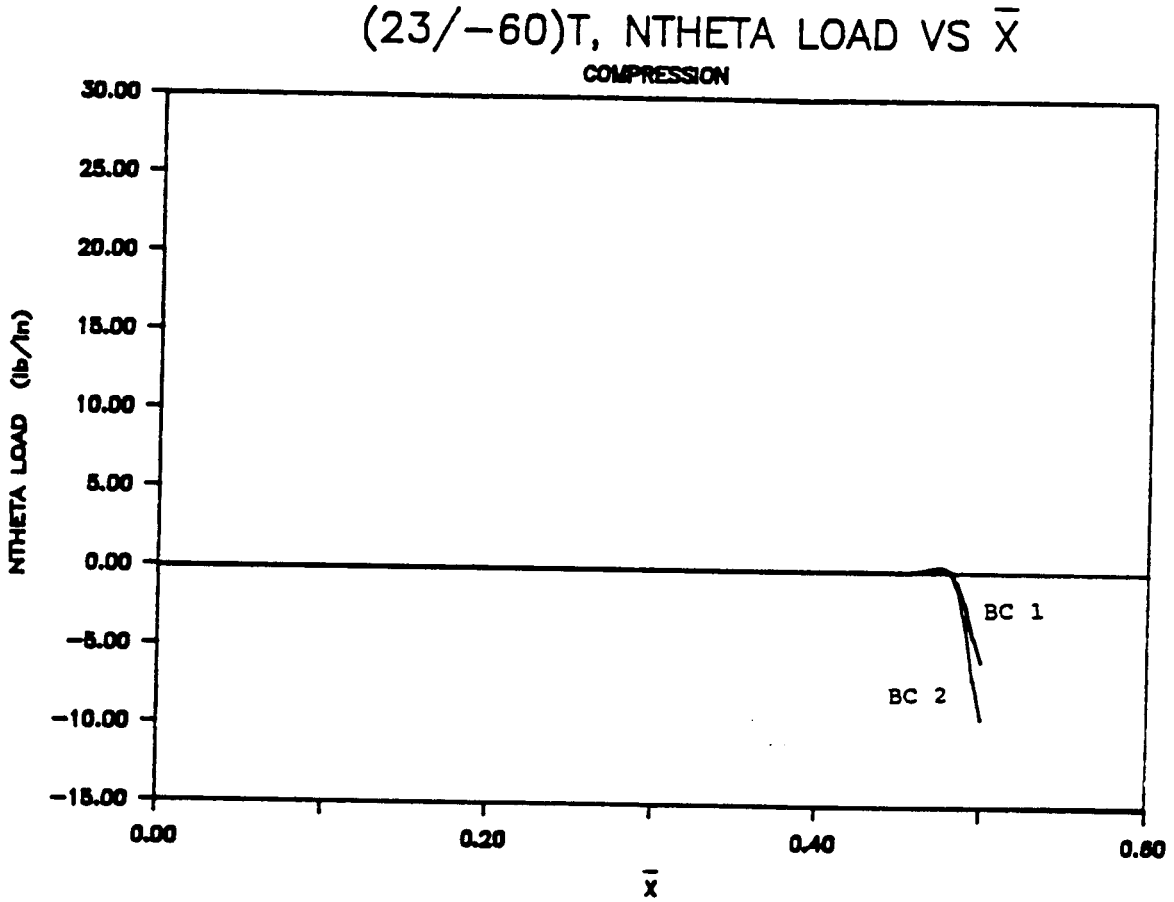

Figure 12 $(23/-60)_T$, N_θ vs $\bar{x}$, Compression

circumferential force resultant and the circumferential displacement are coupled through A_{26} and B_{26} in the third term. These coefficients are zero in metallic and balanced symmetric composite cylinders. For the circumferentially restrained cylinder dv°/dx is zero and the third term has no contribution. In the unrestrained cylinder, there is a gradient in v° and this contributes to the circumferential force resultant and, as noted above, causes it to be larger than when twist is restrained.

The bending moment resultants M_x and M_θ are illustrated in figs. 13 and 14, respectively. Referring to eqs. 112 and 113, for symmetrically laminated composite structures all coefficients in these equations except the D_{ij} are zero. For some symmetrically laminated composite structures D_{16} and D_{26} are small, and for metallic structures they are zero. Therefore, the bending moments depend strongly on the radial displacement only through the axial curvature of the radial displacement, the fourth term. The circumferential and axial displacements have no influence on the moments. Clearly this is not the case for general composite laminates. The axial and radial displacements enter through the B_{ij} terms and influence the moments. In addition, the moments M_x and M_θ are strongly influenced by the presence or lack of circumferential displacement, i.e., dv°/dx. For both M_x and M_θ, the first three terms in the moment expression are relatively

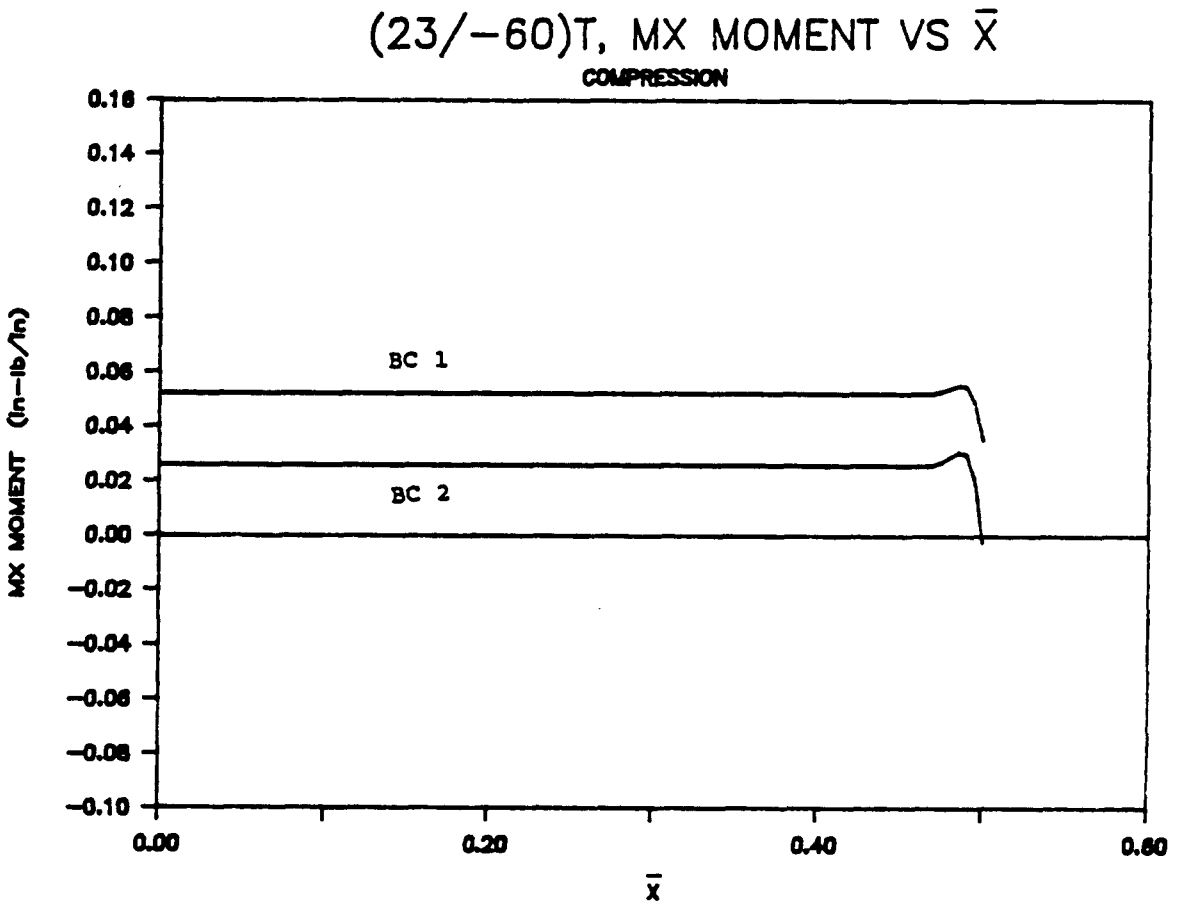

Figure 13 $(23/-60)_T$, M_X vs $\bar{x}$, Compression

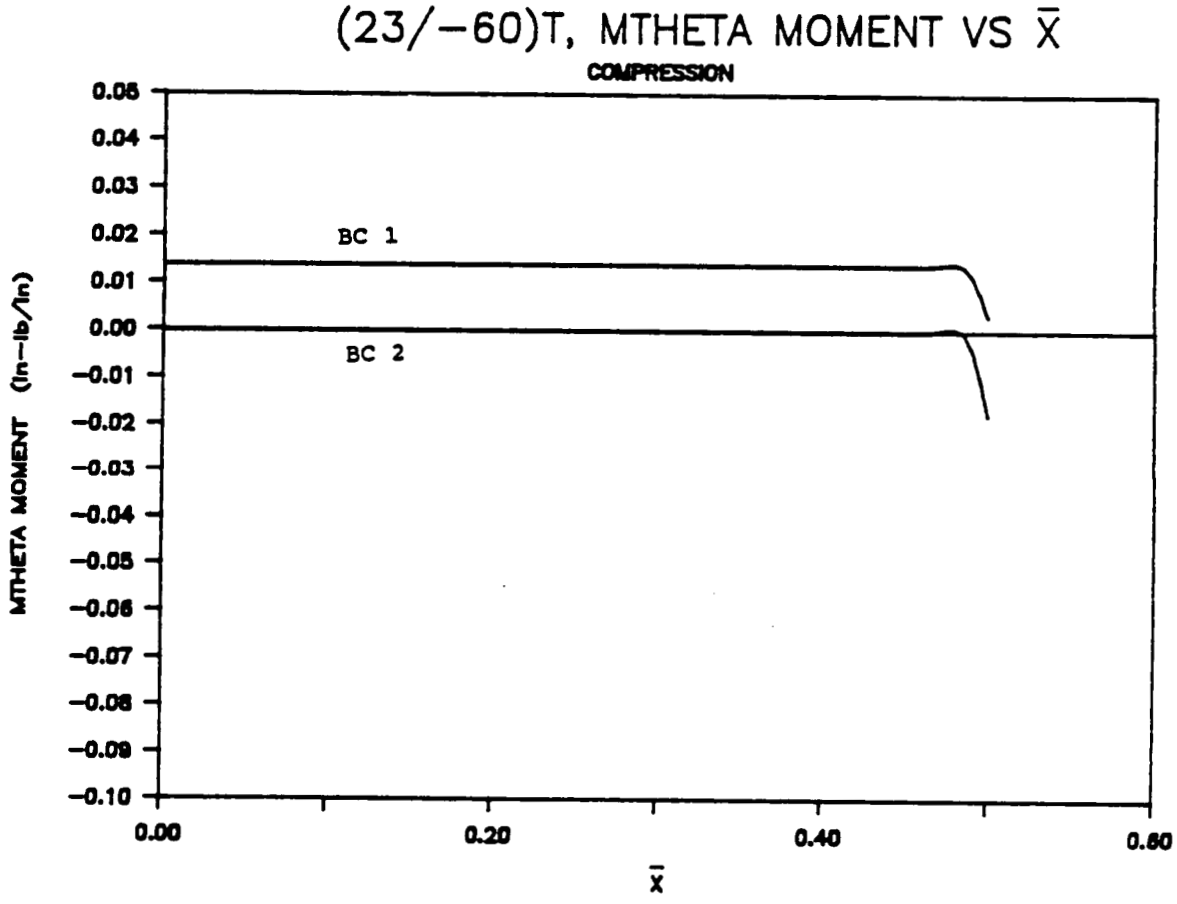

Figure 14 $(23/-60)_T$, M_Θ vs $\bar{x}$, Compression

independent of x. Over the majority of the cylinder the curvature is zero and so the fourth terms are zero. However, near the supported ends, the curvature becomes large and the fourth terms dominate both moment expressions. This dominance is confined to a small region near the end and thus constitutes a boundary layer there. For the case of M_θ and bc 2, there is no moment resultant except for in the boundary layer.

5.1.2 Torsion

As with compression, the twisting of one end of the $(23/-60)_T$ cylinder relative to the other results in several unexpected responses. The circumferential displacement as a function of axial distance from the center of the cylinder is illustrated in fig. 15. This displacement is linear with distance, and is the counterpart to fig. 7 for the axial compression case. The results for both the axially restrained case, bc 1, and the axially free case, bc 2, are identical, the response being determined by V_6 in eq. 164. The shear force resultant, $\overline{N_{x\theta}}$, required to produce the twist is shown in fig. 16. There is considerable difference in the shear force required for the two boundary conditions. The presence of an axial restraint considerably stiffens the cylinder in torsion, a

C-2

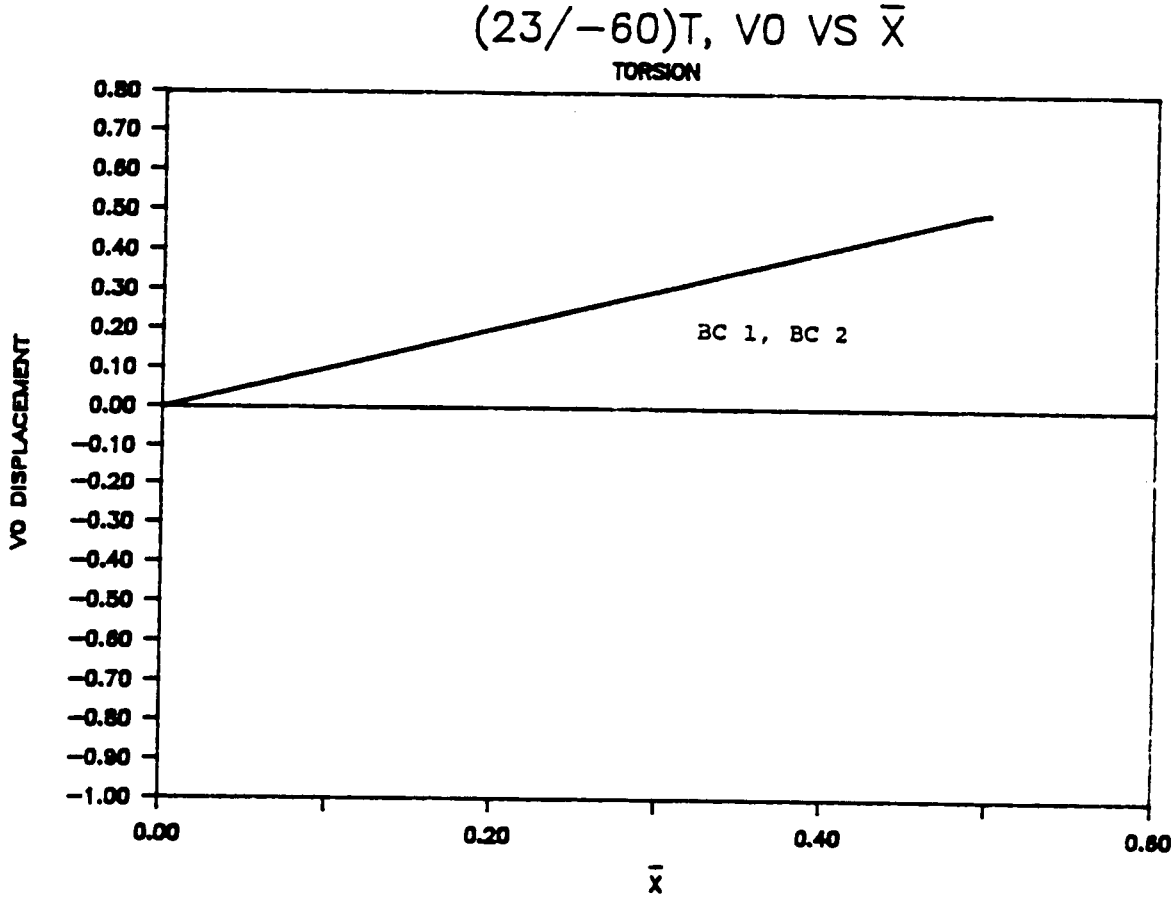

Figure 15 $(23/-60)_T$, $v^{\circ}(\bar{x})$ vs $\bar{x}$, Torsion

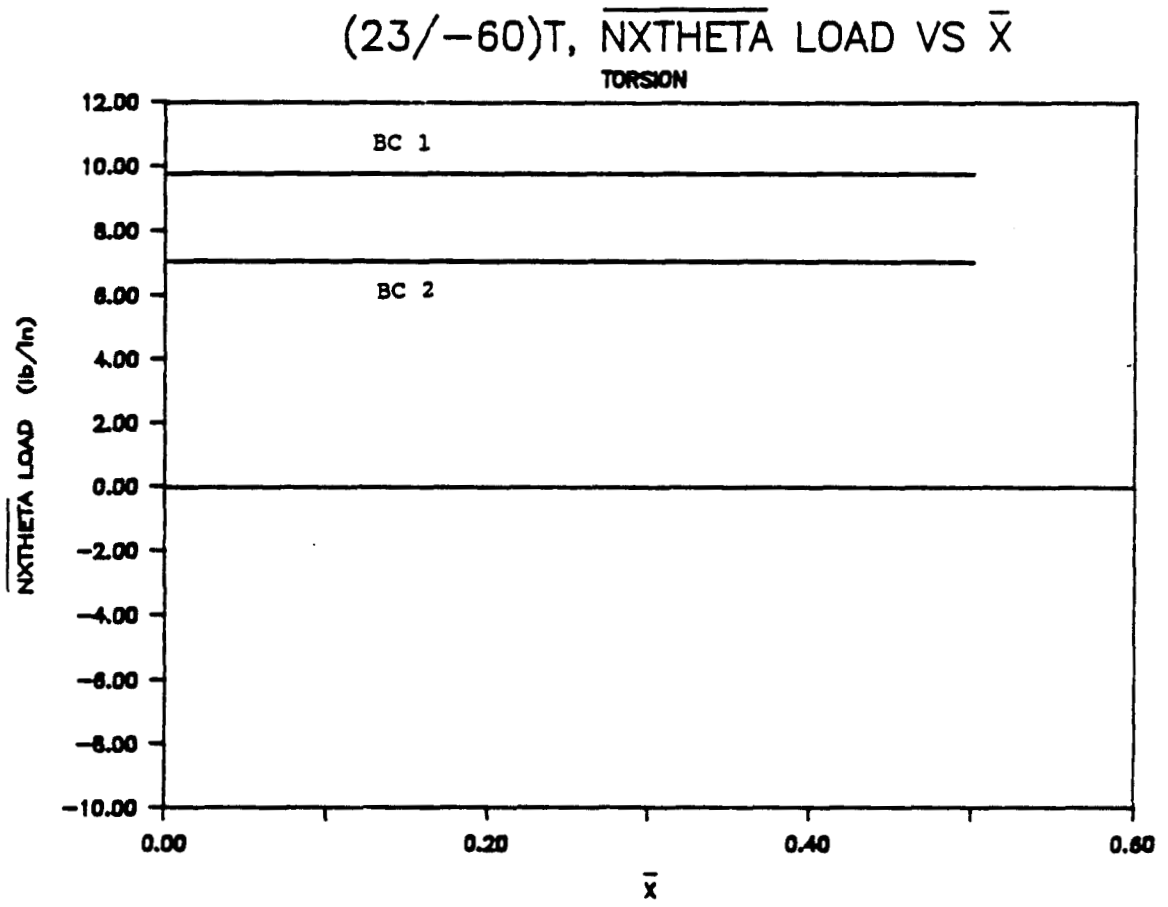

Figure 16 $(23/-60)_T$, $\overline{N_{x\theta}}$ vs $\bar{x}$, Torsion

direct result of the elastic coupling within the cylinder. Examination of the expression for the shear force resultant, eq. 111, indicates that the axial displacement, or lack of it, enters the problem through the coefficients A_{16} and B_{16}. The character of the axial displacement for the two conditions is shown in fig. 17, the axially unrestrained case exhibiting a linear variation of axial displacement with length and the axially restrained cylinder showing very little variation with length. As with compression, this linearity in the unrestrained case is due to the dominance of the U_6 term of eq. 163. The presence or lack of axial displacement causes, through A_{16} and B_{16}, the difference in shear force resultant values. The axial-twist coupling is further illustrated by examining the difference in the axial force resultant caused by the twist for the two cases. It is indicated in fig. 18 that to restrain the axial motion of the cylinder during twist, bc 1, an axial force the same order of magnitude as the force required to compress the torsionally restrained cylinder, fig. 8, is necessary. It should be noted that neither N_x nor $\overline{N_{x\theta}}$ exhibit boundary layers in either of the two loading cases studied so far. This is because the governing differential equations, eqs. 95 and 96, indicate the two resultants cannot vary with x. They must assume the boundary value along the complete length of the cylinder.

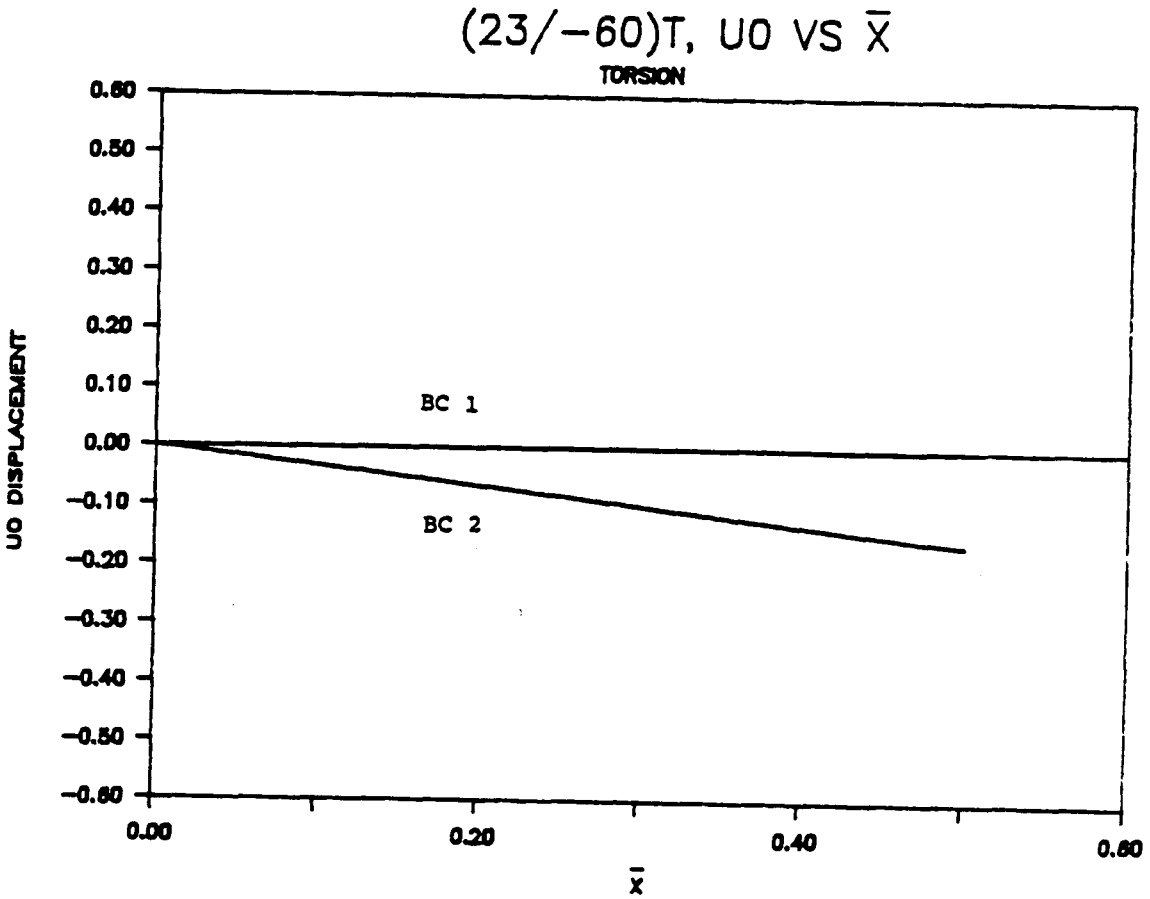

Figure 17 $(23/-60)_T$, $u^*(\bar{x})$ vs $\bar{x}$, Torsion

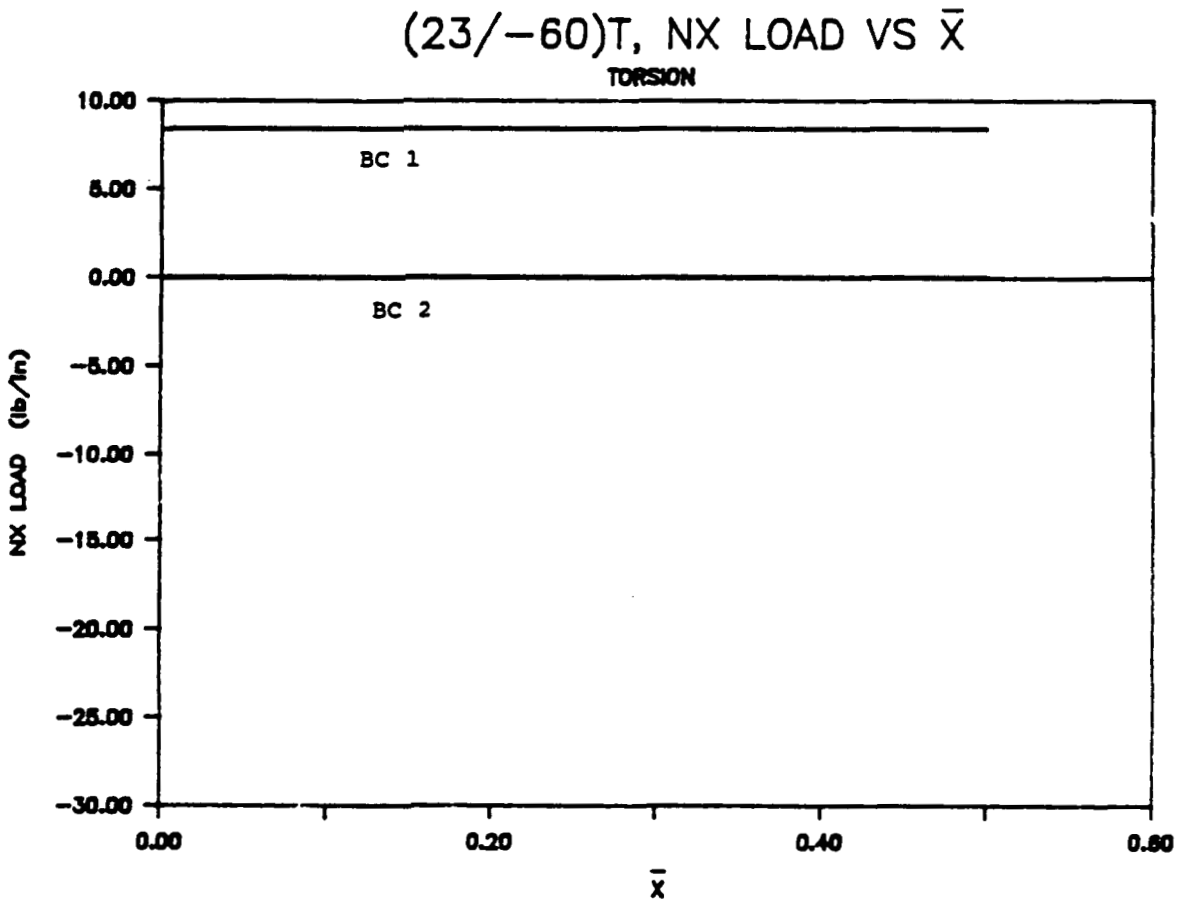

Figure 18 $(23/-60)_T$, N_X vs $\bar{x}$, Torsion

For the case of twist, perhaps the most unusual effect is the coupling between twist and radial displacement, fig. 19. Because the laminate is unsymmetric, these two displacements are coupled, particularly through the B_{16} term in eqs. 111 and 112. It is shown in the figure that twisting of the cylinder causes its radius to increase. Due the boundary condition restraining radial displacement at the ends of the cylinder, there is a boundary region in the radial displacement at the ends. Figure 19 looks very similar to fig. 11, the radial displacement caused by the axial compression. The character of fig. 11 would be much the same for the case of a metal or balanced symmetric composite cylinder. However, there would be no radial displacement due to twist for a metal cylinder and so the results of fig. 19 are unique to composites, and in particular, unsymmetric composites. Furthermore, there is a sign sensitivity to the coupling in that if the cylinder was twisted the other direction, the radial displacements would be negative. In addition, the sign of B_{16} can be reversed by reversing fiber angles, i.e., fabricating a $(-23/60)_T$ laminate. Then the radial displacement would also decrease. This radial displacement-twist coupling is felt to be the most significant effect found to this point in the study.

The character of the moment resultant normally

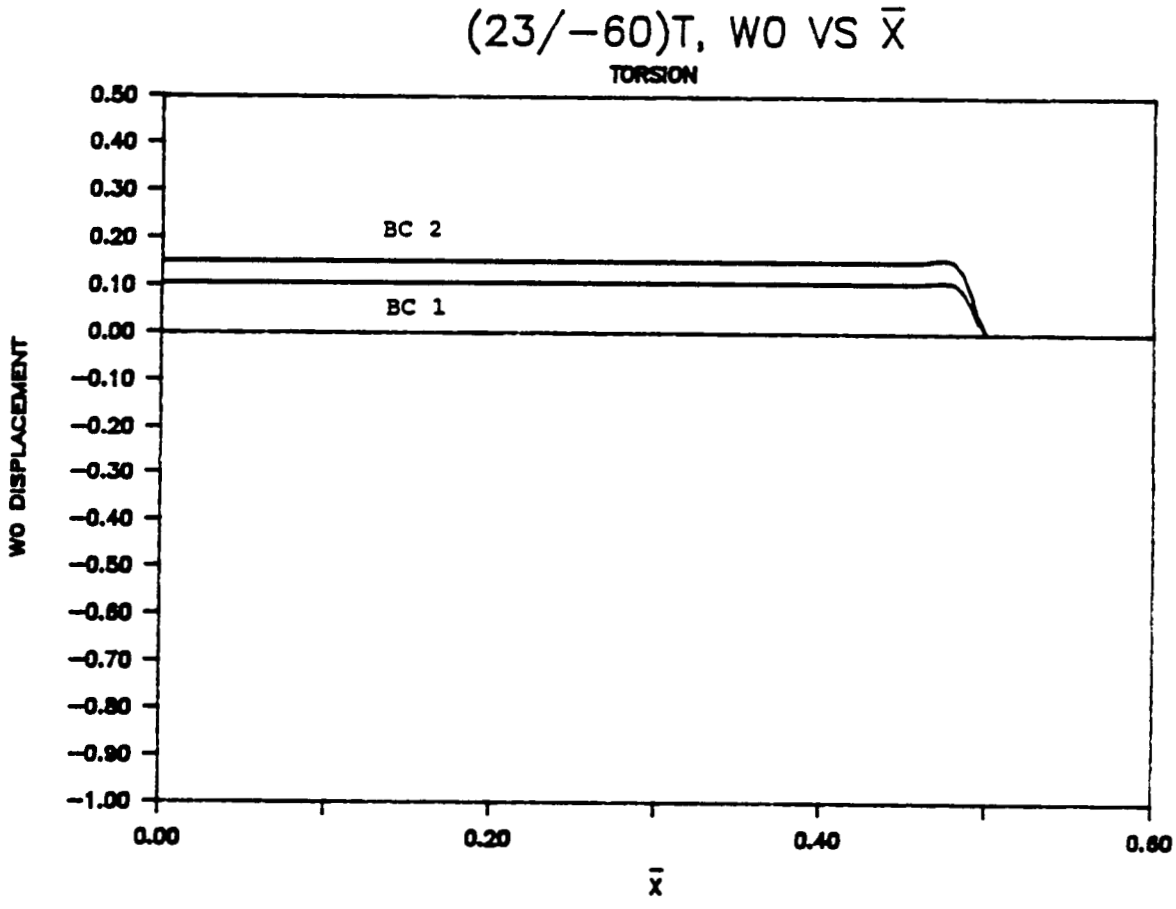

Figure 19 $(23/-60)_T$, $w^*(\bar{x})$ vs $\bar{x}$, Torsion

associated with the radial displacement, namely M_x, is illustrated in fig. 20. Due to bending in the axial direction, there is an increased moment at the end of the cylinder. It is interesting to note that even though there is no curvature in the axial direction over the majority of cylinder length, i.e., w° is a constant over much of the cylinder, there is a moment generated. This is because with composites, moments are associated with displacement gradients other than just curvatures, in particular, gradients of inplane displacements, and with displacements themselves. This has been discussed before and can be seen by examining eqs. 112 and 113. With metals and balanced symmetric laminates, it is only curvatures that are associated with moments.

The character of the other stress resultants associated with twisting the cylinder are illustrated in figs. 21 and 22. As with the axial compression case, the circumferential force resultant N_θ increases at the end of the cylinder, and the moment resultant M_θ is small and constant over the majority of the cylinder, exhibiting an increased value in the boundary layer region.

5.1.3 Temperature Change

Due to the elevated temperature processing associated

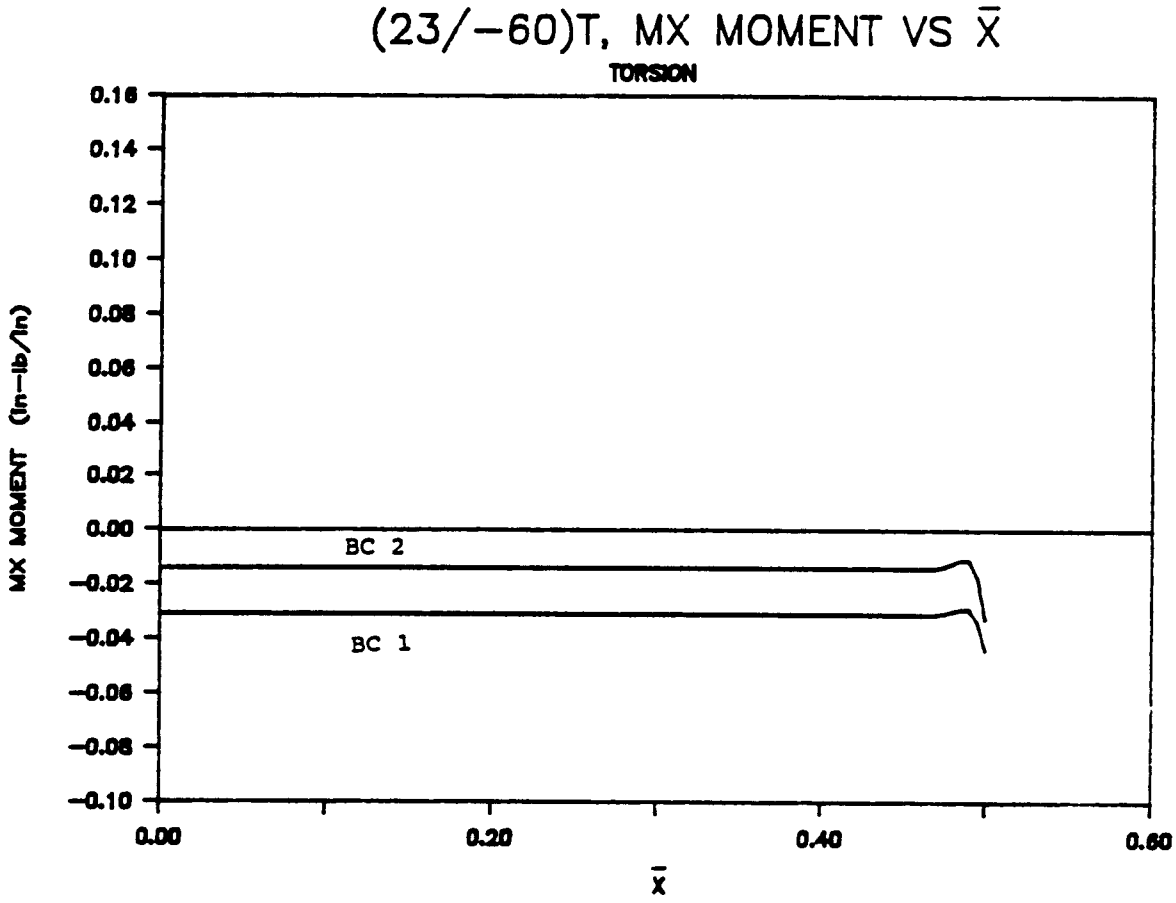

Figure 20 $(23/-60)_T$, M_X vs $\bar{x}$, Torsion

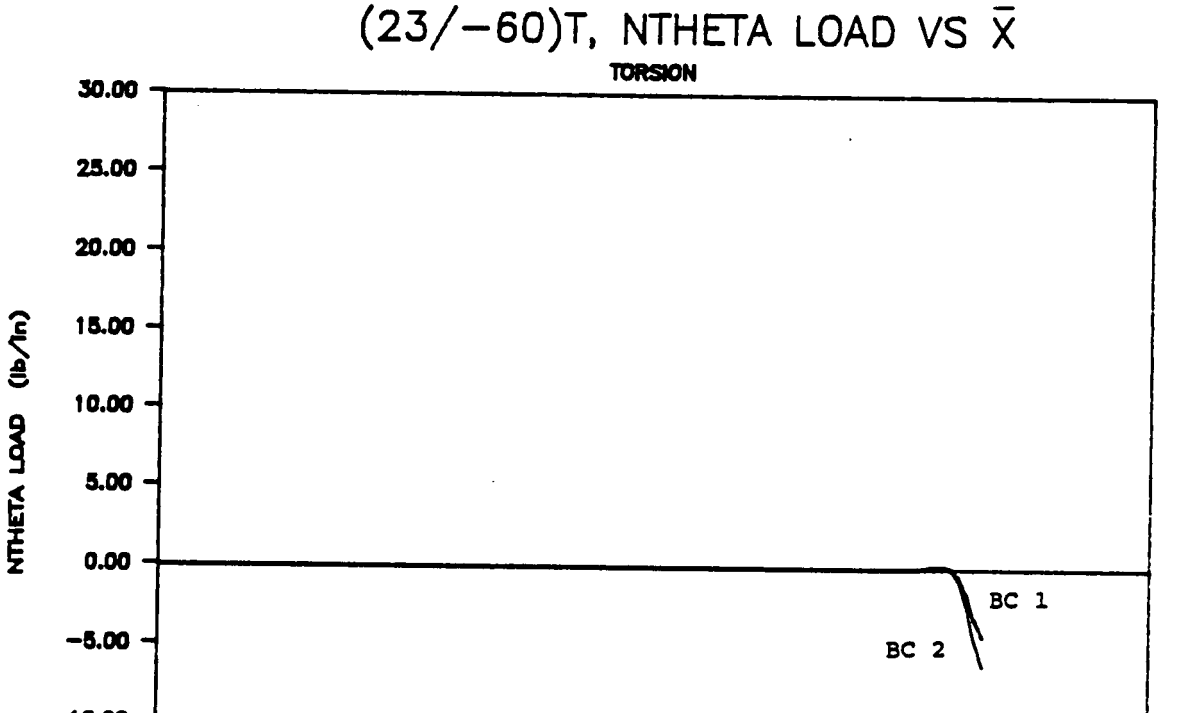

Figure 21 $(23/-60)_T$, N_θ vs $\bar{x}$, Torsion

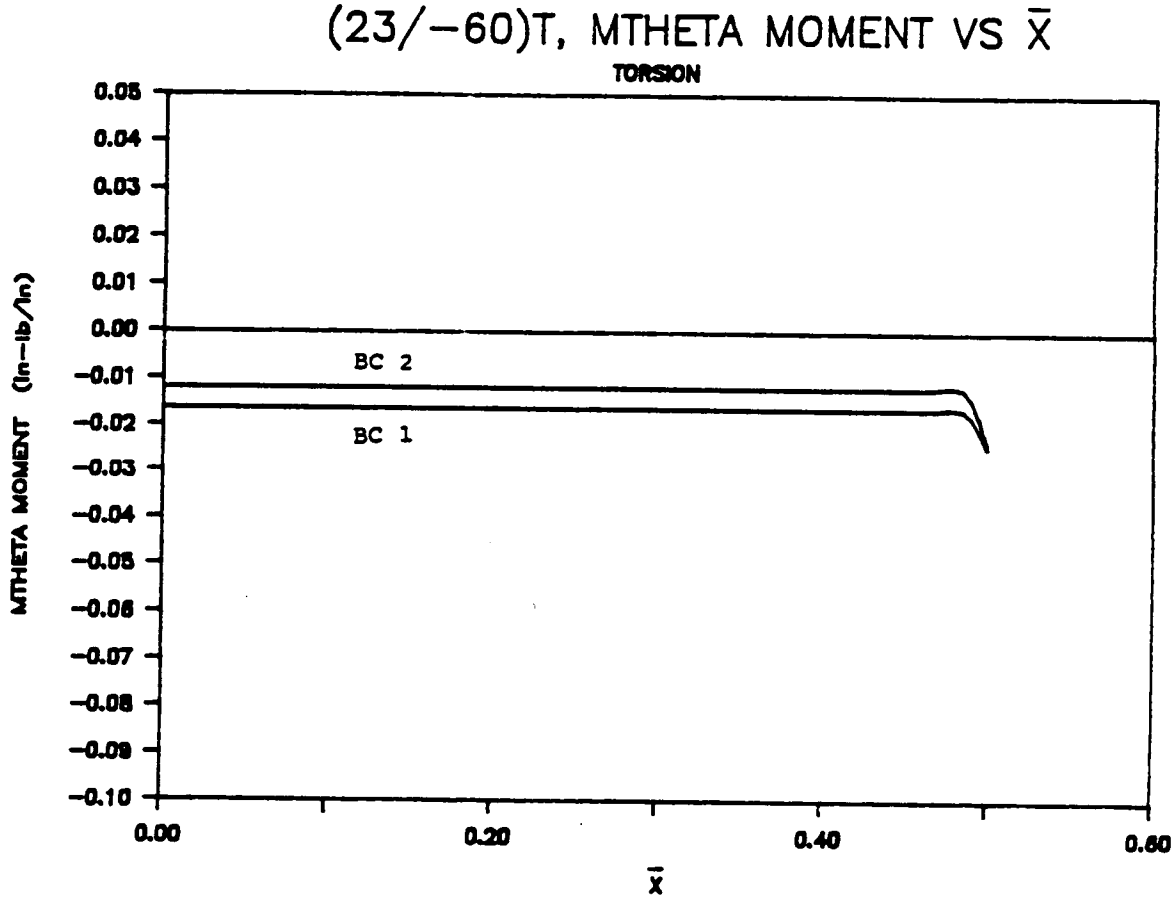

Figure 22 $(23/-60)_T$, M_θ vs $\bar{x}$, Torsion

with most polymer-matrix composites, the thermally-induced deformations and stress resultants, from which thermally-induced stresses can be determined, should be computed to determine their influence on the initial shape of the cylinder, or the initial stress state. For a linear theory, which is used here, these deformations and stress resultants superpose on the response due to axial compression or twist. If deemed important, the thermally-induced responses can be computed in a separate step and the results added to the results for the mechanically-induced response. For a nonlinear theory, the thermally-induced deformations and stress resultants are an important first step and should be the starting point in any analysis directed at understanding the response due to loads. If the loads are being applied at a temperature lower than the processing temperature, deformations and stresses are present before the load is applied. For a nonlinear theory, these thermally-induced responses do not simply add to the nonlinear response. They are a more integral part of the solution. Including or not including the thermally-induced responses as the initial starting condition from which to apply the mechanical load may lead to entirely different predictions for the response due to the load. In this study the intent is to simply examine the thermally-induced response itself, without adding it to the mechanically-induced results, or implying what the

thermal response may mean as regards nonlinear effects of mechanical loads.

The processing temperature of AS4/3501 is 350 °F and if it is assumed that the cylinder is at a service temperature of 70 °F, this represents a -280 °F temperature change. The axial displacement response of the cylinder as a result of this temperature change is shown in fig. 23. The axial displacement of the right-half of the cylinder is negative everywhere, meaning the cylinder length contracts due to the temperature change. The displacement response is linear with position except at the extreme end, where there is a slight perturbation from the linear response. The circumferential displacement as a function of axial position is shown in fig. 24. This response is also linear with axial position except for a slight perturbation at the end. The reason for the perturbation is quite clear when the radial displacement response, fig. 25, is examined. Away from the ends, the cylinder contracts uniformly in the radial direction as the temperature is lowered from the processing temperature. However, at the end of the cylinder the radial displacement changes rapidly from this uniform state. As the end of the cylinder is approached the radius decreases more, and then suddenly increases. This change from the uniform state occurs over a very short axial distance, resulting in large displacement gradients and thus a boundary layer in this region.

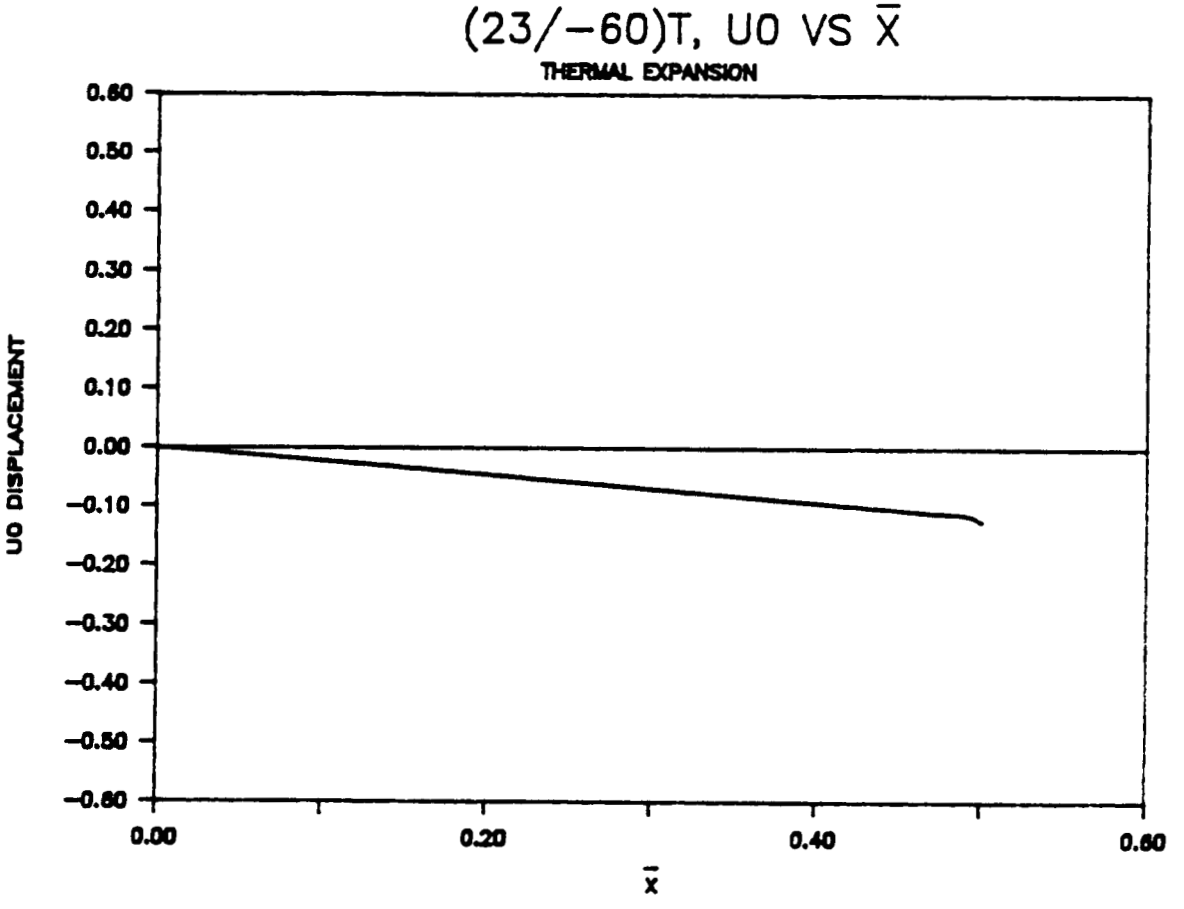

Figure 23 $(23/-60)_T$, $u^*(\bar{x})$ vs $\bar{x}$, Thermal Expansion

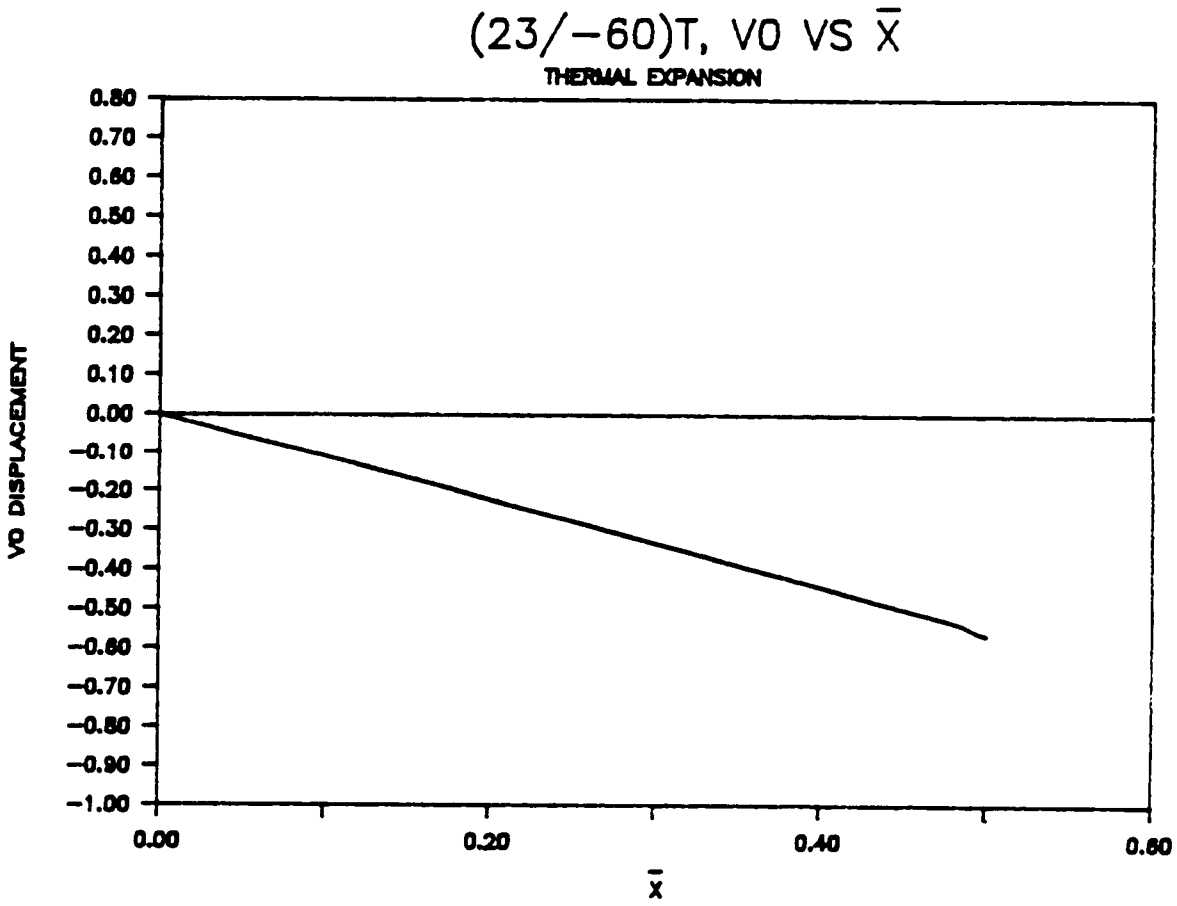

Figure 24 $(23/-60)_T$, $v^*(\bar{x})$ vs $\bar{x}$, Thermal Expansion

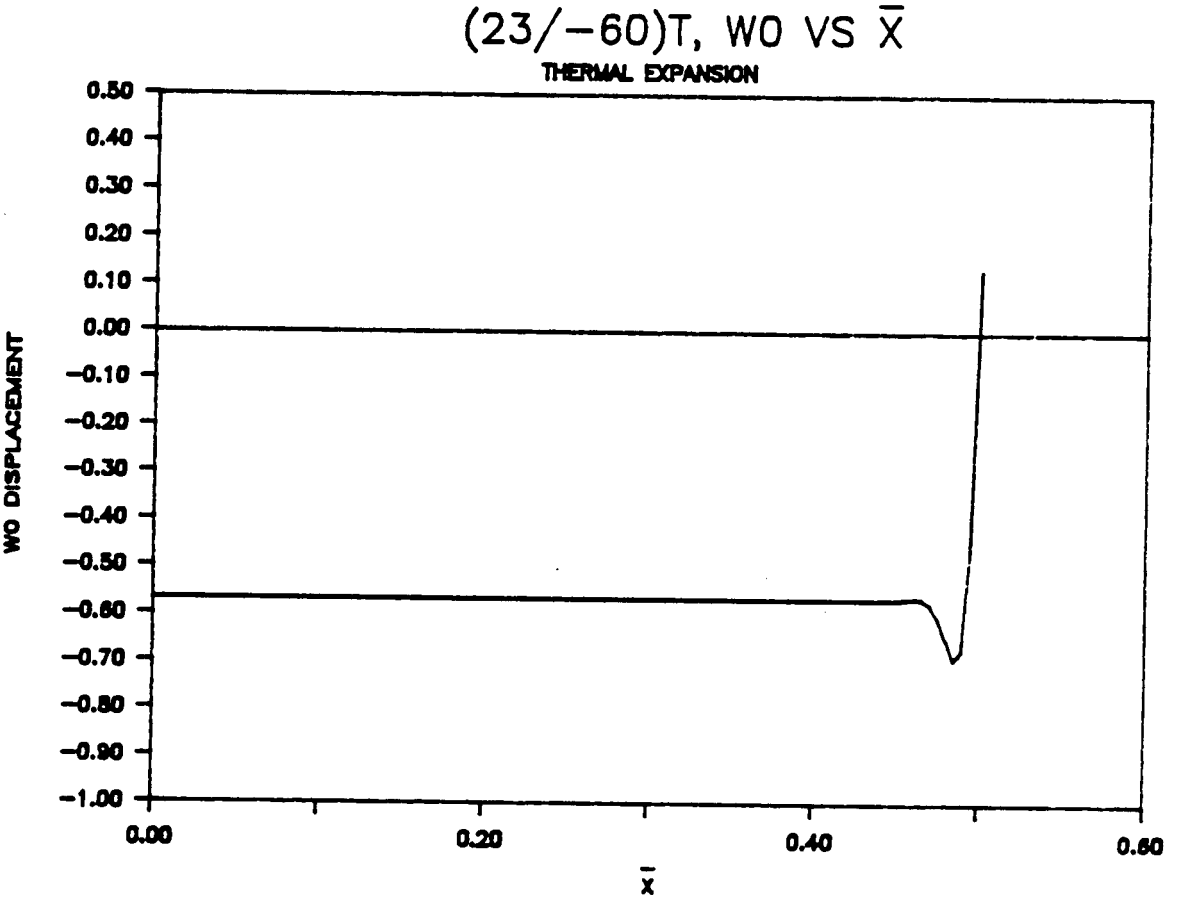

Figure 25 $(23/-60)_T$, $w^*(\bar{x})$ vs $\bar{x}$, Thermal Expansion

There are thermally-induced loads associated with this deformed shape. Due to the traction-free boundary conditions, the axial force resultant, the shear force resultant, and the axial moment resultant, N_x, $\overline{N_{x\theta}}$, and M_x, respectively, must be zero at the end of the cylinder. The other resultants are not specified anywhere along the cylinder. As can be seen in fig. 26, the axial moment resultant along the length of the cylinder is uniform and nonzero over much of the length, increases slightly, then rapidly decreases to zero as the end of the cylinder is approached. If the $(23/-60)_T$ laminate was fabricated and processed as a flat plate and then cooled to 70 °F, the unsymmetric nature of the laminate would cause it to warp significantly and develop large curvatures [1,2,3]. However, the cylinder cannot develop curvatures in the circumferential direction nor in the axial direction except near the end where it is traction free. With the laminate naturally wanting to develop curvature but not being able to because of geometric constraints, force and moment resultants develop in the cylinder. However, with the end of the cylinder being traction free, three of the force and moment resultants must be zero there. If they are not zero away from the ends, they must 'adjust themselves' and vanish at the end. This is the case with M_x. As a result an axial curvature develops in the radial displacement near the end of the cylinder.

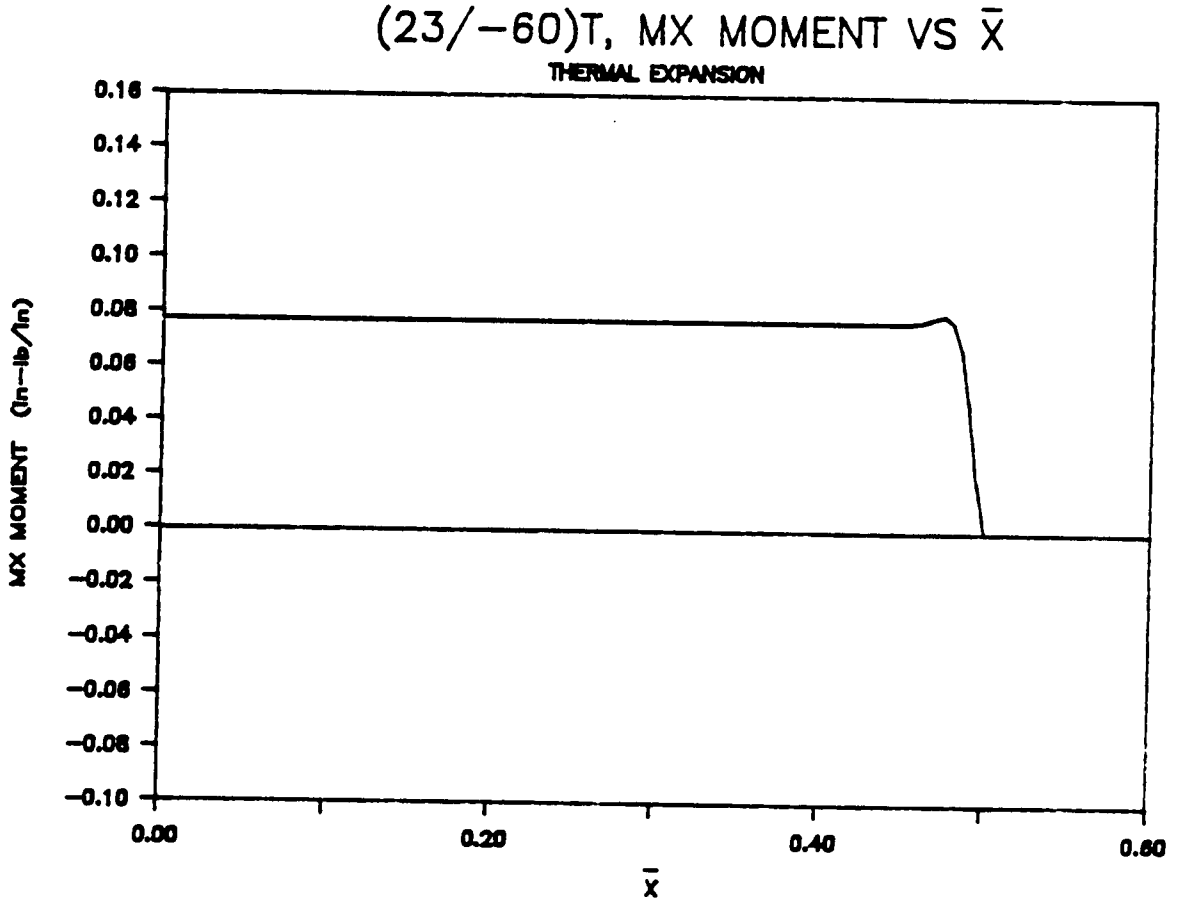

Figure 26 $(23/-60)_T$, M_X vs $\bar{x}$, Thermal Expansion

The circumferential force resultant N_θ, fig. 27, behaves in the opposite manner. This force resultant is zero over most of the length of the cylinder. Toward the end the resultant becomes negative and then rapidly becomes positive. Since there are none, this behavior is not associated with any imposed kinematic constraint at the end of the cylinder, as it is with the axial compression and twist cases. Rather, this behavior is due to the coupling of the stress resultants through the various displacement components, most notably the radial displacement. The circumferential moment resultant, M_θ, is uniform over most of the cylinder and then varies rapidly near the end, as illustrated in fig. 28. The axial and shear force resultants are exactly zero over the entire length of the cylinder. As stated before, the governing equations stipulate that neither of these resultants vary with x, and since they are zero at the ends, they are zero everywhere along the length.

In summary, it is clear the $(23/-60)_T$ cylinder exhibits a high degree of elastic coupling. Though it is a particular case, this cylinder typifies the fact that with composite materials, twist, extension, and bending can be coupled. The most significant finding is the coupling of radial displacement with twist displacement for the cylinder subjected to torsion.

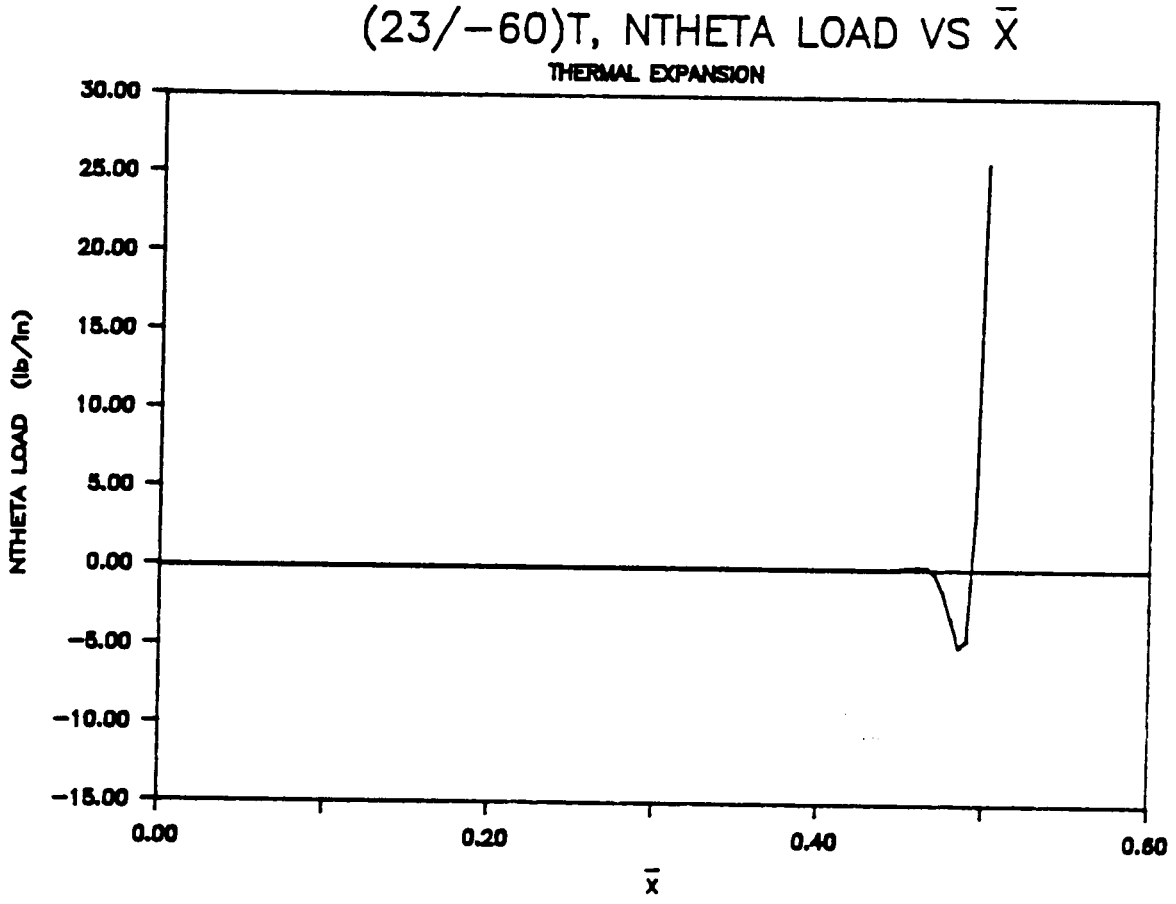

Figure 27 $(23/-60)_T$, N_θ vs $\bar{x}$, Thermal Expansion

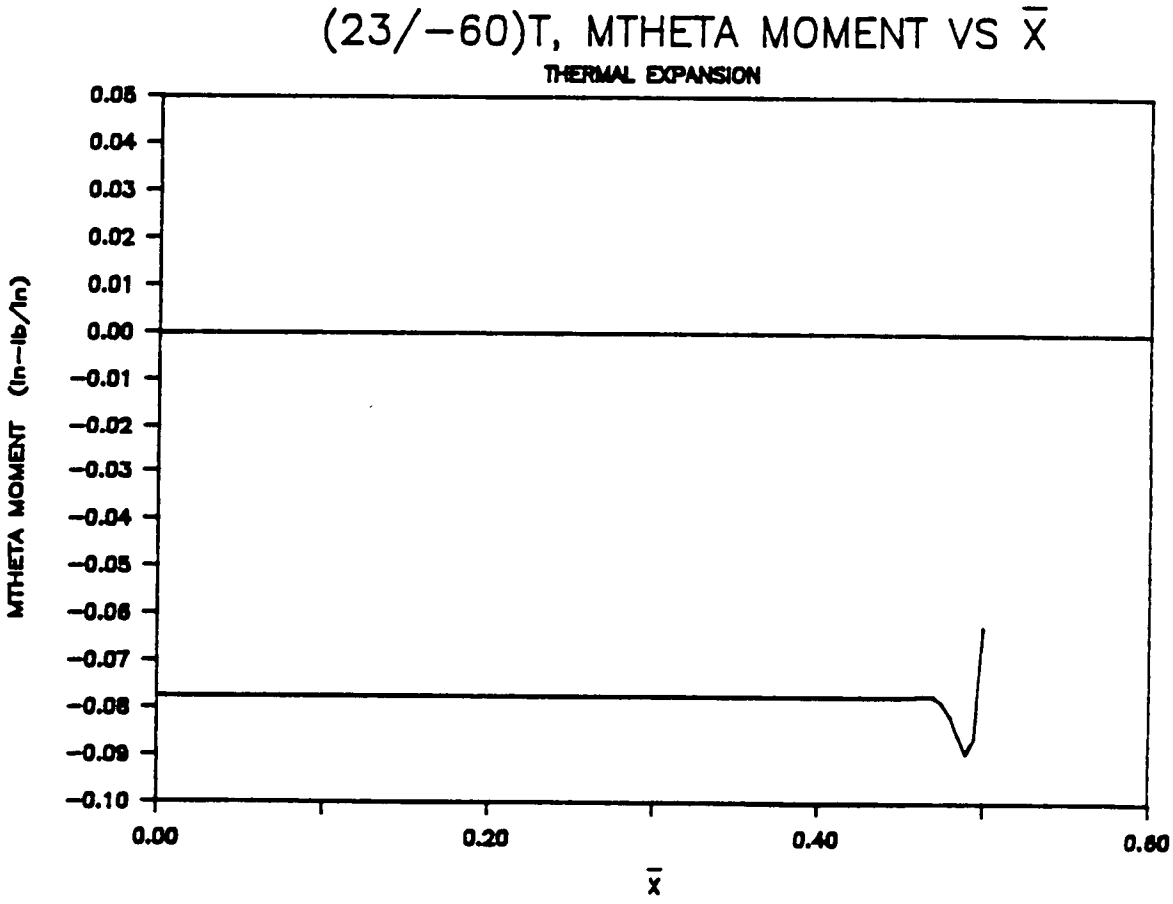

Figure 28 $(23/-60)_T$, M_θ vs $\bar{x}$, Thermal Expansion

5.2 Response of a Quasi-isotropic Cylinder and Two Variants

The results for the $(23/-60)_T$ cylinder indicate the wide range of responses that are possible with general composite laminates. The coupling of the radial displacements with the axial and circumferential displacements, and the accompanying coupling of the force and moment resultants, are characteristics that can be tailored for particular applications. The $(23/-60)_T$ laminate is quite unorthodox when compared to current designs. Unfortunately, unorthodox designs can often be viewed with skepticism due simply to lack of familiarity. Positive features are often overlooked. Therefore, it is of value to examine slight variations in existing designs, and explore the characteristics of these designs. Specifically, a popular conventional design is the quasi-isotropic laminate. This laminate consists of equal percentages of +45°, -45°, 0°, and 90° laminae, the percentage being 25% for all four angles. In the plane of the laminate the effective Young's modulus, Poisson's ratio, and shear modulus are independent of direction, i.e., isotropic. However, the shear modulus is not related to Young's modulus and Poisson's ratio by the well known relation

$$G = \frac{E}{2\,(\,1 + \mu\,)} \quad . \qquad (188)$$

Because of the lack of a relation between these three properties, the term quasi-isotropic is used. A typical 16 layer quasi-isotropic laminate is given by the stacking arrangement

$$(\,\pm 45/0/90\,)_{2s} \quad ,$$

where the subscript s implies the laminate stacking arrangement is symmetric with respect to the laminate midplane. Thus both the lamina at the inner radius and the lamina at the outer radius are oriented at +45°. The laminae on either side of the mean radius are oriented at 90°. Quasi-isotropic designs are popular because many metal-based design concepts are usable and because of the lower density of graphite/polymer composites, a simple substitution of a quasi-isotopic laminate for aluminum saves 25% weight. Accordingly, then, except for the presence of the D_{16} and D_{26} terms, a quasi-isotropic cylinder behaves very much like a metallic cylinder.

Two variants of the above quasi-isotropic design are

design 1 $\quad (\,+45/-45/0_4/+45/-45_2/+45/90_4/-45/+45\,)_T$

.... (0° layers closer to inner radius)

design 2 $(+45/-45/90_4/+45/-45_2/+45/0_4/-45/+45)_T$

.... (90° layers closer to inner radius)

These designs have the same number of layers as the above quasi-isotropic design and these layers have the same orientations as the quasi-isotropic design. In fact, all three laminates have the same A matrix, the matrix associated with inplane stiffness, and so all three laminates are quasi-isotopic in their inplane properties. However, both designs 1 and 2 are unsymmetric. Design 1 is distinguished by having the 0° layers grouped together and placed close to the inner radius. Design 2 has the 90° layers grouped and placed close to the inner radius. The placement of the 0° and 90° layer groups provides some eccentricity in the material properties. The eccentricity of design 1 is exactly opposite to the eccentricity of design 2. The motivation for considering eccentricity is as follows: It is well known that the axial buckling response of a cylinder is influenced by having axial stiffeners on the inside or outside of the cylinder. Among other things, the stiffeners provide eccentricity and can delay the onset of buckling. For a certain range of geometric parameters, stiffeners on the inside are more beneficial than stiffeners on the outside. For other ranges of parameters, stiffeners on the outside are most beneficial. Whether the stiffeners are on the inside or

outside determines the sense of the eccentricity. The idea here is to provide the eccentricity by material coupling rather than by the addition of stiffeners. This may save weight and certainly simplifies fabrication. A complete understanding of whether this material coupling is beneficial cannot be determined until a buckling analysis is conducted. That is beyond the scope of this study but it is felt examining the linear response of unsymmetric cylinders is a worthwhile starting point. It is also worthwhile determining the differences between similar symmetric and unsymmetric designs. That is done in this section.

The A matrix of all three designs is:

$$A_{11} = A_{22} = .69181\ E6\ \text{lb/in}\ ,$$

$$A_{12} = .19659\ E6\ \text{lb/in}\ ,$$

$$A_{16} = A_{26} = 0.\ \text{lb/in}\ ,$$

$$A_{66} = .24761\ E6\ \text{lb/in}\ , \qquad (189)$$

The B matrix of a symmetric laminate is of course zero and the B matrix of design 1 is:

$$B_{11} = - B_{22} = -7524.\ \text{lb}\ ,$$

$$B_{12} = B_{16} = B_{26} = B_{66} = 0.\ \text{lb}\ , \qquad (190)$$

while the B matrix of design 2 is:

$$B_{11} = -B_{22} = 7524.\ \text{lb} \quad ,$$

$$B_{12} = B_{16} = B_{26} = B_{66} = 0.\ \text{lb} \quad , \qquad (191)$$

The D matrices of the symmetric design, and design 1 and design 2 are, respectively,

$$D_{11} = 364.14\ \text{lb-in} \quad , \quad D_{12} = 137.89\ \text{lb-in} \quad ,$$

$$D_{16} = 23.513\ \text{lb-in} \quad , \quad D_{22} = 307.71\ \text{lb-in} \quad ,$$

$$D_{26} = 23.513\ \text{lb-in} \quad , \quad D_{66} = 165.10\ \text{lb-in} \quad ,$$

(192)

$$D_{11} = 352.44\ \text{lb-in} \quad , \quad D_{12} = 121.37\ \text{lb-in} \quad ,$$

$$D_{16} = 18.810\ \text{lb-in} \quad , \quad D_{22} = 352.44\ \text{lb-in} \quad ,$$

$$D_{26} = 18.810\ \text{lb-in} \quad , \quad D_{66} = 148.58\ \text{lb-in} \quad .$$

(193)

As can be seen, the major difference between designs 1 and 2 is in the B matrix....the signs of B_{11} being reversed. The sign reversal on B_{11} is due to a reversal of the material eccentricity. It should be noted that the B matrix for either case is sparsely populated, and $B_{22} = -B_{11}$. At this point it is interesting to compare the ABD

matrices for these three laminates, eqs. 189-193 with the ABD matrix of the $(23/-60)_T$ laminate, eqs. 185-187. The two main differences are: (1) For the $(23/-60)_T$ laminate, the B matrix is completely full and contains no zero elements. For designs 1 and 2, all elements in the B matrix except 2 are zero, and these two are of equal magnitude. (2) For the symmetric design and design 1 and 2, A_{16} and A_{26} are zero, for the $(23/-60)_T$ case they are not. The lack of the A_{16} and A_{26} terms means extension and twist cannot directly couple. The D matrices are full for all cases (a characteristic of most laminates).

The next sections describe the response of the three designs to the compression, torsion, and a temperature change. Any differences in the response among the three designs are noted.

5.3 Response to Compression

The axial displacement for the three cylinders as a function of length along the cylinder is illustrated in fig. 29. The boundary conditions considered are boundary condition 1, eqs. 165-168, namely the cylinder restrained against circumferential displacement at the ends. As expected, the response is quite linear with x with the U_6 term being dominant, and the three cylinders exhibit nearly

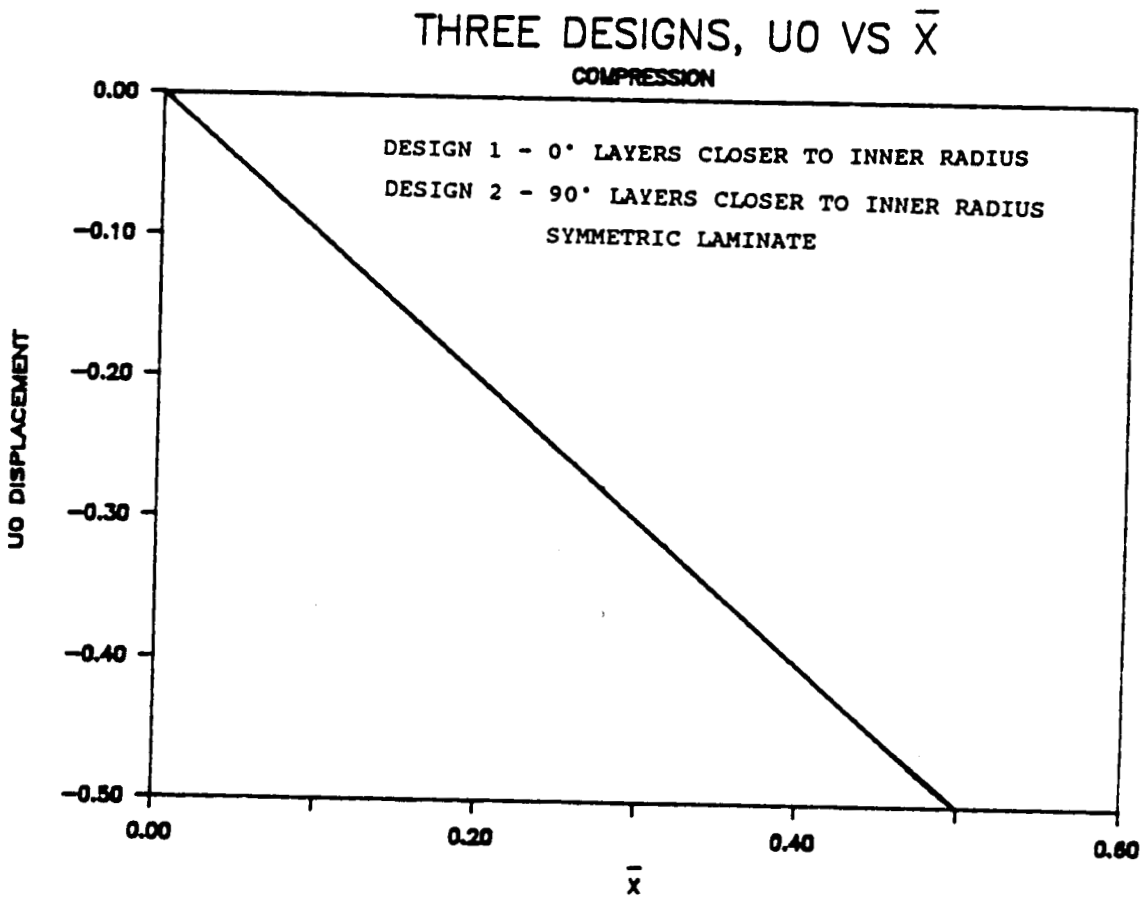

Figure 29 Three Designs, $u^{\circ}(\bar{x})$ vs $\bar{x}$, Compression

identical response. Though not visible on the scale of the figure, the differences that do occur are at the end. The axial force resultant required to compress the cylinder one laminate thickness is shown in fig. 30. The three cases are shown and these forces are identical. The forces are constant with x, because as mentioned earlier, the differential equations require this.

Slight differences in the response are apparent when the radial displacements are studied. This is illustrated fig. 31. All three cylinders have identical radial displacement away from the end and exhibit a boundary layer at the end. The unsymmetric design 1, the design with the 0° laminae closest to the inner radius, results in the least amount of radial displacement variation within the boundary layer. Design 2 exhibits the most, and the symmetric design is between the two. Overall, design 1 is more like the symmetric design than design 2 is. If it is to have an effect at all, one might expect the smaller gradient and smaller reverse curvature of design 1 within the boundary layer to delay the onset of buckling, whereas the larger gradient and larger reverse curvature of design 2 might aggravate buckling.

The axial moment resultants that accompany the three radial displacement characteristics are shown in fig. 32. Away from the ends there is no axial moment generated in the symmetric cylinder. The only moment generated is in

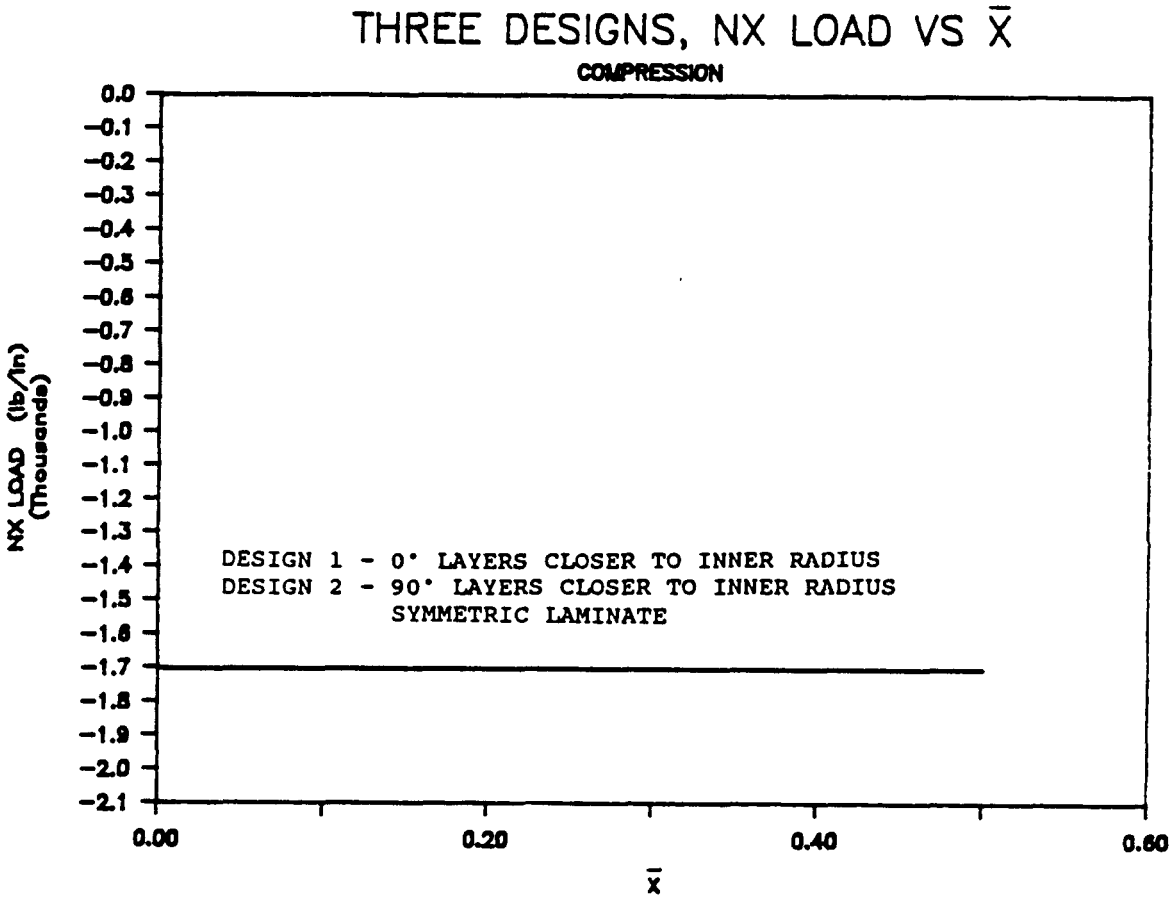

Figure 30 Three Designs, N_x vs $\bar{x}$, Compression

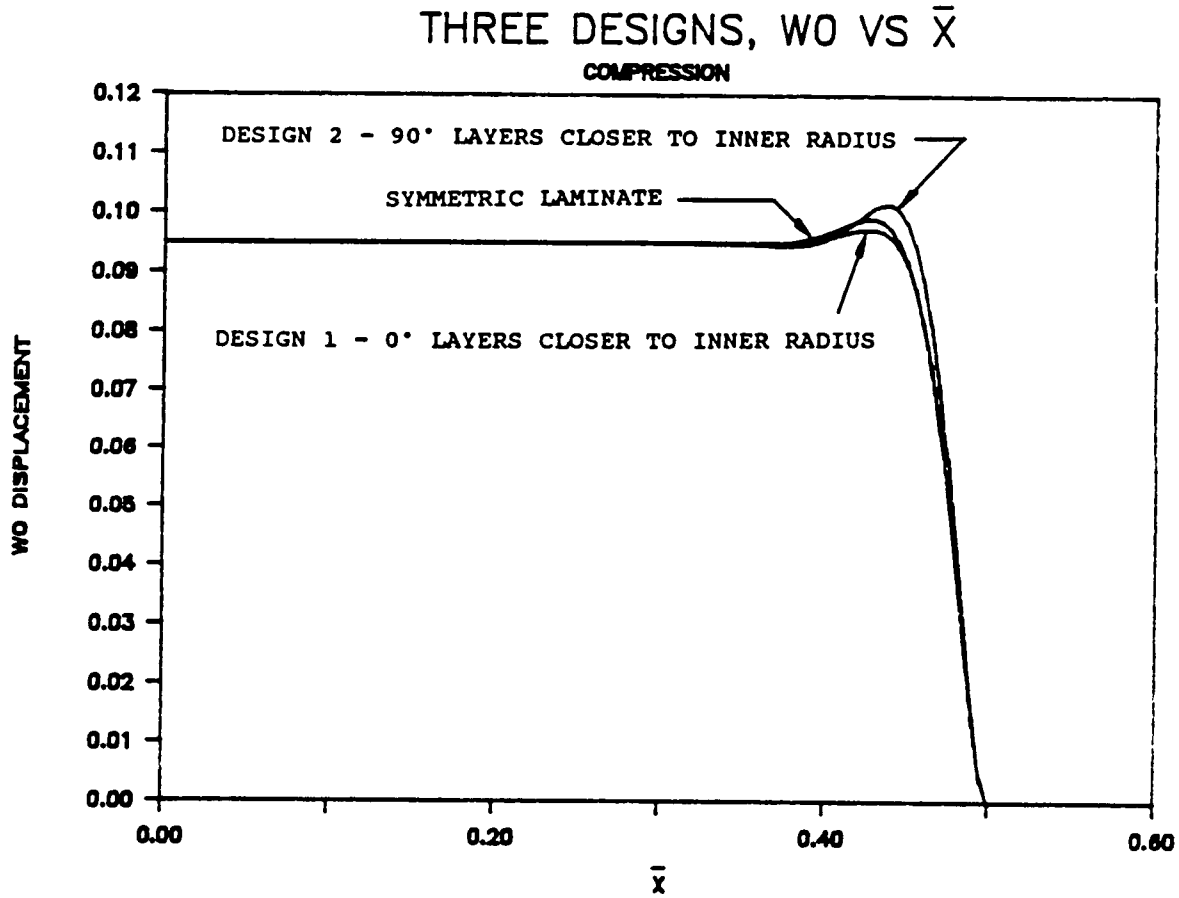

Figure 31 Three Designs, $w^*(\bar{x})$ vs $\bar{x}$, Compression

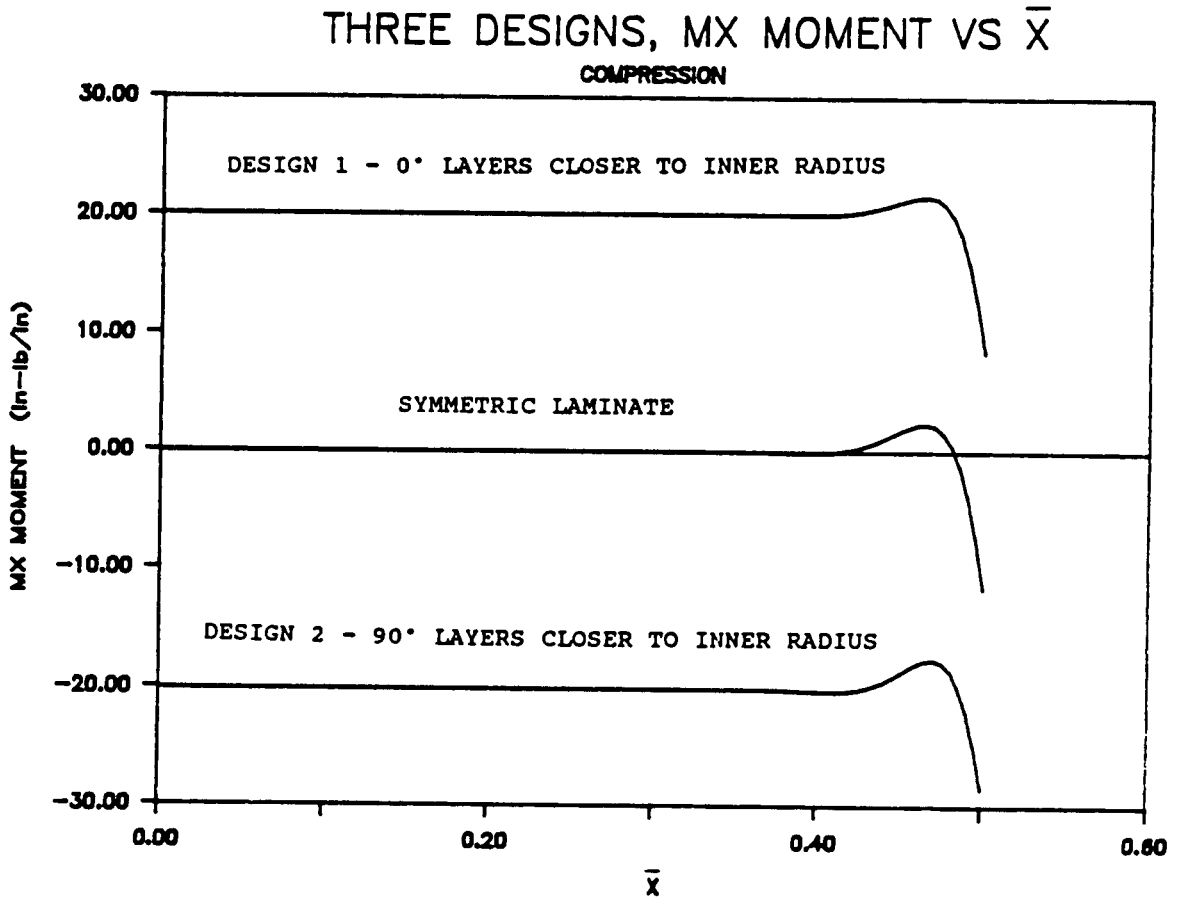

Figure 32 Three Designs, M_x vs $\bar{x}$, Compression

the boundary layer. However, the axial compression of both unsymmetric designs generates moments away from the ends, the moments being exactly opposite. The moment away from the end is altered as the end of the cylinder is approached. Except for slight differences at the ends the three moment characteristics are essentially a positive or negative vertical shift of symmetric case.

The circumferential force resultants for the three cases, fig. 33, differ very little. On the otherhand, the circumferential moment resultants shown in fig. 34 are quite different. In addition to having a nonzero value over much of the cylinder length, unsymmetric design 1 shows a large change in the circumferential moment near the end. Design 2 also exhibits rapid changes in the value of the circumferential moment near the end. It is interesting that all three designs converge to the same value of circumferential moment at the end of the cylinder, independent of the value of the moment at midcylinder, and independent of the local character of the variation within the boundary layer.

Finally, the shear force resultant that accompanies axial compression is not zero but is very small ranging from 10^{-10} to 10^{-9}. The presence of the D_{16} term in eq. 111 is responsible for this.

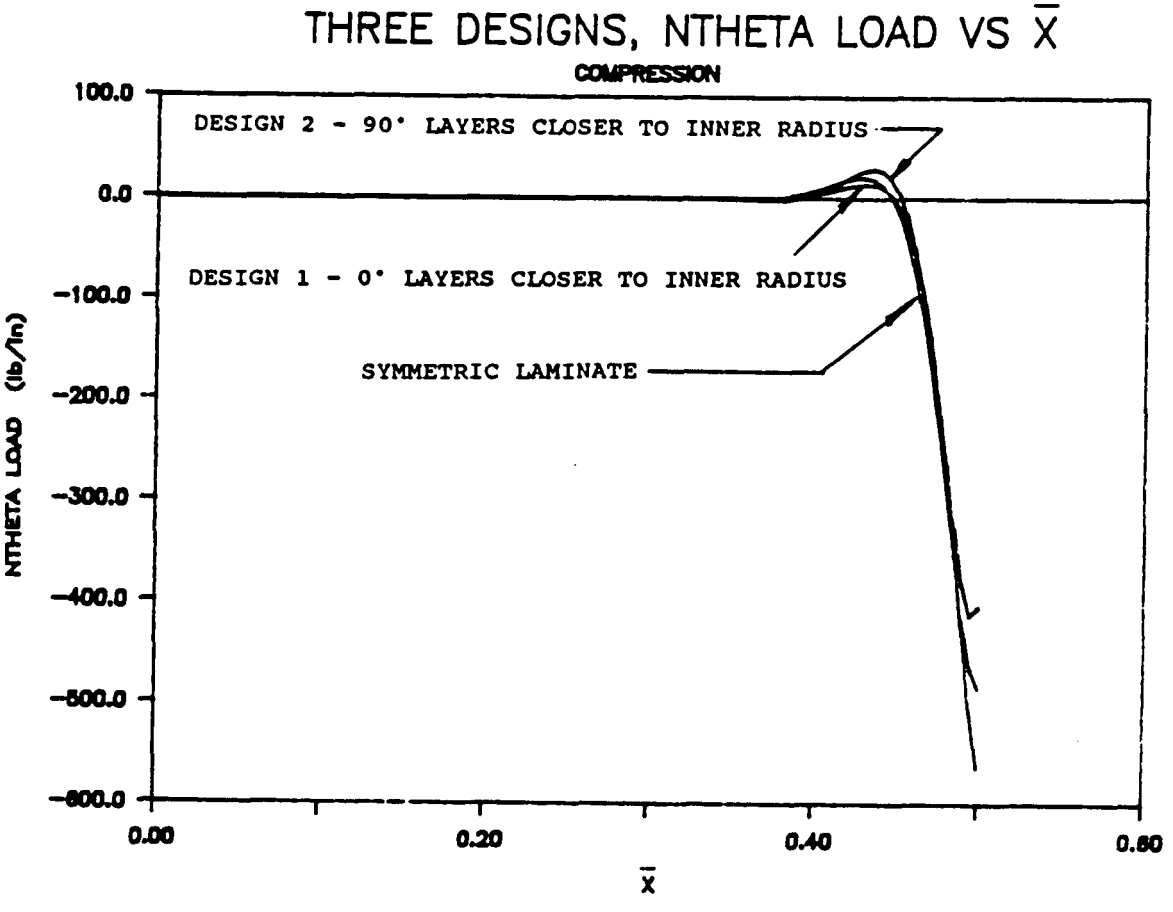

Figure 33 Three Designs, N_θ vs $\bar{x}$, Compression

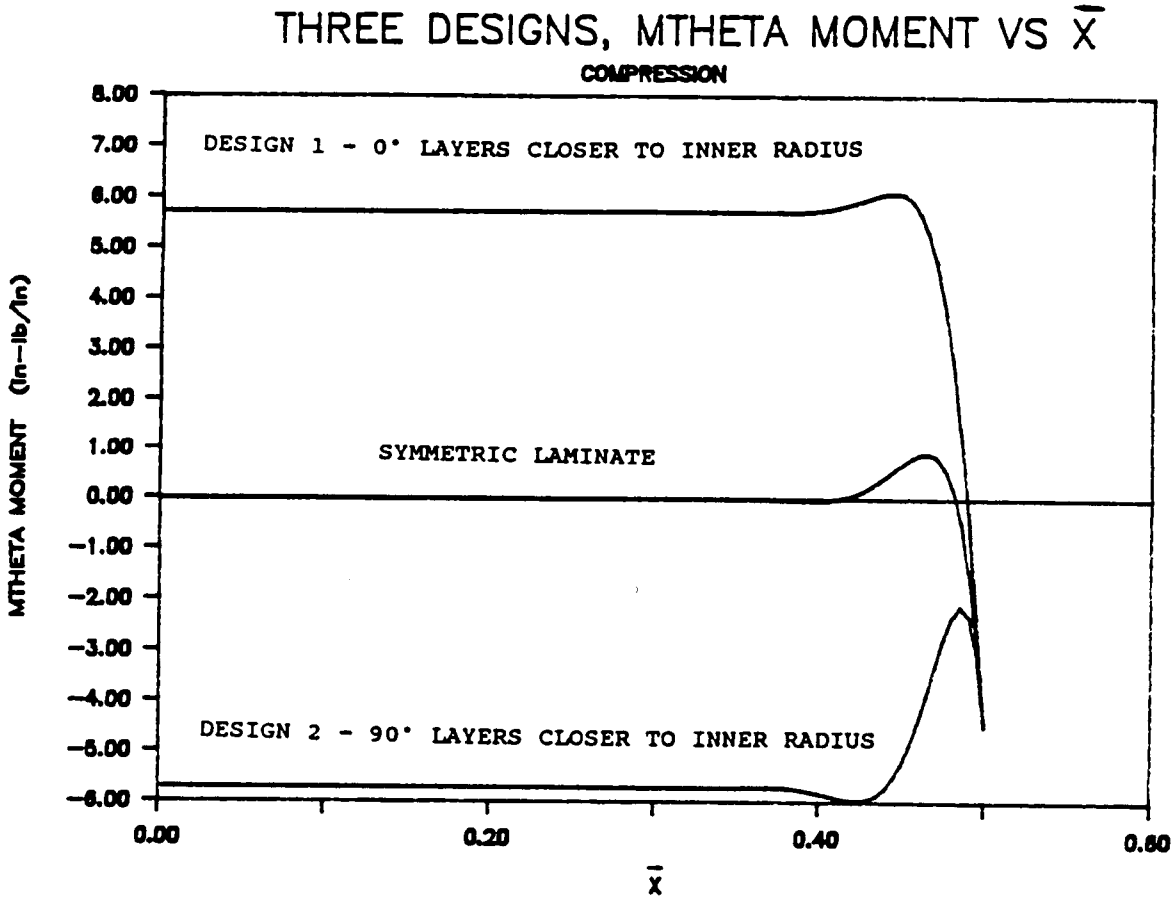

Figure 34 M_θ vs $\bar{x}$, Compression

5.4 Response to Twisting

The twisting responses of the three cylinders to boundary condition 1, eqs. 173-176, cylinders restrained against axial motion, are illustrated in figs. 35-38. The twisting of the three different cylinders does not produce as much response as the twisting of the $(23/-60)_T$ cylinder. Most notably absent for all three designs is any radial displacement. Reviewing eq. 161, for these cases the unknowns C and D are exactly zero as is the constant β. Equation 145 indicates that $\beta = 0$ because $A_{26} = B_{26} = 0$. This makes the radial displacement exactly zero for all three designs. As seen in fig. 35, the circumferential displacement of all three cylinders is very similar, the variation of displacement being quite linear with position along the cylinder. As stated above the unknowns C and D are exactly zero. Since these unknowns are zero, the only term in eq. 164 to produce a response is the V_6 term. Therefore, the response is linear from this term. The shear force resultants, $\overline{N_{x\theta}}$, fig. 36, are also quite similar for the three cylinders. The similar results are to be expected if the expression for $\overline{N_{x\theta}}$, eq. 111, is examined. The material constants A_{16}, A_{26}, B_{16}, and B_{26} are zero for all three cylinders and the shear force depends only on A_{66}, D_{66}, and the circumferential displacement gradient. Since A_{66}, D_{66}, and the gradient

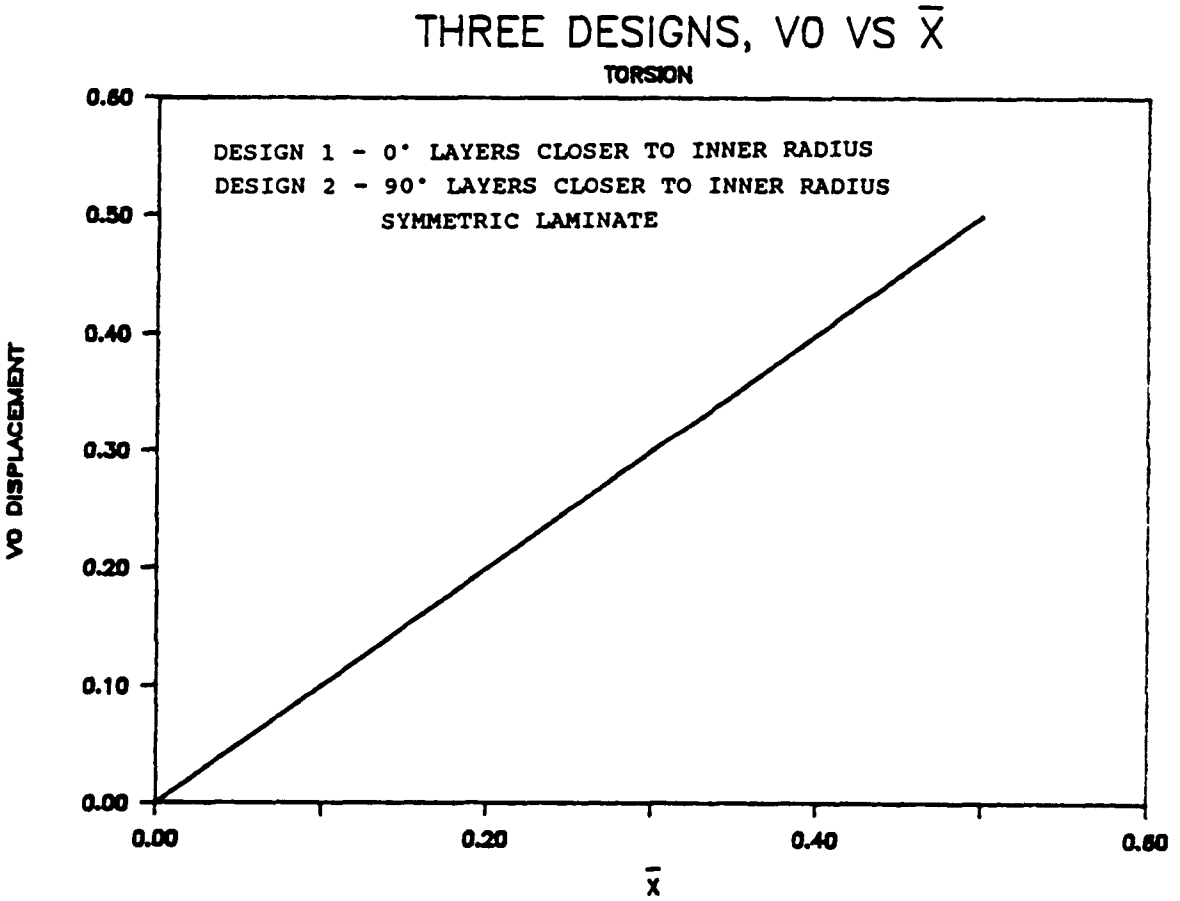

Figure 35 Three Designs, $v^{\circ}(\bar{x})$ vs $\bar{x}$, Torsion

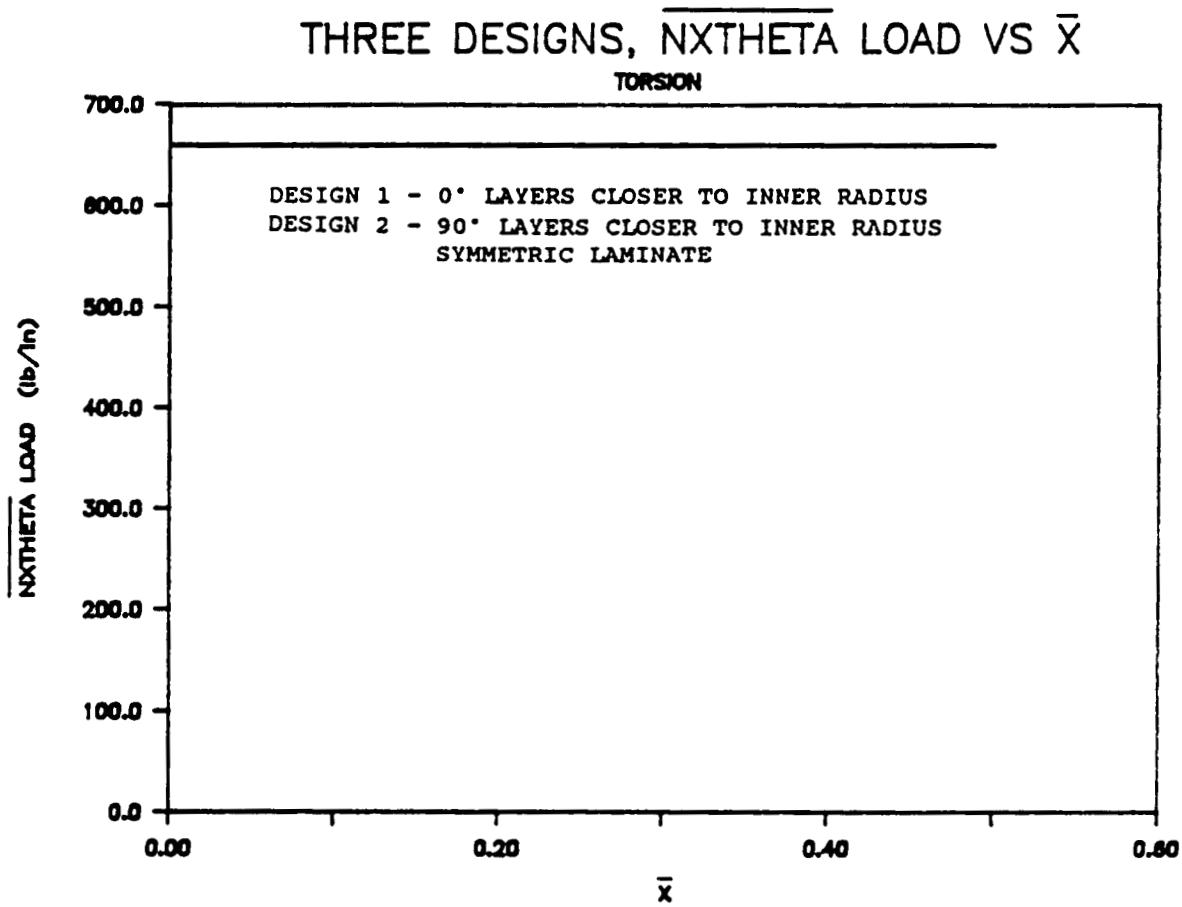

Figure 36 Three Designs, $\overline{N_{x\theta}}$ vs $\bar{x}$, Torsion

are similar for the three cylinders, the shear force resultants are similar. As might be expected, because of its metal-like behavior, there is no axial or radial displacement response for the quasi-isotropic design. Recalling eqs. 161 and 163, these displacements are exactly zero which is due to the unknowns C, D, U_6 being exactly zero for all three designs. As a result there is no axial or circumferential force resultant. The axial and circumferential bending moments, figs. 37 and 38, although small are not exactly zero. The reason can be seen by examining eqs. 112 and 113. The only nonzero terms are the D_{16} and D_{26} terms multiplied by the circumferential gradient. As mentioned previously and as seen in fig. 35, this gradient for the three designs is very similar and is the primary response that causes the bending moment. The difference between the symmetric and unsymmetric designs 1 and 2 is in the D_{16} and D_{26} terms. This material property term differs slightly between the symmetric and unsymmetric cases, causing slight differences in the bending moments.

5.5 Response to a Temperature Change

Again, since graphite-epoxy is processed at an elevated temperature, the effects of this elevated

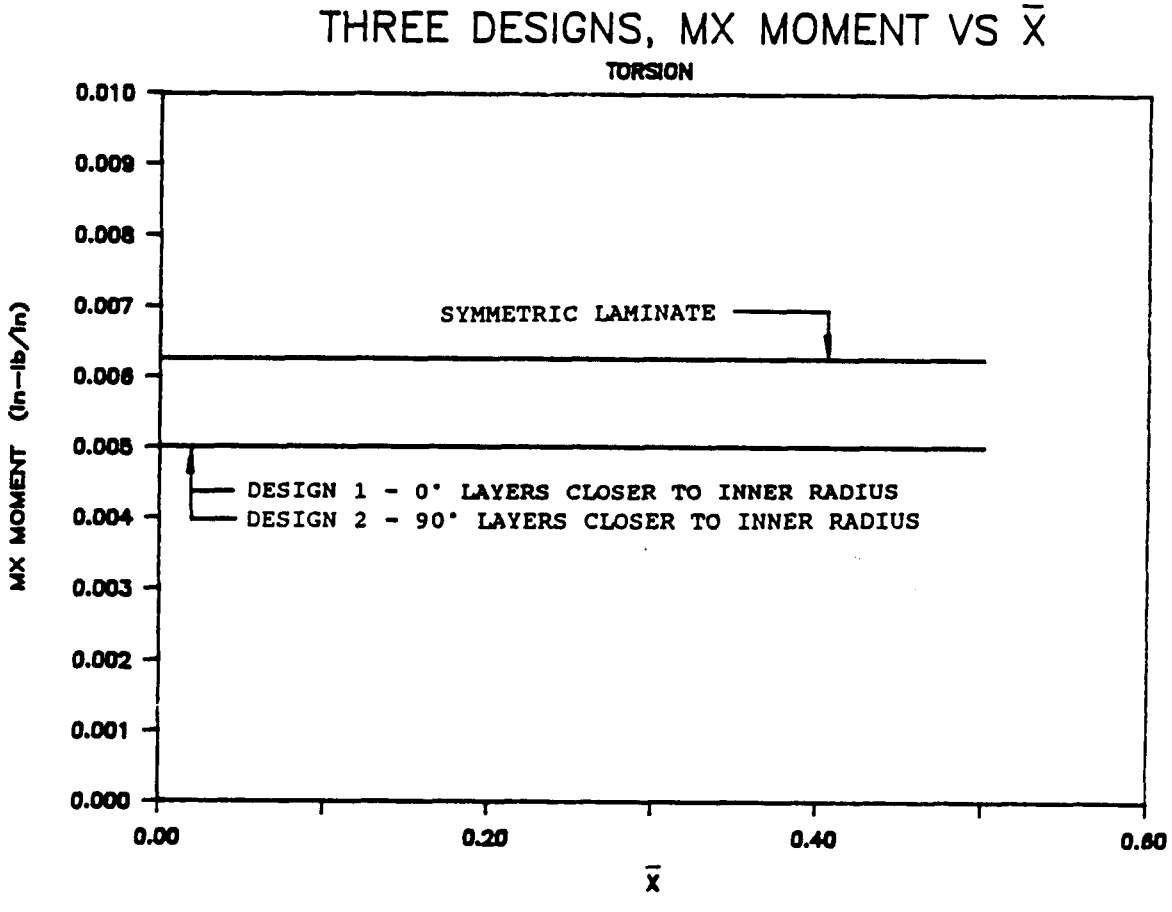

Figure 37 Three Designs, M_X vs $\bar{x}$, Torsion

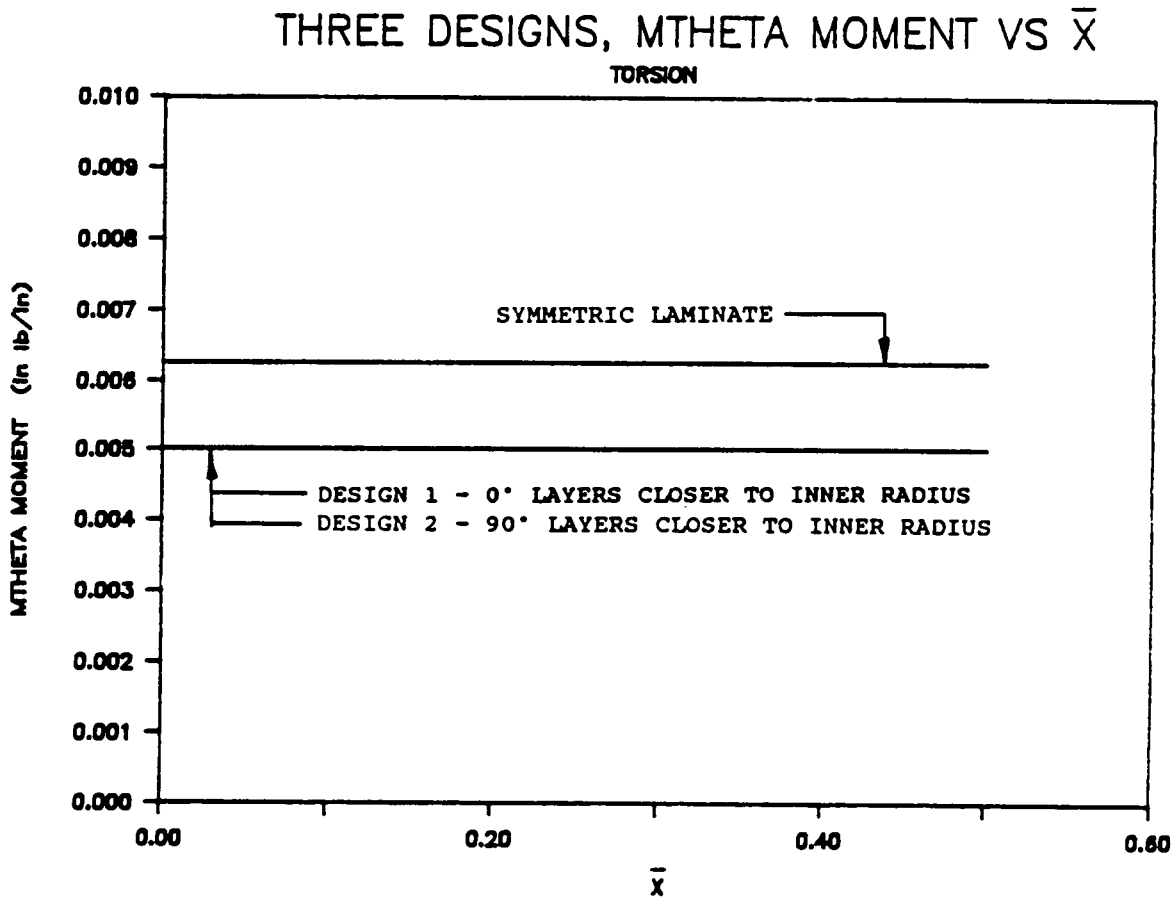

Figure 38 Three Designs, M_θ vs $\bar{x}$, Torsion

temperature on the displacements and stress resultants when the cylinder is at a lower temperature are of interest. Assuming the same -280 °F temperature change as with the $(23/-60)_T$ laminate, the response of the three cylinders is shown in figs. 39-43. The axial contraction due to the negative temperature change is illustrated in fig. 39. The axial contraction response of the three cylinders is practically identical, except at the ends where there are slight differences. These differences are much more significant when the radial displacement is examined. This is shown in fig. 40. Overall, the three cylinders contract radially. With the symmetric design, the contraction is uniform along the entire length of the cylinder. The two unsymmetric designs exhibit behavior different than the symmetric design, and different from each other. The radial displacement of design 1 actually becomes positive right at the end of the cylinder. The transition from uniform contraction to expansion takes place in a short boundary layer region. In fact, within the boundary layer, the radial contraction becomes more pronounced before suddenly changing to a radial expansion. With design 2 on the otherhand, the uniform contraction decreases as the end of the cylinder is approached, before suddenly becoming greater. The behavior of the unsymmetric laminates is due solely to the presence of the B_{11} and B_{22} terms.

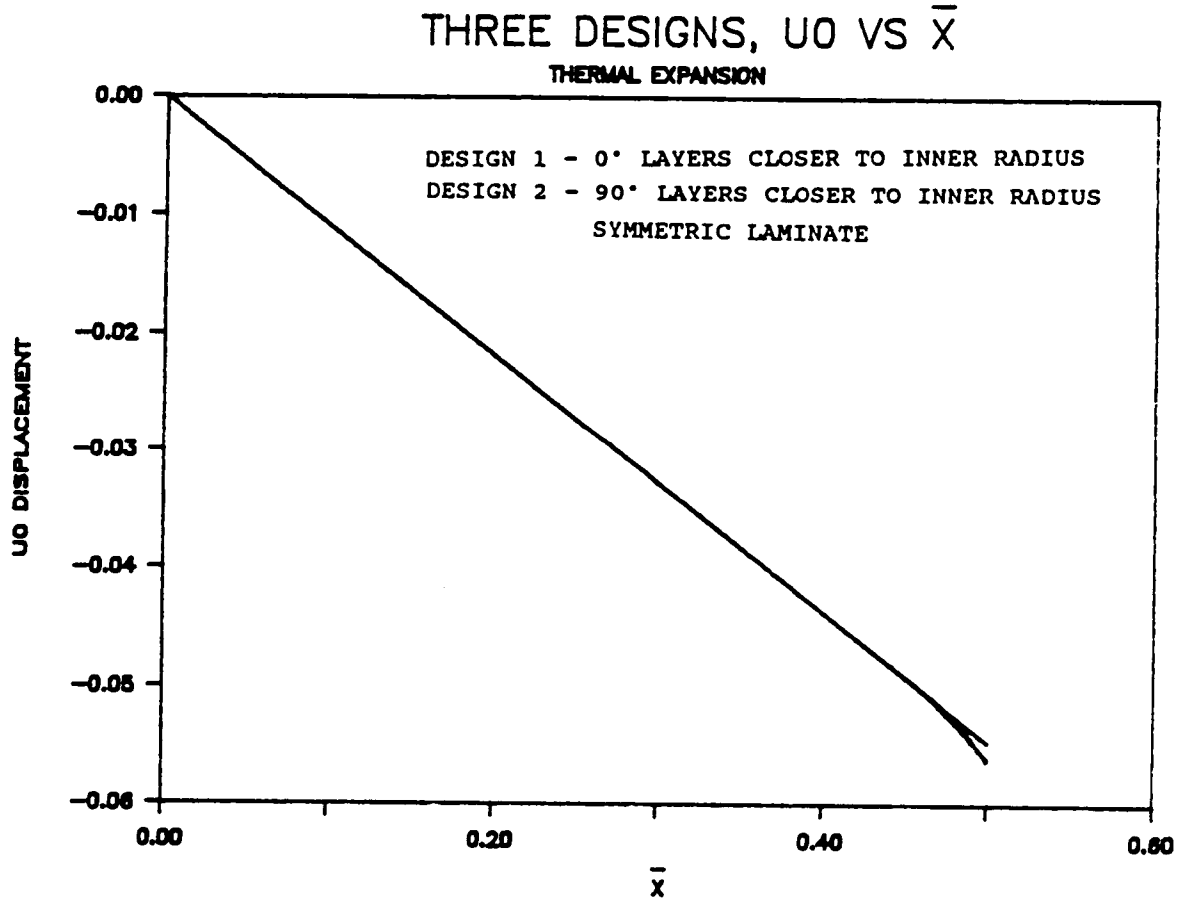

Figure 39 Three Designs, $u^*(\bar{x})$ vs $\bar{x}$, Thermal Expansion

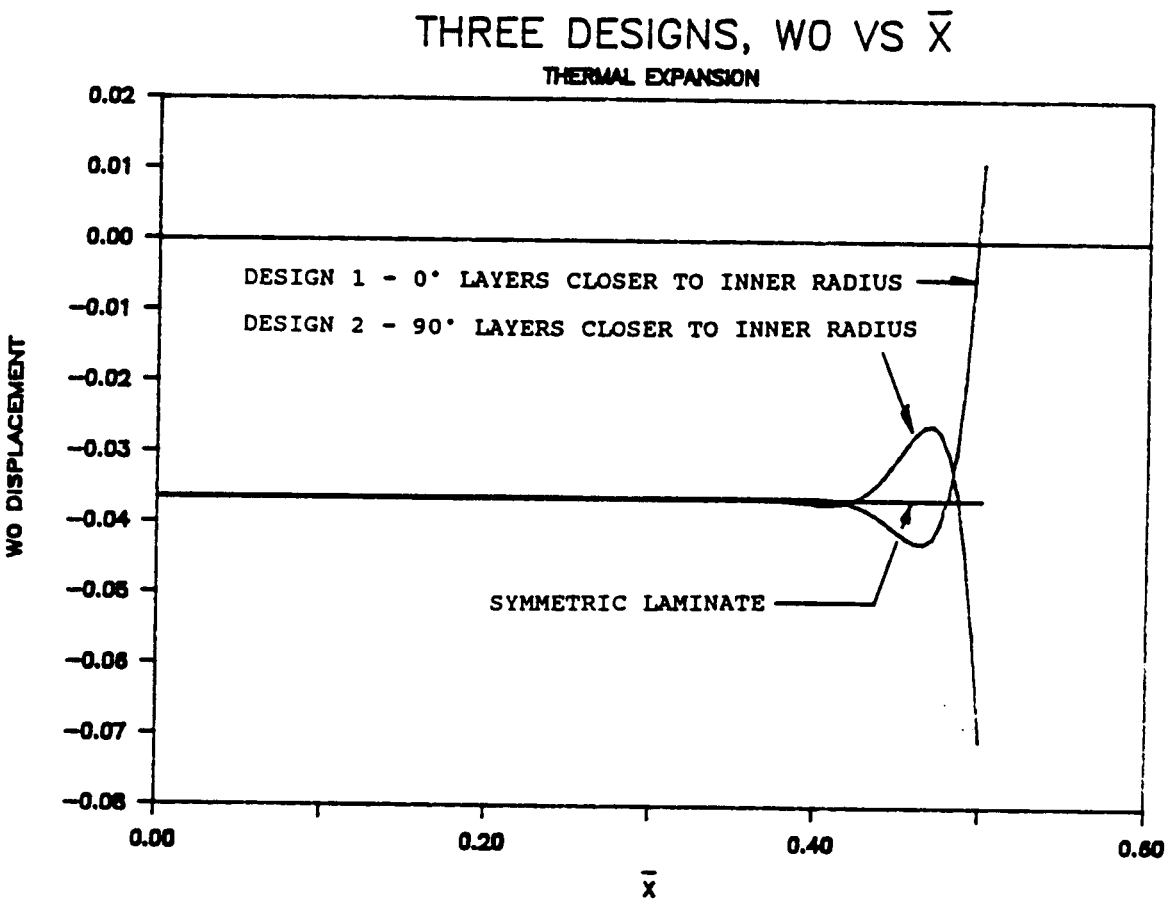

Figure 40 Three Designs, $w^*(\bar{x})$ vs $\bar{x}$, Thermal Expansion

The axial moments that accompanies the radial deflections are illustrated in fig. 41. No moment is induced in the symmetric laminate, whereas both unsymmetric laminates experience an axial moment. The moments for both cases are uniform over most of the cylinder length and suddenly go to zero in the boundary layer. With the symmetric cylinder there are no thermally-induced circumferential displacements, nor is there a shear force resultant. For the unsymmetric cylinders the circumferential responses are not exactly zero but are on the order of 10^{-8} and 10^{-9}, respectively. The resultants in the circumferential direction consist of both forces and moments for the two unsymmetric cases, figs. 42 and 43. For the symmetric case, there are no circumferential stress resultants. For the two unsymmetric cases the circumferential force resultants are zero over most of the cylinder, and then rapidly become nonzero, changing signs once near the end of the cylinder. The moment resultants are of opposite magnitude over most of the cylinder, then change rapidly to dissimilar values at the ends.

In summary, unsymmetric designs 1 and 2, though showing more coupling than the symmetric case, are not as highly coupled as the $(23/-60)_T$ cylinder. This indicates that the degree of coupling can be controlled, and because of the similarity of some of the responses of the

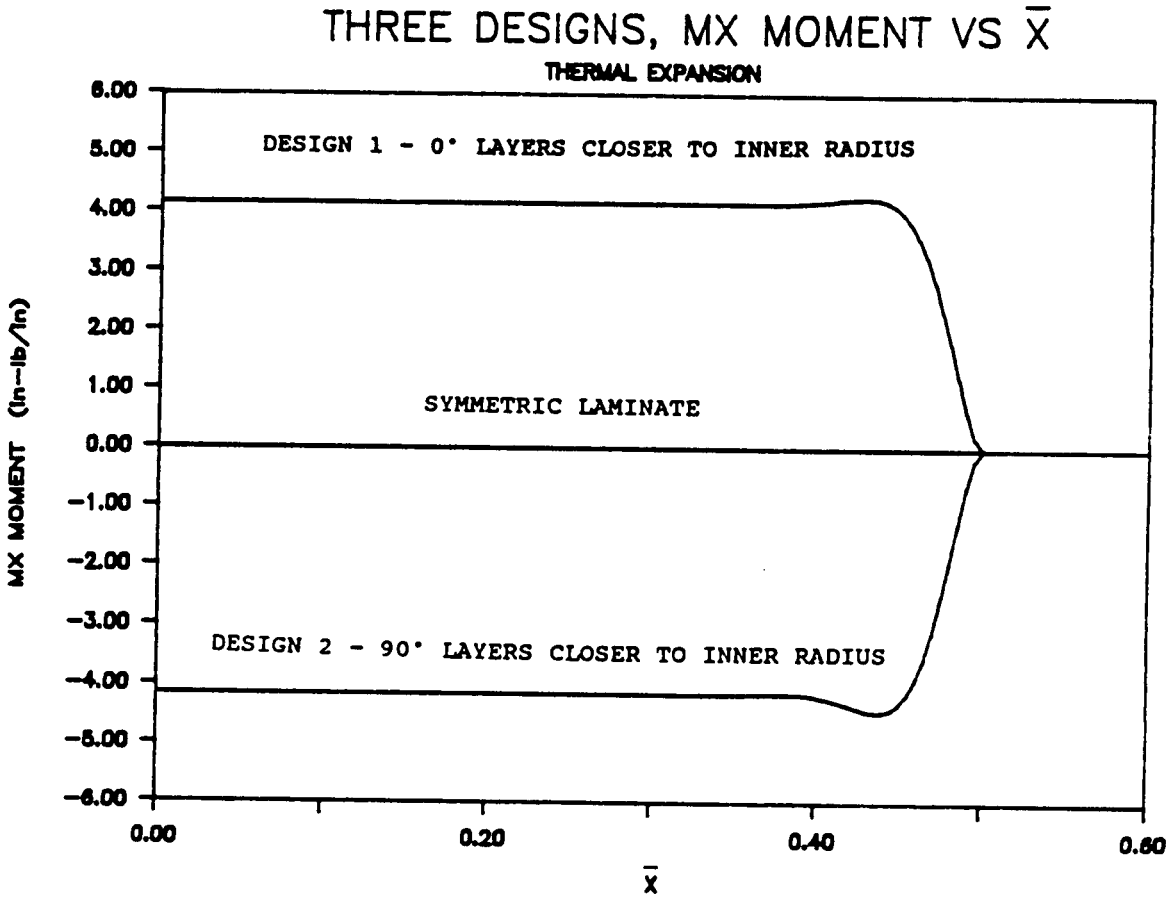

Figure 41 Three Designs, M_X vs $\bar{x}$, Thermal Expansion

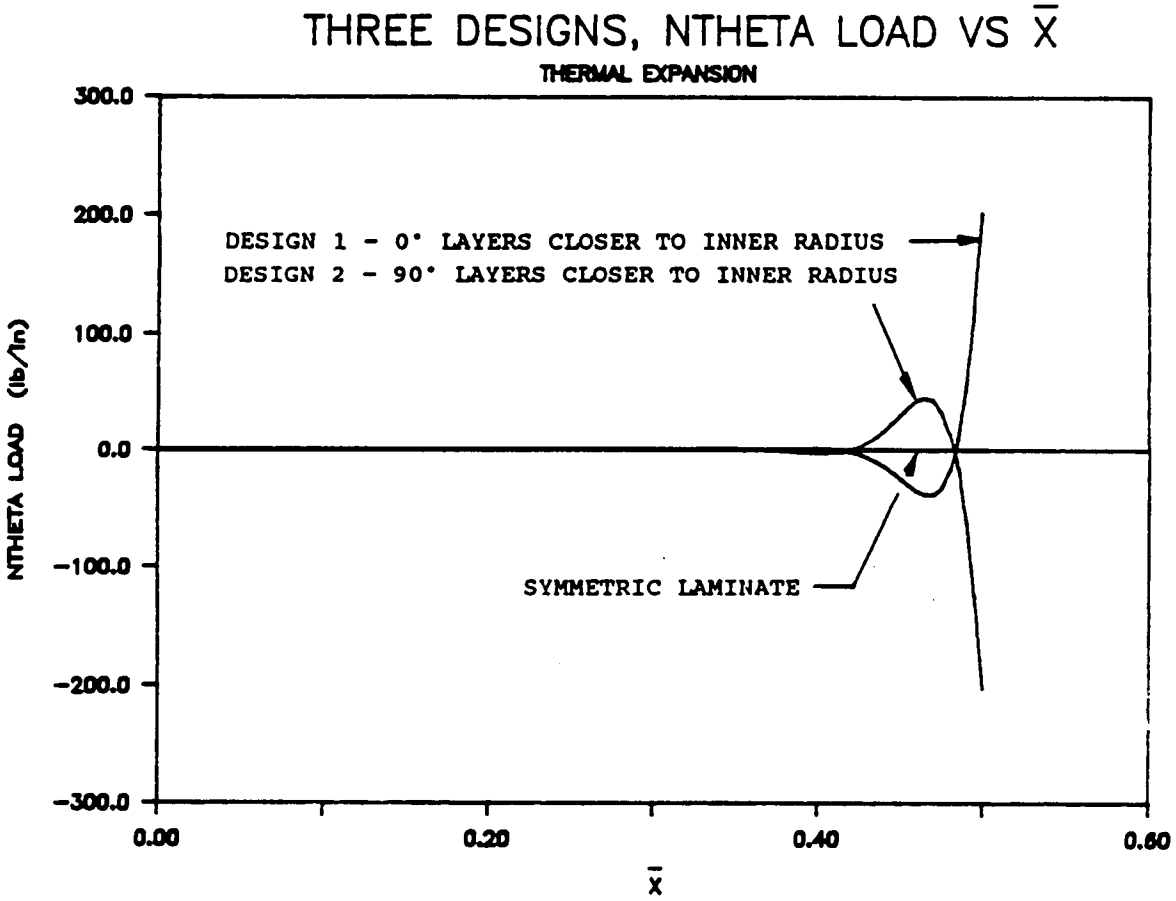

Figure 42 Three Designs, N_θ vs $\bar{x}$, Thermal Expansion

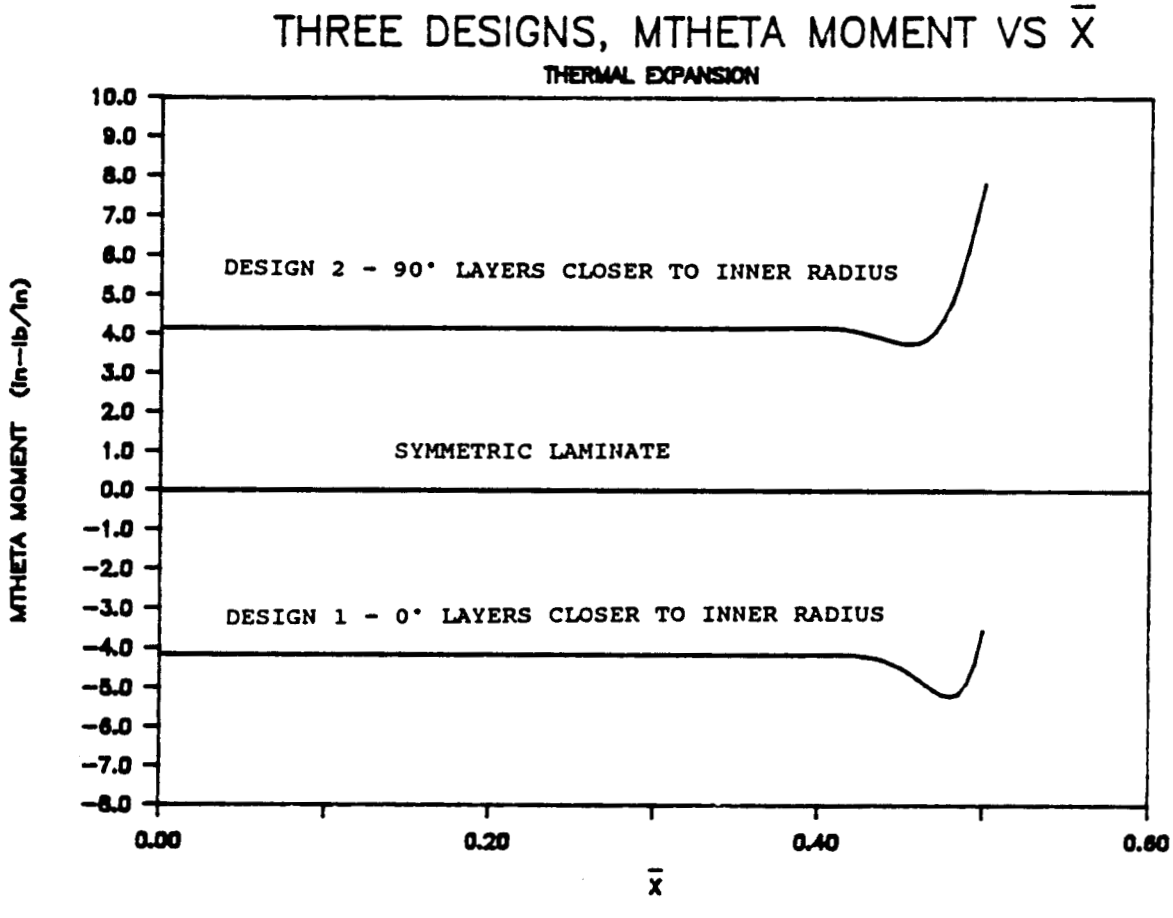

Figure 43 Three Designs, M_θ vs $\bar{x}$, Thermal Expansion

symmetric case and the two unsymmetric cases, designs 1 and 2, certain responses obtainable with symmetric laminates can be retained. The most significant finding for the three cases just discussed is the difference in the radial displacements in the boundary layer when the cylinders are subjected to axial compression, i.e., fig. 31.

Chapter 6 Conclusions and Recommended Future Research

Presented has been the development of equations governing the axisymmetric response of fiber-reinforced composite cylinders to compressive, torsional, and thermal loads. The composite cylinders have been assumed to be general, exhibiting the highest degree of elastic couplings possible. The governing equations were developed by assuming Sanders' kinematic hypothesis was valid, and by using variational methods. Several sets of boundary conditions were considered, depending on the problem. Three FORTRAN programs were developed to implement a closed-form solution to the governing equations. Numerical results obtained from the programs for several example problems were presented and discussed. Based on examining the governing equations and the numerical results, several important conclusions can be drawn. These are as follows:

For the most highly coupled case (the $(23/-60)_T$ laminate), a response totally unlike the response of metal cylinders or more conventional composite cylinders is exhibited. Compressive loading of a cylinder causes torsional stress resultants or circumferential displacements depending on the boundary conditions, and torsion loading causes axial stress resultants or displacements, again depending on boundary conditions. Furthermore, compressive loading of a cylinder causes

radial displacements beyond the normal displacements associated with Poisson effects. Most significant, torsional loading of a cylinder causes radial displacements. . . .an unusual effect. Boundary layer response is exhibited in most cases, the degree of response in the boundary layer depending on the particular case. Typically the boundary layer is characterized by large curvatures and sign reversals of the responses. It does not appear that the boundary layer response is any greater or any less in more general laminates, i.e., the $(23/-60)_T$ laminate or designs 1 and 2, than in more conventional laminate, i.e., the symmetric quasi-isotropic design. It does appear that perhaps the magnitude of the response in the boundary layer can be controlled to some degree by laminate design, i.e., designs 1 and 2 vs. the symmetric laminate in fig. 31. The advantage, or disadvantage of the highly coupled nature of response of cylinders can only be assessed in the context of a specific application. However, it is clear that there is no limit to the type of response that can be achieved.

Three directions for future research are clear. First, it would be useful to fabricate cylinders that exhibit a high degree of coupling and verify that the predictions are valid. The thermal response is felt to be particularly important because at the service temperature the cylinders are not at a constant radius toward the ends.

This would be a problem in attaching the cylinder to other structural components.

Second, the calculation of the response of a cylinder to nonaxisymmetric loadings is an important next step. Specifically, the response to bending loads is felt to be important enough to recommend it as a next step.

Finally, determining the influence of geometric and perhaps material nonlinearities is considered important, particularly geometric nonlinearities. The radial deformation of the cylinder cannot exceed one-half to one wall thickness before geometric nonlinearities become an issue. Inclusion of these effects can be complicating but they are important at higher load levels in both compression and torsion. Nonlinear effects in the thermal case are not felt to be as important.

REFERENCES

1. Hyer, M. W., "Some Observations on the Cured Shapes of Thin Unsymmetric Laminates," J. Composite Materials, vol. 15, Mar. 1981, pp. 175-194.
2. Hyer, M. W., "Calculations of the Room-Temperature Shapes of Unsymmetric Laminates," J. Composite Materials, vol. 15, July. 1981, pp. 296-310.
3. Chaudhuri, Reaz A., Balaraman, K., and Kunukkasseril, Vincent X., "Arbitrarily Laminated, Anisotropic Cylindrical Shell Under Internal Pressure", AIAA Journal, Vol. 24, No. 11, 1851-1858, Nov. 1986.
4. Sanders, J. Lyell, Jr., "Nonlinear Theories for Thin Shells," Quarterly of Applied Mathematics, Vol. 21, No. 1, pp. 21-36, 1963.
5. Dym, Clive L., and Shames, Irving H., Solid Mechanics: A Variational Approach, McGraw-Hill Company, Inc., 1973.
6. Tsai, Stephen W., Composites Design, Think Composites, 1987.
7. Donnell, L. H., Beams, Plates, and Shells, McGraw-Hill Company, Inc., 1976.
8. Reismann, H. and Pawlik, P. S., Elasticity, Theory and Application, John Wiley & Sons, Inc., 1980.